VISIBLE LIGHT-ACTIVE NON-METAL DOPED TITANIUM DIOXIDE MATERIALS FOR PHOTOCATALYTIC OXIDATION

A THESIS

SUBMITTED TO THE DEPARTMENT OF CHEMISTRY

AND THE GRADUATE SCHOOL OF ENGINEERING AND SCIENCE

OF BİLKENT UNIVERSITY

IN PARTIAL FULFILLMENT OF THE REQUIREMENTS

FOR THE DEGREE OF

MASTER OF SCIENCE

By

PELİN ALTAY

August 2014

I certify that I have read this thesis and that in my opinion is it is fully adequate, in scope and quality, as a thesis of the degree of Master in Science

……..

Asst. Prof. Dr. Emrah Özensoy (Supervisor)

I certify that I have read this thesis and that in my opinion is it is fully adequate, in scope and quality, as a thesis of the degree of Master in Science

……..

Asst. Prof. Coşkun Kocabaş

I certify that I have read this thesis and that in my opinion is it is fully adequate, in scope and quality, as a thesis of the degree of Master in Science

……..

Associate Prof. Niyazi Alper Tapan

Approved for the Graduate School of Engineering and Science

……..

Prof. Dr. Levent Onural

Director of the Graduate School of Engineering and Science

ABSTRACT

VISIBLE LIGHT-ACTIVE NON-METAL DOPED TITANIUM DIOXIDE MATERIALS FOR PHOTOCATALYTIC OXIDATION

PELİN ALTAY

M.S. in Chemistry

Supervisor: Asst. Prof. Dr. Emrah Özensoy

August, 2014

One of the most important technologies for a better human life is environmental purification which has drawn attention and gained importance over the past years. Titanium dioxide has been the apple of the eye of both air and water purification systems for its strong ability of oxidation, low cost, nontoxicity, inertness and availability. However, being a wide band gap semiconductor, titanium dioxide can mostly absorb UV photons ($\lambda < 387$ nm) in the sun light, which is only about 3% of the total solar radiation. In this regard, sensitizing titanium dioxide based materials capable of visible light absorption via doping methods is a challenging but yet a rewarding effort.

In the current work, a variety of doping protocols have been employed in conjunction with sol-gel titanium dioxide synthesis protocols in an attempt to prepare visible-active photocatalytic powders. This study has been a preliminary work to propose a simple sol-gel synthesis route for the preparation of visible-active titanium dioxide in order to combine with previously studied UV active titanium dioxide powders to create tandem systems that will harvest both visible and UV light for water and air purification. Along these lines, two different sets of samples were prepared and investigated.

The first set of samples was prepared by a sol-gel route with the addition of non-metallic compounds of Ti which are TiN, TiC and TiS_2. Non-metal atom to titanium mol ratio was kept at 0.1:1 and the syntesized powders were characterized by XRD, Raman Spectroscopy, BET, UV-VIS Diffuse Reflectance Spectroscopy in order to investigate the effect of calcination temperature, surface area and band gap on photocatalytic activity. Besides, these commercial TiN, TiC and TiS_2 powders that were used as dopants, were also annealed in open air to prepare partially oxidized titanium materials.

Secondly, inexpensive sources of non-metal compounds such as boric acid, diethanolamine (DEA), triethylamine (TEA), thiourea, urea and cyclohexanol were added in an alternative sol gel synthesis route. Dopant compound to titanium dioxide mol ratio was also kept at 0.5:1. Structural and electronic characterization of this family of materials were also carried out in addition to photocatalytic activity tests.

Photocatalytic activity measurements were done in liquid phase via the degradation of an organic contaminant, Rhodamine B, in a custom-designed VIS-illuminated photocatalytic reaction cells. Photocatalytic performance of all samples were compared with that of a commercially available Degussa P25 TiO_2 benchmark catalyst. Photocatalytic preformance tests revealed improved photocatalytic activity for non-metal compound added titanium dioxide compared to unmodified titanium dioxide prepared with the same method. Also, several samples presented even higher photocatalytic activity compared to Degussa P25. Characterization experiments showed hinderance in anatase to rutile transformation due to foreign atoms. It was also observed that although a small band gap is important for the photocatalytic activity, there are other critical parameters such as particle size, surface area, crystallinity, active facets, oxygen vacancies which have to be fine tuned for photocatalytic performance optimization.

Keywords: TiO_2, Heterogeneous Bulk Doping, Sol-Gel, Non-Metal Compounds, VIS light, Photocatalytic Oxidation

ÖZET

FOTOKATALİTİK YÜKSELTGEME SÜREÇLERİ İÇİN GÖRÜNÜR IŞIKLA AKTİFLEŞEN, AMETAL BİLEŞİKLERİ İLE KATKILANDIRILMIŞ TİTANYUM DİOKSİT MALZEMELERİ

PELİN ALTAY

Kimya Yüksek Lisans Tezi

Danışman: Y. Doç. Dr. Emrah Özensoy

Ağustos, 2014

Daha iyi bir insan hayatı için en önemli teknolojilerden biri çevre kirliliğinin engellenmesidir. Titanyum dioksit, güçlü oksidasyon yetkinliği, düşük maliyeti, zehirsiz olması, yüksek yapısal kararlılığı ve kolay erişilebilmesi gibi özelliklerinden dolayı hava ve su arıtma sistemlerinin göz bebeği haline gelmiştir. Ancak, geniş elektronik bant aralığına sahip olmasından dolayı, titanyum dioksit sadece güneş ışığının %3'ünü oluşturan UV ışığını soğurabilmektedir. Bu malzemenin güneş ışığını kullanabilmesi, çevre arıtımı için gereken işletim maliyetini oldukça düşürecektir. Bu yüzden, titanyum dioksiti güneş spektrumunun büyük bir parçasını kullanabilmesi için görünür ışık aktif malzemelere dönüştürmek önemli bir hedef haline gelmiştir.

Bu çalışmada, görünür ışık ile aktifleşen titanyum dioksit tozlarının hazırlanması amacıyla çeşitli ametal bileşiklerinin titanyum dioksit sol-jel sentez protokolüne eklenmesi incelenmiştir. Bu çalışma bir ön çalışma olup, hedeflerinden en önemlisi, daha önce çalışılan UV aktif titanyum dioksit tozları ile birleştirilerek; özel tasarım bir hava arıtım teknolojisi için, UV ve VIS aktif ikili (eşlenik) sistemlerde kullanılmasıdır. Bu sebeple, mevcut çalışmada iki temel fotokatalizör ailesi sentezlenerek, yapısal ve fotokatalitik performans özellikleri incelenmiştir.

İlk grup numuneler, titanyumun ametal bileşikleri olan TiC, TiN ve TiS_2'ün sol-jel yöntemine eklenmesi ile hazırlanmıştır. Katkı atomun titanyuma olan mol oranı 0.1:1 olarak belirlenmiş ve sentezlenen tozlar XRD, Raman spektroskopisi, BET ve UV-VIS DR spektroskopisi ile karakterize edilmiş ve kalsinasyon sıcaklığı, yüzey alanı ve elektronik bant aralığının fotokatalitik aktiviteye olan etkisi araştırılmıştır. Sol-jel yöntemine ek olarak, sol-jel yönteminde katkı olarak kullanılan TiC, TiN ve TiS_2 tozların, ayrıca havaya açık fırında tavlanmasıyla, kısmi olarak yükseltgenmiş fotokatalitik malzemeler de elde edilmiştir.

İkinci olarak, farklı bir sol-jel yöntemiyle, borik asit, dietanolamin, trietilamin, tiyoüre, üre ve siklohekzanol gibi ucuz ametal bileşikleri ile katkılandırılmış titanyum dioksit türleri sentezlenmiştir. Hesaplama kolaylığından ötürü eklenen katkı bileşiğinin titanyum dioksite olan mol oranı, 0.5:1 olarak belirlenmiştir. Aynı karakterizasyon metodları, aynı parametrelerin fotokatalitik aktiviteye olan etkisini incelemek amacıyla kullanılmıştır.

Fotokatalitik aktivite ölçümleri, tasarımı ve kurulumu mevcut çalışma çerevesinde gerçekleştirilen, görünür ışık aydınlatmalı, özel-tasarım fotokatalitik reaksiyon hücrelerinde, sıvı fazda organik bir kirletici olan Rhodamine B boyasının bozunması kullanılarak yapılmıştır. Bütün malzemelerin fotokatalitik performanslar, ticari Degussa P25 referans katalizör ile karşılaştırılmıştır. Fotokatalitik performans testleri, katkılandırılmış titanyum dioksit malzemelerinin, saf titanyum dioksit malzemesinden daha iyi görünür ışık aktivitesine sahip olduğunu göstermiştir. Ayrıca, bazı malzemelerin performansının Degussa P25'den bile daha iyi olduğu görülmüştür. Karakterizasyon yöntemleri anataz fazından rutil fazına geçişte katkı atomlarından dolayı bir gecikme olduğunu göstermiştir. Buna ek olarak, elektronik bant aralığı değerinin küçük olmasının, görünür ışık aktivitesi için önemli olsa da, bunun bir zorunluluk olmadığı; fotokatalitik aktiviteyi etkileyen başka bir çok önemli parametrenin (parçacık boyutu, yüzey alanı, kristalinite, aktif fasetler, oksijen boşlukları vb.) de varlığı saptanmıştır.

Anahtar Kelimeler: TiO_2, Heterojen Kütle Katkılandırması, Sol-Jel, Ametal Bileşikler, Görünür Işık, Fotokatalitik Oksidasyon

ACKNOWLEDGEMENT

Firstly I wish to thank my supervisor Asst. Prof. Emrah Özensoy. He was always ready to answer any question I had no matter how trivial, he replied to all my enquiries with great haste. He was a constant source of ideas, knowledge and encouragement and without him I could not have achieved as much.

I offer my sincere appreciation to Asst. Prof. Özgür Birer and Cansu Yıldırım for their help on the Diffuse Reflactance UV-VIS measurements.

I would like to offer my special thanks to Dr. Deniz Erdoğan for fruitful discussions on this research work. She has been a collegue and good friend over the past two years.

My completion of this project could not have been accomplished without our technician Ethem Anber, who helped constructing the photocatalytic batch reactor.

To my friends and companions in the lab; Zafer Say, Kerem Emre Ercan, Merve Tohumeken, Merve Demirkıran, Mustafa Karatok, Abdurrahman Türksoy, Evgeny Vovk, Syed A. A. Shah, Sean W. McWhorter, Aybegüm Samast, Sinem Apaydın. You were (almost) all with me from the start and you've made the whole experience far more enjoyable so thank you.

I also wish to acknowledge the financial support provided by the Scientific and Technical Research Council of Turkey (TUBITAK) (Project Code: 113Z543).

I am ever so grateful to my family, Sevgi, Ercan and Çisem, for being there whenever I am in need. Nobody knows better than I how they have encouraged me and supported me from my early youth up to now. Also, I owe sincere and earnest thankfulness to Paşabeyoğlu family who has been there for me over the years.

Finally, to Anıl Paşabeyoğlu: my deepest gratitude. Your encouragement when the times got rough are much appreciated and duly noted. It was a great comfort and relief to know that you support my decisions and inspire me to do more. My heartfelt thanks.

"I finished it."

To My Family

and Anil

"Ad astra per aspera"

TABLE OF CONTENTS

LIST OF FIGURES

LIST OF TABLES

1. INTRODUCTION

1.1 Historical Overview of TiO_2

TiO_2 has been used as a white pigment from ancient times, and thus its safety for both humans and the environment is guaranteed by history [1]. In 1938, Goodeve et al. reported that active oxygen species produced on the TiO_2 surface can bleach dyes under UV light irradiation [2]. In 1956, Kato and Mashio were the first ones that used the terminology "photocatalyst" for TiO_2 [3]. At the time of "oil crisis", Fujishima and Honda published an article in Nature [4] that drew attention of many people to TiO_2. They demonstrated the powerful semiconductor capabilities of TiO_2 in the splitting of water in a photoelectrochemical cell for hydrogen production from water. This revolutionary work ignited researchers to demonstrate titanium dioxide's unique properties in many areas. After Fujishima and Honda, in 1977 Frank and Bard showed CN^- reduction in water, followed by Ollis, who used TiO_2 for the mineralization of organic pollutants in 1983 [5]–[8]. However, TiO_2 gained its worldwide fame after 1990's at which Gratzel published a paper on dye sensitized solar cells [9]. Then the novel concept of light-cleaning materials coated with a TiO_2 film photocatalyst under UV light was investigated [10].The application areas of TiO_2 has been shown in Figure 1 [11].

In the last decade, many different TiO_2 materials have been prepared and main challenges such as broad absorption capability and reduced recombination probability have been identified [12]–[21]. Yet, main problem still remains as these materials utilize only UV light for photocatalysis. Several strategies have been performed to optimize photocatalytic materials for visible light absorption such as crystal growth and shape control, surface sensitization or modification, heterostructuring, and metal/non-metal doping [22]–[32]. Doping with non-metal anions or non-metal molecules can strongly enhance the absorption of a photocatalyst by influencing the electronic structure of TiO_2, however, many problematic issues exist as will be discussed in following chapters.

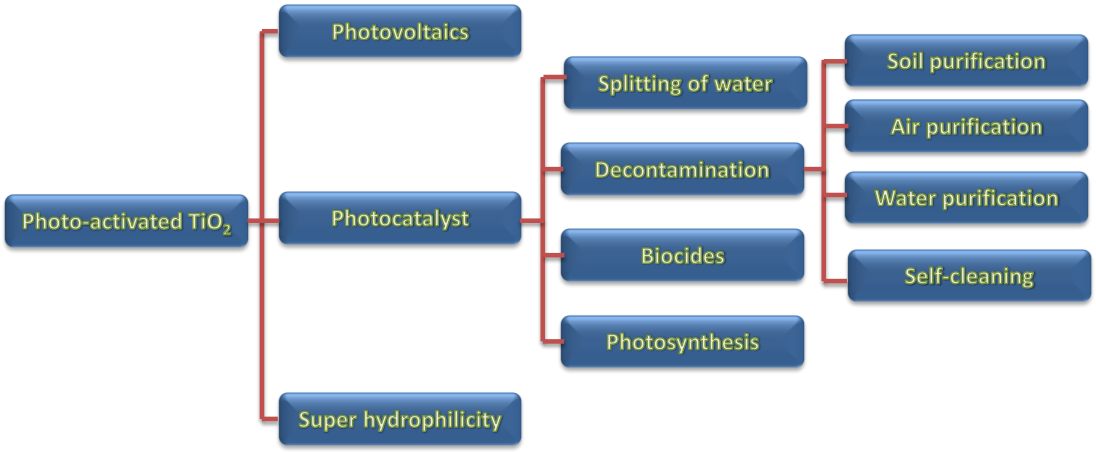

Figure 1. Various applications of photo-activated titania photocatalysis in environment and energy fields.

1.2 Physical Properties of TiO_2

Titanium was discovered in by Reverend William Gregor in England, in 1791 but it was Heinrich Klaporth, a German chemist, who coined the name after Titans in Greek Mythology when it was rediscovered in rutile ore several years later. The primary source and the most stable form of titanium dioxide is rutile ore. Its name is derived from the Latin *rutilus*, red, because of the deep color observed in some specimens when the transmitted light is viewed [33]. Rutile is one of three main polymorphs of titanium dioxide, the other polymorphs being; anatase and brookite [34], [35]. While brookite was named after an English mineralogist, H. J. Brooke, anatase was named from the Greek word "anatasis", meaning extension, due to its longer vertical axis compared to that of rutile.

In all three polymorphs, Ti^{4+} ions are coordinated to six O^{2-} atoms, resulting TiO_6 octahedra, and only the arrangement of octahedral changes giving different polymorphs [33]–[36]. Titanium dioxide is typically an n-type semiconductor due to oxygen deficiencies [37] that has a band gap of 3.2 eV for anatase [38]–[40], 3.0 eV for rutile [41]–[43], and ~3.2 eV for brookite [44]–[46]. Titanium dioxide (TiO_2) is the most widely investigated photocatalyst due to its strong oxidative properties, low cost, non-toxicity, chemical and thermal stability [47]–[49].

1.2.1 Anatase to Rutile Phase Transformation

Being a metastable phase, anatase is more commonly seen for particles synthesized at room temperature and rutile is mostly observed at higher temperatures [50]. Phase transformation temperature between these two phases is used for the estimation of the energy barrier for the corresponding structural transformation [51]. Phase transformation temperature is dependent on the particle size and the reason can be explained associated with the defect density which is relevant to particle size [52]. The anatase to rutile transformation is not instantaneous; it is time-dependent because two Ti-O bonds break in the anatase structure, allowing rearrangement of the Ti-O octahedra, forming a dense rutile phase [53]–[55]. It is often overlooked that all titania is contaminated with some levels of impurities. The presence of unintentional impurities or intentional dopants has a strong effect on the kinetics of the anatase to rutile transition [56]. Either intentional or unintentional, "dopant" atoms can have the effect of hindering or enhancing the transition to rutile. If the solubility limit for impurities or dopants is exceeded, then their precipitation can facilitate the phase transformation through heterogeneous nucleation [57], [58]. As a matter of fact, the phase transformation is also dependent on oxygen vacancies since they destabilize the lattice, promoting the transformation. In the case of nitrogen, a different mechanism operates. Nitrogen has a comparable size with oxygen, therefore O replacement with N does not create a vacany. As a result, nitrogen addition may have a limited lattice desatabilization effect, and may act as an inhibitor for phase transition. Controversely, it has been also reported that nitrogen doping increases the level of oxygen vacancies [59], [60] promoting the anatase to rutile transormation.

Carbon is a very strong reducing agent and, during calcination, it would be likely to enhance the transformation to rutile through the formation of oxygen vacancies [61]. Boron and sulfur on the other hand, are known as inhibitors for the anatase to rutile transformation [61]–[63].

1.3 Mechanistic Aspects of Photocatalysis on TiO_2

1.3.1 Electronic Processes

In photocatalysis, light impinging on a catalytic surface is used to drive chemical reactions [64], [65]. In other words, it can be considered as a photon-assisted generation of catalytically active species.

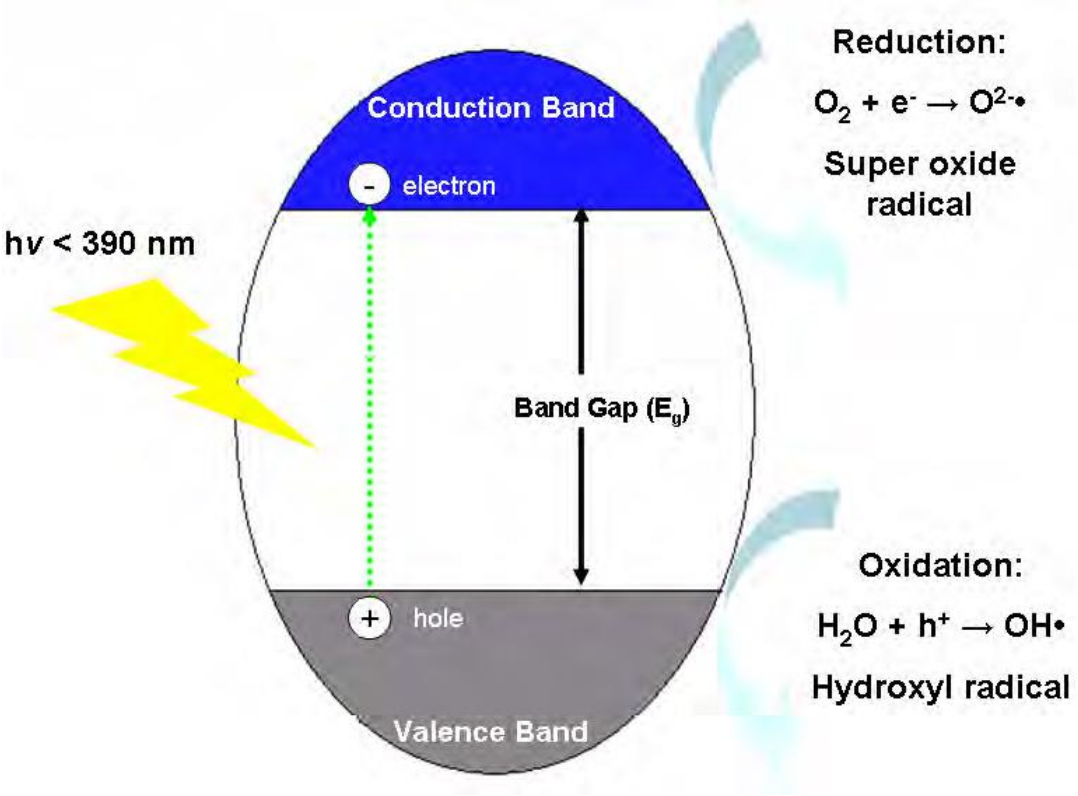

Figure 2. Schematic of photocatalytic mechanism. Reprinted from ref. 66 Copyright 2012 with permission from Elsevier [66].

In photocatalysis, light with an energy greater than the band gap of the semiconductor, excites an electron from the valence band to the conduction band (Figure 2). the band gap of anatase is 3.2 eV, therefore UV light (< 390 nm) is required to initiate the photocatalytic process. Light (< 390 nm) excites an electron (e^-_{CB}) to the conduction band generating a positive hole (h^+_{VB}) in the valence band. Charge carriers can be trapped as Ti^{3+} and O^- defect sites in the TiO_2 lattice, or they can recombine, dissipating energy [67].

Alternatively the charge carriers can migrate to the catalyst surface and initiate redox reactions on the adsorbates [68]. Positive holes generated by light become trapped by surface adsorbed H_2O. The H_2O gets oxidized by h^+_{VB} producing H^+ and OH• radicals, which are extremely powerful oxidants. The hydroxyl radicals subsequently oxidize organic species from the surrounding environment to CO_2 and H_2O and in most cases these are the most important radicals formed in TiO_2 photocatalysis [69].

Electrons in the conduction band can be rapidly trapped by molecular oxygen adsorbed on the particle. Trapped molecular oxygen will be reduced by excited electrons to form superoxide (O_2^-•) radicals that may further react with H^+, to generate peroxide radicals (•OOH) and H_2O_2 [70], [71]. Equations 1.1 – 1.8 given below summarize these chemical reactions.

$$e^-_{CB} + h^+_{VB} \rightarrow energy \quad (1.1)$$

$$H_2O + h^+_{VB} \rightarrow \bullet OH + H^+ \quad (1.2)$$

$$O_2 + e^-_{CB} \rightarrow O_2^- \bullet \quad (1.3)$$

$$\bullet OH + VOC \rightarrow H_2O + CO_2 \quad (1.4)$$

$$O_2^- \bullet + H^+ \rightarrow \bullet OOH \quad (1.5)$$

$$\bullet OOH + \bullet OOH \rightarrow H_2O_2 + O_2 \quad (1.6)$$

$$O_2^- \bullet + VOC \rightarrow CO_2 + H_2O \quad (1.7)$$

$$\bullet OOH + VOC \rightarrow CO_2 + H_2O \quad (1.8)$$

1.3.2 Electron-Hole Recombination

Recombination of electron-hole pairs on the photocatalyst surface is a major limitation in semiconductor photocatalysis [72]. The photocatalytic efficiency can be significantly enhanced if recombination is reduced. Doping with ions [73]–[75], heterojunction coupling [76]–[78] and nanosized crystals [79], [80] have all been

reported to promote separation of the electron-hole pair, reducing recombination and therefore improving the photocatalytic activity of the semiconductor material. Recombination competes strongly with the photocatalytic process. It may occur on the surface or in the bulk and is generally enhanced by impurities, defects, or other factors introducing bulk or surface imperfections [81].

1.3.3 Effect of Physical Properties

The photocatalytic efficiency of a TiO_2 photocatalyst depends not only on the electronic properties but also physical/structural properties of the materials. The availability of active sites on the material surface also plays a major role in the ability of the photocatalytic material to degrade organic contaminants [33]. Therefore, properties such as crystal size and structure, pore size/volume, density of surface OH groups, surface charge, number and nature of trap sites and absorption/desorption characteristics all contribute as important factors in the photocatalytic activity of TiO_2 [82]. Large surface area will result in an increase in the number of active sites available for photocatalytic degradation reactions. A delicate balance between surface area and recombination must be achieved in order to produce an effective photocatalyst. Smaller crystal size will result in a larger surface area but a spectral blue shift can be observed for crystal sizes below 10 nm. This is believed to be the result of the quantum size effect. The quantum size effect may produce a blueshift in the absorbance band edge as a consequence of exciton confinement with decreasing particle size [83]. Recombination is also promoted with larger surface areas. This is usually because a larger surface area leads to an increased number of crystal defects. The surface defects will act as recombination centres for the photoinduced electron/hole pair [33]. Surface hydroxyl groups which participate in the photocatalytic process in a number of ways, also affect the photocatalytic efficiency of the materials. They trap photoexcited electrons and produce OH• radicals and they can also act as active absorption sites for pollutants [33]. Calcination of TiO_2 at a high-temperature will also result in the removal of surface hydroxyl groups. Because rutile is produced from the high temperature calcination of anatase, rutile possesses fewer surface hydroxyl groups decreasing the photocatalytic activity.

1.4 Non-metal Doping of TiO_2 Photocatalysts

TiO_2 has been proved to be photocatalytically active under UV irradiation but it can only harvest a minor portion of the solar energy that actually reaches the Earth surface [84], [85]. Therefore, increasing the activity of titania for visible light through introduction of impurity atoms is a major research focus.

Over the last several years, it has been demonstrated that TiO_2 doped with non-metal elements such as carbon (C) [86]–[90], nitrogen (N) [30], [91]–[101], sulfur (S) [102]–[106], or boron (B) [62], [107]–[112] shows a positive response in the visible-light region and a higher photocatalytic activity. Although nature and effectiveness of doping titanium dioxide with these non-metal elements are still under debate, increasing number of studies in the field has been made in each year (Figure 3).

There are three major points to be considered regarding the influence of non-metal atom doping on the TiO_2 structure [113]:

(1) Band gap narrowing
(2) Impurity energy levels
(3) Oxygen vacancies

These effects will be discussed in the next sections in detail.

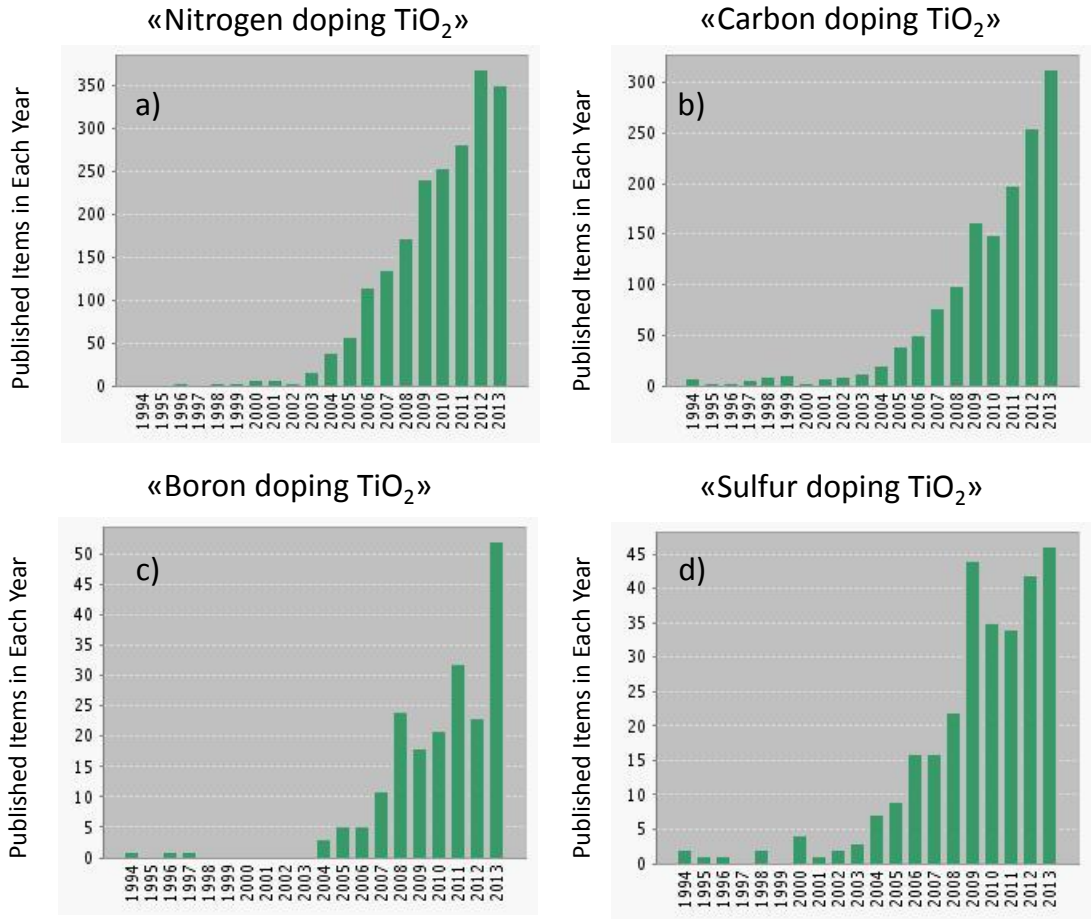

Figure 3. Rising interest in the photocatalysis field of non-metal doped titania materials. Source: ISI Web of Knowledge, 14/07/14. Search terms: (a) "Nitrogen Doping TiO_2" (b) "Carbon Doping TiO_2" (c) "Boron Doping TiO_2" (d) "Sulfur Doping TiO_2".

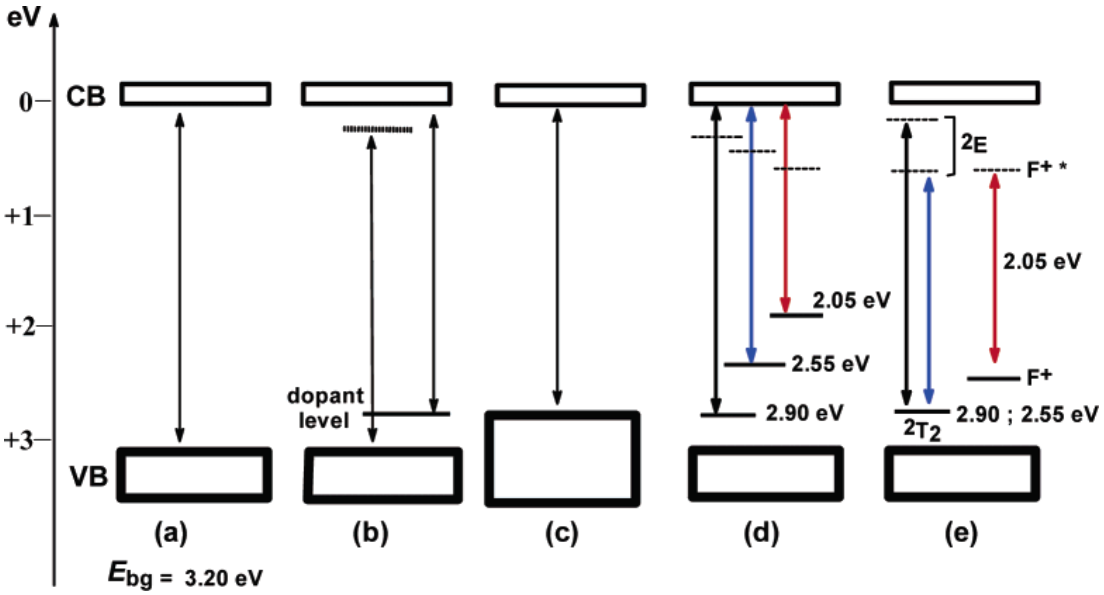

Figure 4. Various schemes illustrating the possible changes that might occur in the electronic structure of anatase TiO_2 upon doping with various nonmetals: (a) band gap of pristine TiO_2; (b) doped TiO_2 with localized dopant levels near the VB and the CB; (c) band gap narrowing resulting from broadening of the VB; (d) localized dopant levels and electronic transitions to the CB; and (e) electronic transitions from localized levels near the VB to their corresponding excited states for Ti^{3+} and F^{+} centers. Reprinted with permission from ref. 113. Copyright 2006 American Chemical Society. [114].

1.4.1 Nitrogen Doped TiO_2

Nitrogen doped titania is by far the most intensively studied system among the other non-metallic doped materials. N atoms can be easily introduced to titania lattice due to their comparable atomic size to oxygen, small ionization energy and high stability. Asahi et al. [30] found that mixing of 2p states of N with 2p states of O results in the formation of a new valence band with a shifted valence band edge towards higher energies, narrowing down the band gap of titania (Figure 4d). Shortly after this study, Ihara et al. [60] reported that visible light activity of nitrogen doped titania does not originate from nitrogen states but from oxygen defect sites in grain boundaries generated upon nitrogen doping. As it was calculated later, nitrogen

doping decreases the formation energy of oxygen vacancies from 4.2 to 0.6 eV [115]. Currently, there appears to be some agreement on the mechanism of nitrogen doped visible light absorption explained by Irie and Nakamura [100], [116]. They explained that TiO_2 oxygen lattice sites substituted by nitrogen atoms form an occupied midgap (N-2p) level above the (O-2p) valence band. Irradiation with UV light excites electrons in both the valence band and the narrow (N-2p) band, but irradiating with visible light only excites electrons in the narrow (N-2p) band. A broad spectral band seen around $410 < \lambda < 535$ nm (3.02-2.32 eV) has been attributed to a set of states centered at ~2.9 eV below the lower edge of the conduction band [99] that probably involves color centers (F) associated with oxygen vacancies created during the doping of TiO_2 (Figure 4e).

1.4.2 Carbon Doped TiO_2

The effective mechanism of how carbon dopant enhances the photoactivity remains not fully understood. The fact that so called "carbon doped titania" materials can be synthesized via very different routes has caused conflicting findings in the literature and raised controversy. The role of carbon has not been agreed on although it is widely accepted that carbon doping leads to a red-shift in the activation energy.

The state of carbon dopant in the titania lattice is found to be either in the form of a substitutional anion with -4 oxidation state [90], [117]–[120], or an interstital cation with +4 oxidation state [87], [121]–[124] or sometimes in the form of both [125]. Mechanism of photocatalytic enhancement is associated to different factors such as the existence of Ti-C, O-Ti-C, C-O or C-C bonds, and/or oxygen vacancy mid-gap states [124]. On the other hand, Serpone et al. argued that oxygen vacancies giving rise color centers that display visible light activity are the real reason; not the narrowing of the intrinsic band gap of titania [114].

Di Valentin et al. [126] suggested that when oxygen concentration is low, carbon substitutes oxygen, creating oxygen vacancies; whereas when oxygen concentration is high, interstital carbon and/or substitution of titanium is favored.

1.4.3 Boron Doped TiO_2

Boron doping was first reported by Zhao et al. in 2004 [127]. They prepared boron doped titania via sol-gel route using boric acid as dopant, and the results show a decreased band gap value of 2.93 eV and high photocatalytic activity. Finazzi et al. [128] reported that boron can be incorporated as substitutional boron replacing oxygen, giving rise to mid gap states or as interstitial boron. Boron as interstitial impurity behaves as three electron donor with formation of B^{3+}, although Finazzi et al. suggested that substitutional boron is less stable than interstitial boron.

In addition to improvement of photoactivity for boron doped titania systems, controversial effects were also reported. Chen et al. [62] observed a band gap increase upon B doping and they have attributed it to quantum size effects, while Zhao et al. [127] detected a red shift in the absorption spectrum. Notably, it has been reported that only oxygen substitution will lead to band gap narrowing, while the interstitial occupancies will produce blue shift.

Geng et al. [129] reported a boron doped anatase titania that is much more efficient and stable than pure titania. Also, Xu et al. [130] suggested that boron atoms could retard the grain growth, hinder anatase to rutile formation, therefore achieving higher surface area and photocatalytic activity compared to pure titania and Degussa P25. In fact, at high boron concentration, the boron atoms are expelled from titania structure during calcination and form diboron trioxide (sassolite) nanoclusters that retard the crystal growth, stabilizing the anatase form [62].

1.4.4 Sulfur Doped TiO_2

Successful incorporation of sulfur into the titania lattice is far more diffucult compared to other discussed non-metals because of its larger ionic radius. Sulfur doping was first performed by Umebayashi et al. [102], by oxidation of TiS_2 powder in air. By ab initio band calculations, it was reported that mixing of S 3p states with O 2p states in the valence band leads to band gap narrowing (Figure 4c). Ohno et al. [131] reported an easy synthesis method with thiourea and it has shown a significant shift to visible range and a high photocatalytic activity in the liquid phase.

1.4.5 "To dope or not to dope"

"To dope or not to dope."- This point was raised by Kamat et al. in 2011 [132], yet no conclusive answer has been found yet. There are many advantageous properties of doping, briefly discussed above for some non-metal dopants but also there are many disadvantages as well. Firstly, introduced dopants can act as recombination centers. Depending on the location of the dopant, diffusing charge carriers can recombine at dopant sites. Secondly, the discrete interstitial states or novel conduction band and/or valence band edges can reduce the reduction or oxidation potential of the modified semiconductor, resulting in decreased activity. Furthermore, homogeneous doping must be achieved to have a shift of the absorption edge.

One of the methods to reduce recombination rate is to produce a heterojunction. This is the case for Degussa P25 commercial photocatalyst, where a combination of anatase (80%) and rutile (20%) results in increased photocatalytic activity. Due to a lower conduction band potential than that of anatase, rutile phase acts as an electron sink for photogenerated electrons from the conduction band of the anatase phase. This intimate contact between these two phases was considered one of the reasons why P25 has high photocatalytic activity under UV and/or VIS irradiation [133].

1.5 Aim of the Current Study

In this work, a variety of non-metal atoms were added to the titanium dioxide sol-gel synthesis protocol for the purpose of preparing visible-active titanium dioxide powders. This study is a preliminary work to obtain a simple sol-gel synthesis route for the preparation of visible-active titanium dioxide which can be combined with previously studied UV-active titanium dioxide based catalytic systems that have been designed in our research group to create tandem systems that will harvest both visible and UV light for air purification.

2. EXPERIMENTAL

2.1 Sample preparation

1.5.1 Preparation of TiN, TiC and TiS_2 Doped Titania

For the synthesis of sol-gel TiO_2 doped with the non-metal compounds of titanium (TiN, TiC, TiS_2), the following protocol was followed. 14.8 ml of titanium(IV) isopropoxide (97 %, Sigma Aldrich) was mixed with 30 ml propan-2-ol (99.5 +%, Sigma Aldrich) for 30 min. TiN (<3 μm, Sigma Aldrich), TiC (<4 μm, ≥99% (Ti), Sigma Aldrich) and TiS_2 (-200 mesh, 99.9%, Sigma Aldrich) were added and mixed for another 30 min to prepare N doped, C doped and S doped TiO_2, respectively. The mol ratio of the dopant non-metal to titanium metal was kept at 0.1:1. The precipitation of the corresponding hydroxide was accomplished after the gradual addition of 45 ml water to the solution. The resulting gray slurry was aged under ambient conditions for 2-3 days and then further dried at 110^{o}C for 3h. The dried sample was ground to fine powder with a glass mortar. For further analysis of the obtained TiO_2, various annealing steps ranging from 500 to 800^{o}C (1 h in air for each temperature) were performed. To compare the effect of the doping, pure TiO_2 was also prepared following the same procedure above, except the addition of non-metal compounds. The compositions and calcination temperatures of these materials are listed in Table 1 [134].

Table 1. Compositions and calcination temperatures of the synthesized pure and TiN, TiC and TiS_2 doped samples.

Calcination Temperature	Dopant: TiN Sample Name	Dopant: TiC Sample Name	Dopant: TiS_2 Sample Name	TiO_2 Sample Name
500 °C	N/TiO_2-500	C/TiO_2-500	S/TiO_2-500	TiO_2-500
600 °C	N/TiO_2-600	C/TiO_2-600	S/TiO_2-600	TiO_2-600
700 °C	N/TiO_2-700	C/TiO_2-700	S/TiO_2-700	TiO_2-700
800 °C	N/TiO_2-800	C/TiO_2-800	S/TiO_2-800	TiO_2-800

1.5.2 Partial Oxidation of TiN, TiC and TiS_2 by Annealing

To prepare partially oxidized TiN, TiC and TiS_2, 3.0 g of the powders was calcined in the furnace which was open to the atmosphere for 1 hour. The temperature was ramped up and cooled down at a rate of 10 ^oC /min during the heating and cooling processes. The compositions and calcination temperatures of these materials are listed in Table 2.

Table 2. Calcination temperatures of the partially oxidized TiN, TiC and TiS_2 samples.

Calcination Temperature	TiN Sample Name	TiC Sample Name	TiS_2 Sample Name
500 ^oC	TiN-500	TiC-500	TiS_2-500
600 ^oC	TiN-600	TiC-600	TiS_2-600
700 ^oC	TiN-700	TiC-700	TiS_2-700
800 ^oC	TiN-800	TiC-800	TiS_2-800

1.5.3 Preparation of Non-Metal Compound Doped Titania

For the synthesis of the non-metal doped sol-gel TiO_2, the following protocol was followed. 14.8 ml of titanium(IV) isopropoxide (97 %, Sigma Aldrich) was mixed with 50 ml propan-2-ol (99.5 +%, Sigma Aldrich) and 1.6 ml acetylacetone (99.3 %, Fluka) for 30 min. This clear yellow solution was vigorously stirred at room temperature. Non-metal compounds were added in the solution for another 30 min of stirring. The mol ratio of non-metal compound to TiO_2 was kept at 0.5:1. Here, six different non-metal compounds were chosen for this purpose. These compounds were;

- Thiourea (Th) (ACS reagent, ≥99.0%, Sigma Aldrich)
- Urea (U) (ACS reagent, reag. Ph. Eur., ≥99.5%, Sigma Aldrich)
- Boric Acid (B) (ACS reagent, ≥99.5%, Sigma Aldrich)
- Diethanolamine (DEA) (ACS reagent, ≥99.0% (GC), Sigma Aldrich)

- Triethylamine (TEA) (≥99%, Sigma Aldrich)
- Cyclohexanol (Cyc) (ReagentPlus®, 99%, Sigma Aldrich)

The precipitation of the corresponding hydroxide was accomplished after the gradual addition of 6 ml of 0.5 M HNO_3 to the solution, which consecutively led to the formation of gel. The resulting yellow slurry was aged under ambient conditions for 3 days and then further dried at 60°C for 48h. The dried sample was ground to fine powder with a glass mortar. For further analysis of the obtained TiO_2, various annealing steps ranging from 150 to 700°C (2 h in air for each temperature) were performed. To compare the effect of the doping, pure TiO_2 (denoted as $PTiO_2$) was also prepared following the same procedure above, except the addition of non-metal compounds. The compositions and calcination temperatures of these materials are listed in Table 3.

Table 3. Calcination temperatures of the synthesized pure and thiourea, boric acid, cyclohexanol, urea, diethanolamine, triethylamine doped samples.

Calcination Temperature	**TiO_2 Sample Name**						
150 °C	Thio-150	B-150	Cyc-150	U-150	DEA-150	TEA-150	$PTiO_2$-150
350 °C	Thio-350	B-350	Cyc -350	U-350	DEA -350	TEA -350	$PTiO_2$-350
500 °C	Thio-500	B-500	Cyc -500	U-500	DEA -500	TEA -500	$PTiO_2$-500
600 °C	Thio-600	B-600	Cyc -600	U-600	DEA -600	TEA -600	$PTiO_2$-600
700 °C	Thio-700	B-700	Cyc -700	U-700	DEA -700	TEA -700	$PTiO_2$-700

2.2 Experimental set-up

1.5.4 Photocatalytic Batch Reactor Set-Up for Liquid Phase

Figure 5. Photocatalytic Batch Reactor system designed for liquid phase degradation experiments.

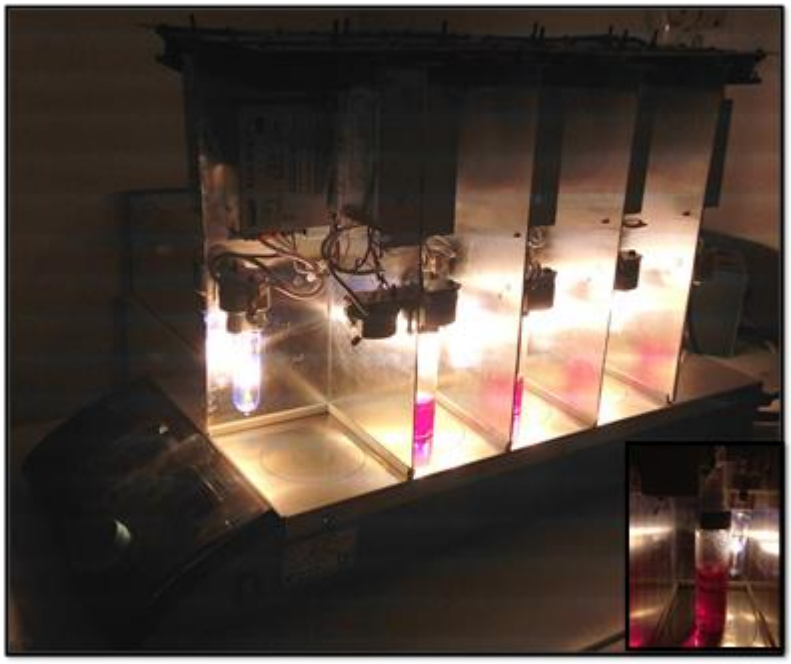

Figure 6. Representative picture of a liquid phase degradation experiment, inset: cell view.

The custom-designed batch photocatalytic reactor system is assembled with the aim of measuring the photocatalytic degradation Rhodamine B dye (≥95% (HPLC), Sigma Aldrich) performances of candidate photocatalysts under visible light exposure. The suspension was continuously stirred with Jeio Tech multiple position magnetic stirrer (MS-52M) at 500 rpm. As the visible light source, Osram 35W high intensity discharge lamp (metal halide lamp with ceramic burner, HCI-TC 35W/942 NDL PB) with UV-filter technology was chosen because of the similarity of its spectrum to the solar irradiation. Although having UV-filter, the lamp had 13 W/m^2 irradiance readout by UVA probe (LP471 UVA, DeltaOhm) in 315-400 nm range, therefore a commercial transparent UV protective film (LLumar window film UV CL SR PS (clear)) that is 99,9% blocking UV was covered around the vial to remove undesired wavelengths. After that, the lamp had 0,013 W/m^2 irradiance in 315-400nm. The visible photon flux of the lamps was measured as 2000 $\mu mol/m^2s$ with a LP471 PAR visible probe (400nm-700nm). On the top, 4x4 cm fans were placed to prevent heating by continuous flow of air. In addition to fans, vials had lids to prevent evaporation and change in concentration.

1.5.5 VIS Lamp

The photoreactors were illuminated with 35W high intensity discharge lamp which is metal halide lamp with ceramic burner including UV-filter technology (Osram, HCI-TC 35W/942 NDL PB). Correlated color temperature was 4200K. In Figure 7, emission spectra of the lamp with and without UV blocking film taken with USB2000+ Miniature Fiber Optic Spectrometer are given.

The photon power density of the VIS-lamp is measured by a photo-radiometer (HD2302.0, DeltaOhm/Italy) with a UVA probe in W/m^2 (LP471 UVA, DeltaOhm) and VIS probe in $\mu mol/m^2s$ (LP471 PAR, DeltaOhm).

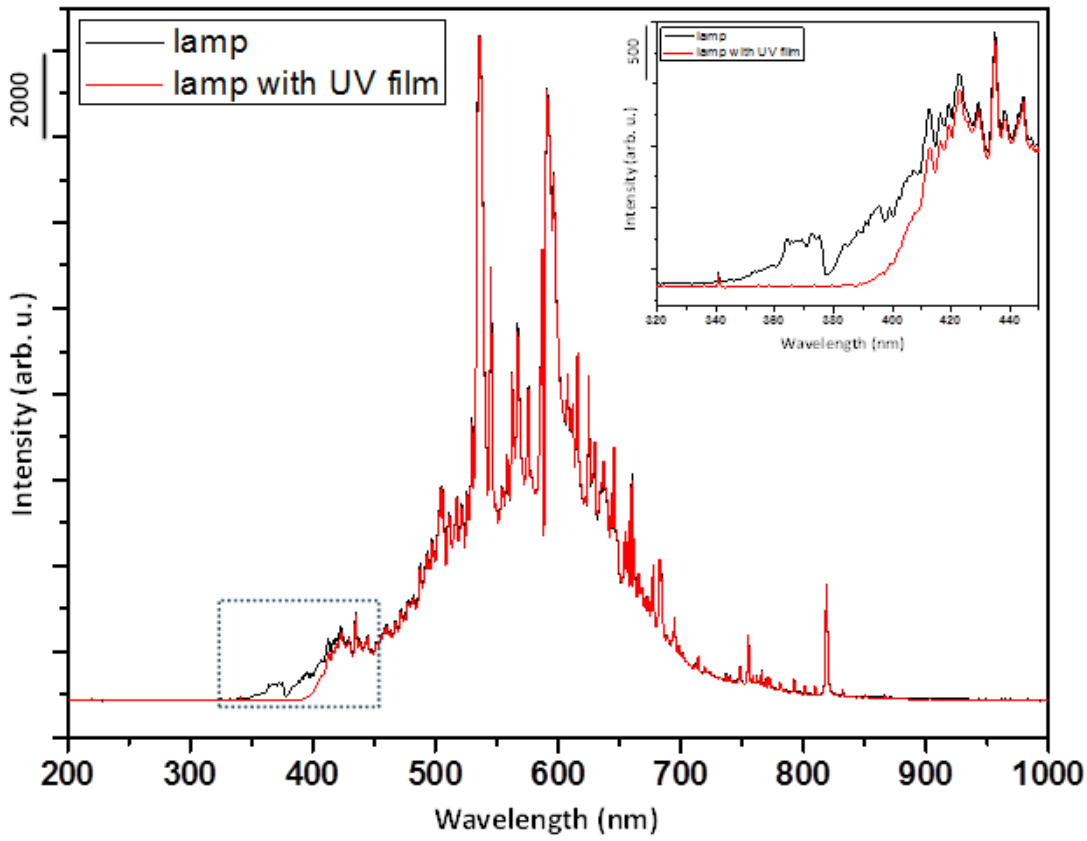

Figure 7. Emission spectra of the light source with and without UV blocking film (Courtesy of Coşkun Kocabaş, Bilkent University, Physics Department)

2.3 Experimental Protocols

2.3.1 Photocatalytic Degradation of Rhodamine B Dye Under Visible Illumination

Photocatalytic studies were carried out on selected powders. The photocatalytic activity of the materials was investigated by degrading an organic pollutant. Rhodamine B is one of the widely used organic pollutants for degradation studies. The standard protocol in our laboratory is as follows; in a typical experiment, sample (50 mg) was added to 30 mL of deionized water and this suspension was sonicated for 20 min. After sonication, 10 mL of 40 mg/L Rh B dye stock solution was added to have a dye concentration of 10 mg/L (20.876 μM). 3 mL aliquot was

then removed to provide initial concentration value. The suspension was allowed to stir in the dark for 60 min to obtain adsorption-desorption equilibrium, eliminating any error caused by initial adsorption. The suspension (under continuous stirring, 500 rpm) was then irradiated by 35 W metal halide lamp (2000 μmol/m^2s in 400-700nm range). Aliquots (3 mL) were removed at timed intervals, centrifuged at 6000 rpm for 30 min, and the visible absorption spectra were recorded using a Cary 300 UV–Vis spectrometer. The absorption of Rh B was measured at 553 nm and the concentration was calculated by using calibration curves. Blank experiments with the VIS-lamp and without catalysts under the same conditions were also performed to measure the photolysis of the dye.

Although the designed system for photocatalytic activity tests has 10 different reaction cells, only 4 of them, namely B1, B2, C2 and D2 are decided to be used due to their comparable reaction conditions.

In the case of the photocatalytic oxidation of an unimolecular reactant on TiO_2, the rate of degradation, r, could be expressed by unimolecular type Langmuir–Hinshelwood (L–H) model [135]:

$$r = -\frac{dC}{dt} = \frac{kKC}{1+KC} \qquad 2.1$$

where k is the reaction rate constant, C is the dye concentration (Rhodamine B), K is the adsorption equilibrium constant. When the dye concentration is very small, this equation becomes:

$$r = -\frac{dC}{dt} = kKC = k_{app}C \qquad 2.2$$

where $kK = k_{app}$ and therefore the rate of degradation obeys (pseudo) first order kinetics for most of the samples. Hence the rate constant for degradation, *k*, was obtained from the first-order plot of kinetic analysis according to equation 2.3:

$$ln\frac{C}{C_0} = kt \qquad 2.3$$

where, C_0 is the initial concentration, C is the concentration after a time (t) of the Rh B dye degradation, and *k* is the pseudo first order rate constant (min^{-1}). The rate constant, *k* can be derived from a plot of $ln(C/C_0)$ versus time.

2.3.2 XRD & BET

X-ray diffraction is a non-destructive technique that reveals the crystal structure of the material under analysis. XRD was used to determine the crystalline phase of all synthesized materials. Fine powdered samples were spread onto a glass holder and X-ray diffractograms were collected using a Rigaku diffractometer, equipped with a Miniflex goniometer and an X-ray source with Cu$K\alpha$ radiation, at λ = 1.54 Å, 30 kV and 15 mA with a diffraction angle range 2θ = 10–80° with a scan rate of $1.4^{o}min^{-1}$. The mass fraction of rutile (X_R) and anatase (X_A) was determined by the Spurr equation [136]

$$\text{Anatase (\%)} = [I_A / (I_A + 1.26\, I_R)] \times 100$$

$$\text{Rutile (\%)} = [1.26\, I_R / (I_A + 1.26\, I_R)] \times 100$$

where I_A is the intensity of the (101) peak and I_R is the intensity of the (110) peak.

Surface area measurements of the samples (which were initially dehydrated at 573 K for 2 hr in vacuum) were determined by N_2 adsorption at 77 K via conventional BET (Brunauer, Emmett, and Teller) method by using a BET surface area analyzer (Micromeritics TriStar Surface Area and Porosity Analyzer).

2.3.3 Raman Spectroscopy

Raman spectra were recorded on a HORIBA Jobin Yvon LabRam HR 800 instrument, equipped with a confocal Raman BX41 microscope, spectrograph with an 800 mm focal length and a nitrogen cooled CCD detector. The Raman spectrometer was equipped with a Nd:YAG laser (λ = 532.1 nm). During the Raman experiments, the laser power was tuned to 20 mW, measured at the sample position, in order to minimize the sample heating effects. The incident light source was dispersed by holographic grating with a 600 grooves/mm and focused onto the sample by using a 50X objective. The confocal hole and the slit entrance were set at 1100 μm and 200 μm, respectively. The spectrometer was regularly calibrated by adjusting the zero-order position of the grating and comparing the measured Si Raman band frequency with the typical reference value of 520.7 cm^{-1}. The powder samples were mechanically dispersed onto a single-crystal Si holder for the Raman measurements and all Raman spectra were acquired within 100-4000 cm^{-1} with an acquisition time of 100 s and a spectral resolution of 4 cm^{-1}.

1.5.6 UV-VIS Absorption Spectroscopy

A Cary 300 UV–Vis spectrometer was used to record absorption spectra of the organic dye Rhodamine B for photo-degradation studies. Spectra were recorded in the region 400 – 700 nm with a scan rate of 600 nm/min. The absorption at maximum wavelength (λ_{max}) Rh B (553 nm) was used to calculate degradation rates as a function of irradiation time.

1.5.7 UV-VIS DR (Diffuse Reflectance) Spectroscopy

Diffuse reflectance spectra were recorded using Shimadzu UV-3600 UV-VIS-NIR spectrophotometer equipped with ISR-3100 UV-VIS-NIR integrating sphere attachment. Barium sulfate (Wako Pure Chemical Indutries, Ltd.) was used as the reference material. The range of 220-1000 nm was scanned with 0.2 nm sampling interval, 20 nm slit width and medium scan speed. For the diffuse reflectance measurements, samples were powdered in an agate mortar and pressed into 2 mm deep custom made powder sample holders by using a glass rod. The acquired diffuse reflectance spectra were converted to Kubelka-Munk function data using the UVProbe 2.33 software. The Kubelka-Munk function, F(R), allows the optical absorbance of a sample to be approximated from its reflectance [137]:

$$F(R) = \frac{(1-R)^2}{2R}$$

The calculation of direct and indirect band gaps was done according to Tauc expression [138]:

$$(h\nu\alpha)^n = A(h\nu - E_g)$$

where h: Planck's constant, ν: frequency of vibration, α: absorption coefficient, E_g: band gap, A: proportional constant, n=1/2 for indirect allowed transition n=2 for direct allowed transition. For a semiconductor sample this allows the construction of a Tauc Plot. When the reflectance spectra are transformed into Kubelka-Munk functions, absorption coefficient becomes proportional to Kubelka-Munk function

F(R). Extrapolation of the linear portion of the plot $[F(R)h\nu]^n$ vs $h\nu$ gives band gap energy for indirect or direct transitions.

3. RESULTS AND DISCUSSION

3.1 Structural Characterization of the Samples

The crytalline structures of the materials have been examined with XRD, Raman and UV-VIS Diffuse Reflectance spectroscopy techniques while specific surface areas of chosen samples have been determined with BET method. The anatase to rutile transition characteristics of doped samples have been compared with that of undoped (pure) TiO_2 prepared by the corresponding synthesis protocol.

3.1.1 TiN, TiC and TiS_2 Doped Titania

3.1.1.1 XRD Experiments

Figure 8a illustrates the thermal behavior of pure TiO_2 synthesized and calcined in air between 500-800^{o}C for 1 h. It is shown that crystalline titania begins to form at 500^{o}C with anatase diffraction pattern (JCPDS 21-1272). However, when the sample is calcined at 600^{o}C, minor diffraction lines coming from the (110) and (101) planes of the rutile phase (JCPDS 04-0551) can be seen at 27,44^o and 36,08^o 2θ respectively. At 700^{o}C, the rutile lines in the XRD pattern become much more apparent. Finally, when the TiO_2 is heated up to 800^{o}C, the crystal structure becomes fully rutile (with some extent of anatase diffraction).

Figure 8b illustrates the thermal behavior of TiN doped TiO_2 (denoted as N/TiO_2) synthesized and calcined in air between 500-800^{o}C for 1 h. It is shown that anatase titania begins to form at 500^{o}C with some unreacted cubic TiN present in the diffraction pattern (JCPDS 21-1272, JCPDS 87-0633). However, when the sample is calcined at 600^{o}C, cubic TiN major peaks at 36,74 ^{o} and 42,66 ^{o} start to disappear and minor diffraction lines coming from the (110) and (101) planes of the rutile phase (JCPDS 04-0551) starts to form at 27,46^o and 36,12^o 2θ respectively. At 700^{o}C, the rutile lines in the XRD pattern become much more apparent. Finally, when the TiO_2

is heated up to 800°C, the crystal structure becomes fully rutile (with some extent of anatase diffraction).

Figure 8c illustrates the thermal behavior of TiC doped TiO_2 (denoted as C/TiO_2) synthesized and calcined in air between 500-800°C for 1 h. It is shown that anatase titania begins to form at 500°C with some unreacted cubic TiC present in the diffraction pattern (JCPDS 21-1272, JCPDS 65-8417). However, when the sample is calcined at 600°C, cubic TiC major peaks at 35,92 °, 41,72 ° and 60,46 ° start to disappear and minor diffraction line coming from the (110) planes of the rutile phase (JCPDS 04-0551) starts to form at 27,44°. At 700°C, the rutile lines in the XRD pattern become much more apparent. Finally, when the TiO_2 is heated up to 800°C, the crystal structure becomes fully rutile.

Figure 8d illustrates the thermal behavior of TiS_2 doped TiO_2 (denoted as S/TiO_2) synthesized and calcined in air between 500-800°C for 1 h. It is shown that anatase titania begins to form at 500°C with no unreacted hcp TiS_2 seen in the diffraction pattern (JCPDS 21-1272, JCPDS 15-0853). Sample preserves its anatase phase at even high calcination temperatures up to 800 °C. At 800°C, the rutile lines in the XRD pattern become dominant but still sample has a higher anatase mass fraction compared to other doped and pure materials calcined at 800 °C. Table 4 summarizes all the calculated mass fraction of anatase and rutile phases for these samples.

By comparing the characteristics of these three particular families of doped titanium dioxides and of pure titania, it can be suggested that nucleation of TiO_2 crystals is hindered due to impurities. It can also be argued that phase transformation from anatase to rutile shifts to a higher calcination temperature. Sanz et al. reported that the formation of Ti-O-Ti bonds between amorphous and anatase phase destabilizes anatase crystals and as a result, anatase phase transforms into rutile phase [139]. Periyat et al. has investigated the anatase to rutile phase transformation of sulfur doped samples prepared by a sol-gel method and observed that samples preserved their anatase forms even at high calcination temperatures, similar to our case [140]. In addition, it has been observed that while nitrogen incorporation has almost no effect on anatase to rutile transformation, carbon and especially sulfur inhibits this transformation. Also, by looking at (101) plane diffraction line seen at $2\theta = 25.3^o$, it can be said that peak is broadened, implying the presence of smaller crystallite size for carbon and sulfur doped samples calcined at 500 °C.

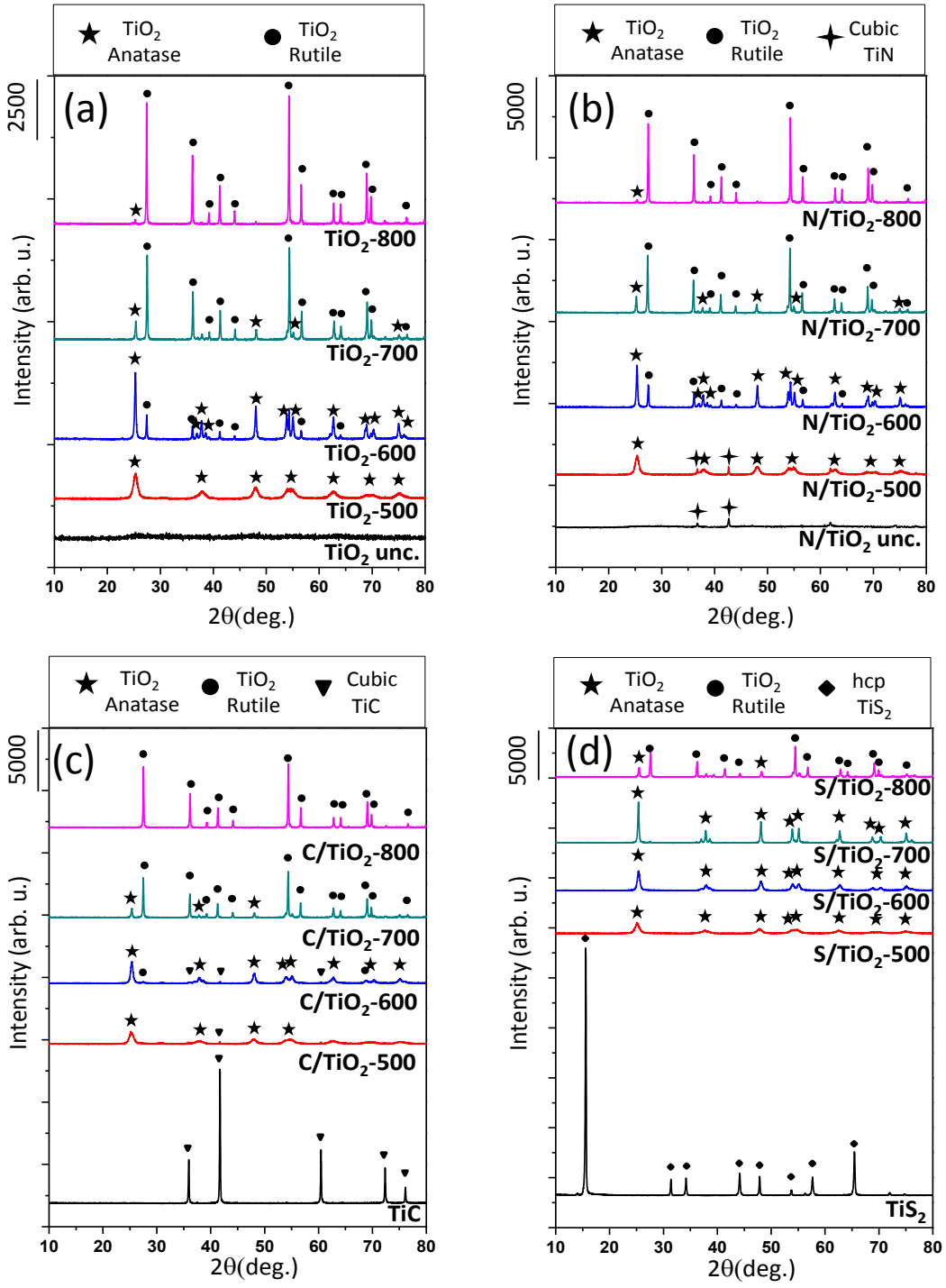

Figure 8. XRD patterns of (a) pure TiO_2 (b) TiN doped TiO_2 (N/TiO_2) (c) TiC doped TiO_2 (C/TiO_2) (d) TiS_2 doped TiO_2 (S/TiO_2) before (as is powders for dopants) and after calcination in air between 500 to 800 ^oC.

Table 4. Calculated mass fraction percentages of anatase (A%) and rutile (R%) phases for pure, N/TiO_2, C/TiO_2 and S/TiO_2

Sample	TiO_2		N/TiO_2		C/TiO_2		S/TiO_2	
T/ ^oC	A %	R %	A %	R %	A %	R %	A %	R %
500	100	-	100	-	100	-	100	-
600	68,22	31,78	59,69	40,31	90,48	9,52	100	-
700	15,03	84,97	18,69	81,31	15,39	84,61	100	-
800	3,62	96,38	3,15	96,85	-	100	23,05	76,95

3.1.1.1 Raman Analysis

Raman spectrum of anatase phase shows six Raman peaks ($1A_{1g}$, $2B_{1g}$, and $3E_g$) at 144 (E_g), 197 (E_g), 399 (B_{1g}), 516 (A_{1g} + B_{1g}), 639 (E_g) and 796 cm^{-1} (E_g) [141]. On the other hand, the rutile phase can be characterized by a Raman spectrum with four Raman active modes (A_{1g} + B_{1g} + B_{2g} + E_g) at 143 (B_{1g}), 447 (E_g), 612 (A_{1g}), 826 cm^{-1} (B_{2g}) and also a two-phonon scattering band at 236 cm^{-1} [142].

Figure 9 represents the Raman data for the thermally treated pure TiO_2 and doped TiO_2. In Figure 9a, the evolution of TiO_2 crystalline phases in pure titania can be observed upon calcination between 500-800^oC for 1h. Here, the Raman spectra are in accordance with the XRD data, showing fully crystalline anatase signals even at 500^oC. At 600^oC, in addition to anatase phase, a weak Raman signal for rutile phase is observed at 447 cm^{-1}. Around 700^oC, rutile formation is clearly observed with the Raman signals at 447 and 612 cm^{-1} and at 800^oC, the crystalline phase becomes almost completely rutile with a minor contribution from anatase.

In panels (b), (c) and (d) of Figure 9, the thermal transformations of N/TiO_2, C/TiO_2 and S/TiO_2 are illustrated. In general, current Raman spectra of the materials are consistent with the XRD data. However, the Raman measurements are more

sensitive in monitoring the surface crystallization fraction compared to XRD data. For instance, in pure TiO_2 and N/TiO_2 at 800°C, the Raman spectrum shows a significant proof of anatase phase while in XRD, the mass fraction of the anatase phases is calculated to be around 3,5%.

3.1.1.1 BET Analysis

BET surface areas of the thermally treated pure titania and N/TiO_2, C/TiO_2, S/TiO_2 were analyzed and the results are given in Table 5. TiC and TiS_2 addition increased the specific surface area compared to unmodified titania while TiN addition had a smaller SSA. Secondly, with increasing calcination temperatures, the S_{BET} values decrease monotonically, showing that the samples are strongly affected by the thermal treatment. The reduction of the surface areas can be explained as a result of sintering and/or phase transformations. All samples starts displaying anatase diffraction lines in XRD at around 500°C. However, by looking at the broadening of the peaks, it can be said that particles sizes of C/TiO_2 and S/TiO_2 are smaller than pure titania. High surface area is lost for S/TiO_2 at 600°C, whereas C/TiO_2 still has a relatively high specific surface area at 600°C. Note that the specific surface area of Degussa P25 at room temperature is around 55 m^2/g [143].

Table 5. BET Specific surface areas (in m^2/g) of the pure, N/TiO_2, C/TiO_2 and S/TiO_2 samples calcined within 500-800°C.

Sample T/ °C	**TiO_2**	**N/TiO_2**	**C/TiO_2**	**S/TiO_2**
500	96.79	71.49	109.46	115.32
600	17.44	14.88	55.92	2.53
700	9.97	9.43	6.87	-
800	-	6.82	-	-

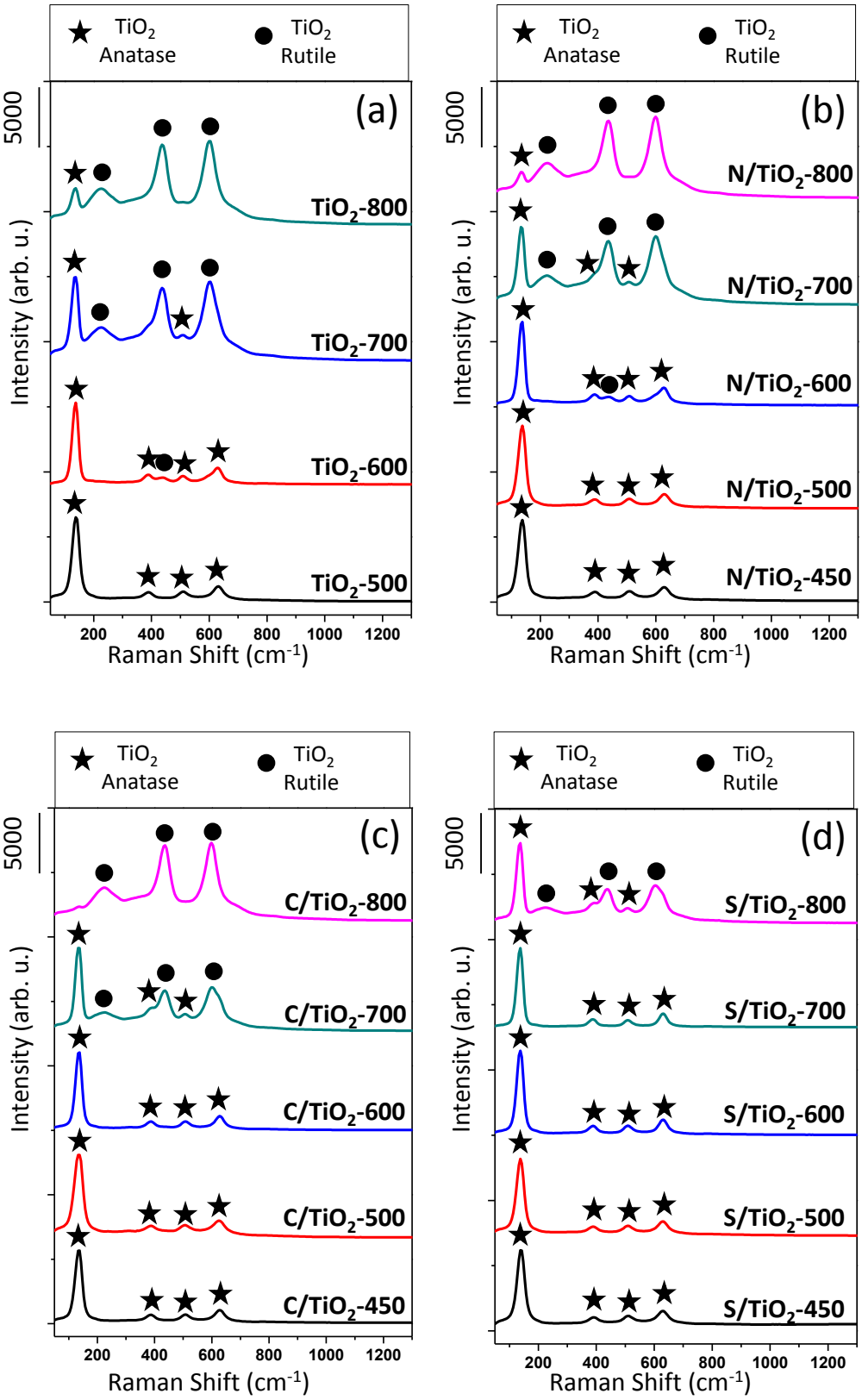

Figure 9. Raman spectra of (a) pure TiO_2 (b) TiN doped TiO_2 (N/TiO_2) (c) TiC doped TiO_2 (C/TiO_2) (d) TiS_2 doped TiO_2 (S/TiO_2) after calcination in air between 450 to 800 ^oC.

3.1.1.1 UV-VIS Diffuse Reflectance Experiments

In order to estimate the electronic band gap energies, UV-VIS Diffuse Reflectance Spectroscopy was employed. Figure 10 shows Kubelka-Munk transformed spectra of pure and doped TiO_2. In Figure 10 (a) and (b), it can be seen that unmodified TiO_2 and N doped TiO_2 samples have increasing visible light absorption with increasing calcination temperature. However in panel (c), C doped samples calcined at 500 ^oC and 600 ^oC show no change in absorption spectra. Only at 700^oC and 800^oC, the samples show a considerable shift to the visible region due to rutile phase formation. In panel (d), S doped TiO_2 samples can be seen. While there is not much change with increasing calcination temperature, a major shift to the visible region has been observed for samples calcined at 800 ^oC but this shift is not related with the rutile formation.

The calculations of direct and indirect band gaps of the samples were done by constructing Tauc plots. Figure 11 shows the Tauc plots of pure, N, C and S doped TiO_2 upon calcination between 500-800^oC for 1h for direct band gap calculations. In Figure 11a, extrapolation of the linear portion of the plot gives direct band gaps values of 3.61, 3.49, 3.3 and 3.23 eV for the TiO_2-500, TiO_2-600, TiO_2-700 and TiO_2-800 respectively. In Figure 11b, direct band gap values of N doped TiO_2 samples are found to be 3.6, 3.51, 3.28 and 3.2 eV, decreasing with increasing calcination temperatures. In Figure 11c, direct band gap values of C doped TiO_2 samples are found to be 3.65, 3.62, 3.28 and 3.17 eV, decreasing with increasing calcination temperatures. In Figure 11d, direct band gap values of S doped TiO_2 samples are found to be 3.62, 3.57, 3.5 and 3.29 eV, decreasing with increasing calcination temperatures. It is not uncommon to observe such high direct band gap values for sol gel synthesized TiO_2. Valencia et al. [144] shows that sol gel synthesized TiO_2 has unexpectedly high calculated direct band gap values.

Figure 12 shows the Tauc plots of pure, N, C and S doped TiO_2 upon calcination between 500-800^oC for 1h for indirect band gap calculations. In Figure 12a, extrapolation of the linear portion of the plot gives indirect band gaps values of 3.28, 3.19, 3.02 and 3.02 eV for the TiO_2-500, TiO_2-600, TiO_2-700 and TiO_2-800 respectively. In Figure 12b, indirect band gap values of N doped TiO_2 samples are

found to be 3.30, 3.13, 3.02 and 3.02 eV, for the N-500, N-600, N-700 and N-800 respectively. In Figure 12c, direct band gap values of C doped TiO_2 samples are found to be 3.30, 3.25, 3.02 and 3.02 eV, for the C-500, C-600, C-700 and C-800 respectively. In Figure 11d, direct band gap values of S doped TiO_2 samples are found to be 3.30, 3.27, 3.26 and 3.02 eV, decreasing with increasing calcination temperatures. TiO_2 is widely considered as indirect band gap material [75], [145], [146].

Figure 13 summarizes the direct and indirect band gap values for samples discussed above.

3.1.1 Partial Oxidation of TiN, TiC and TiS_2 by Annealing

3.1.1.1 XRD Experiments

Figure 14a illustrates the thermal behavior of TiN powder calcined in air between 500-800^oC for 1 h. It is shown that crystalline titania begins to form at 500^oC with rutile diffraction pattern (JCPDS 04-0551), in addition to a small fraction of anatase (JCPDS 21-1272) and a large amount of unreacted TiN (JCPDS 87-0633). When the sample is calcined at 600^oC, almost all TiN is oxidized to rutile TiO_2. At 700^oC, the rutile lines in the XRD pattern become much more apparent. Finally, when the TiO_2 is heated up to 800^oC, the crystal structure becomes fully rutile. Iwase et al. observed a similar path for the annealing of TiN powder except the fully rutile structure was not achieved at temperatures higher than 700 ^oC [134].

In Figure 14b, the thermal behavior of TiC powder calcined in air between 500-800^oC for 1 h is shown. Similar to TiN oxidation, rutile TiO_2 formation begins at 500^oC in addition to an almost nonexistent anatase and a large amount of unreacted TiC (JCPDS 65-8417). At 600^oC, approximately half of the TiC is oxidized to rutile TiO_2. It is observed that TiC is much harder to be oxidized TiN. At 700^oC, all TiC is oxidized to the rutile phase. Finally, when the TiO_2 is heated up to 800^oC, rutile lines in the XRD pattern become much more intense.

In Figure 14c, the thermal behavior of TiS_2 powder calcined in air between 500-800^oC for 1 h is shown. Unlike TiN and TiC, at 500^oC it is oxidized completely to anatase TiO_2 (JCPDS 21-1272). Sample keeps the anatase form up until 800 ^oC where a small amount of rutile phase begins to appear. Umebayashi et al. has also

observed a complete oxidation of TiS_2 powder and persistency of the anatase structure at high temperatures [102].

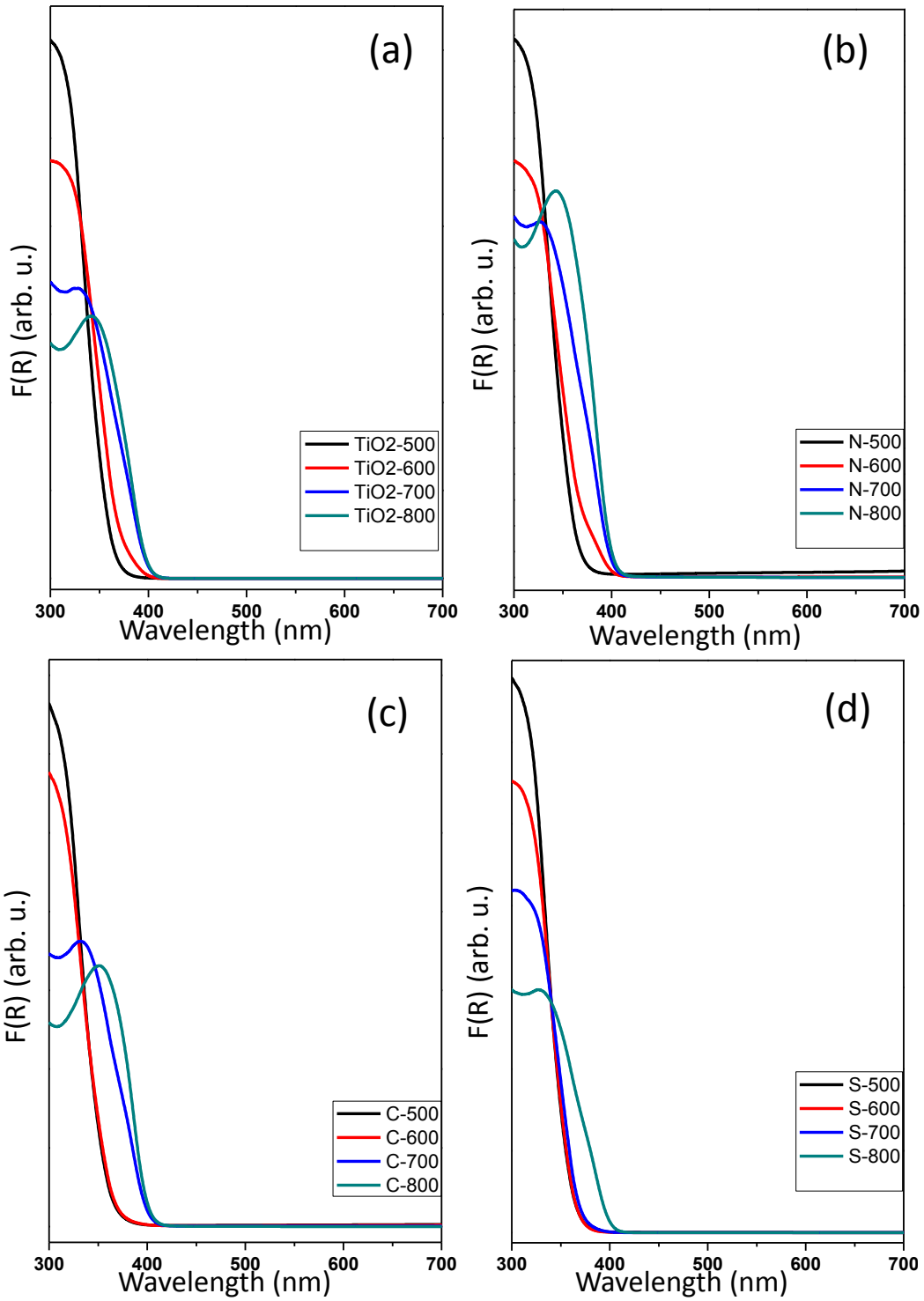

Figure 10. Kubelka-Munk transformed UV-VIS Diffuse Reflectance Spectra of (a) pure TiO_2 (b) TiN doped TiO_2 (N/TiO_2) (c) TiC doped TiO_2 (C/TiO_2) (d) TiS_2 doped TiO_2 (S/TiO_2) after calcination in air between 500 to 800 ^oC.

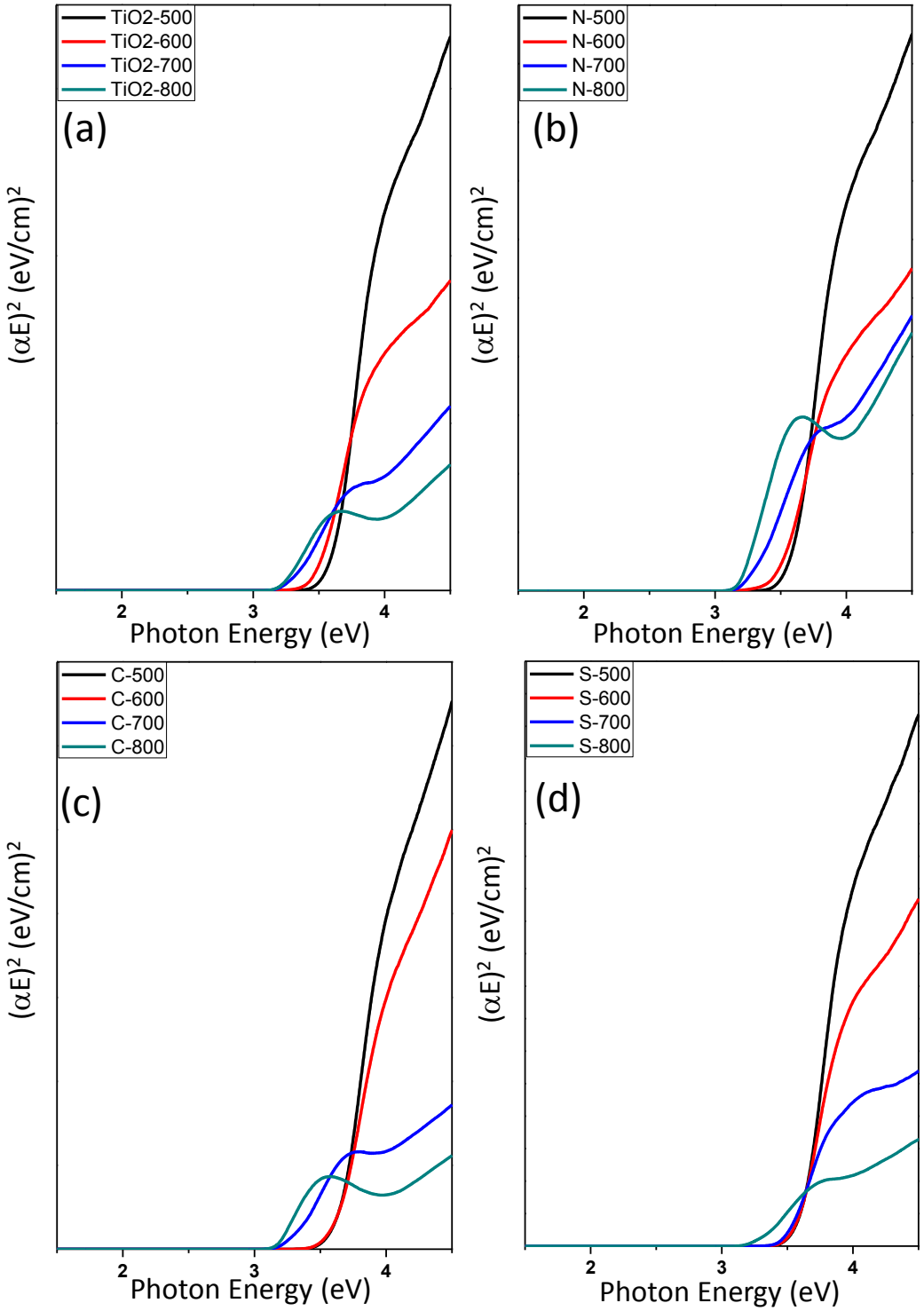

Figure 11. Tauc plots of (a) pure TiO_2 (b) TiN doped TiO_2 (N/TiO_2) (c) TiC doped TiO_2 (C/TiO_2) (d) TiS_2 doped TiO_2 (S/TiO_2) after calcination in air between 500 to 800 ^oC for the direct band gap calculations.

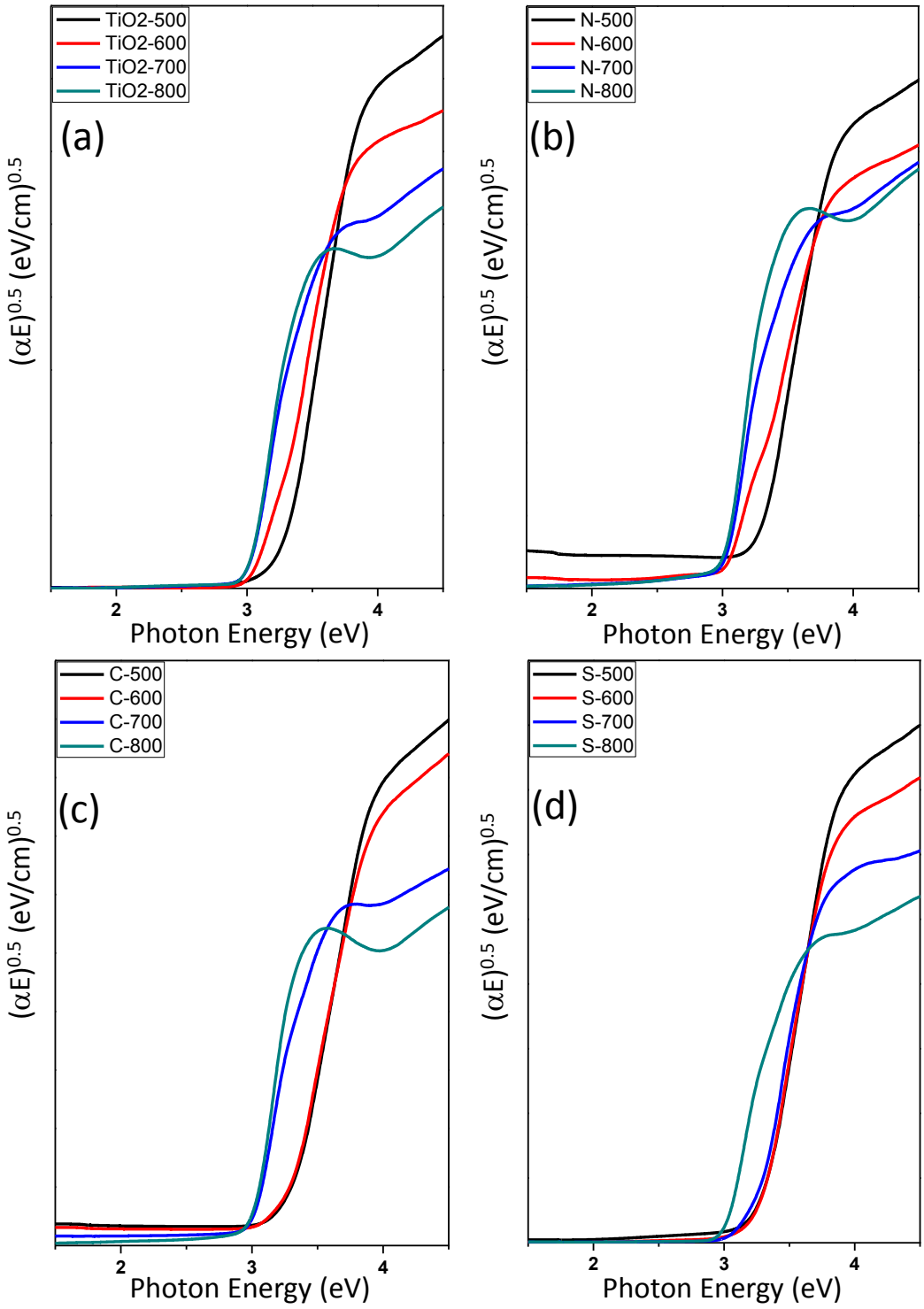

Figure 12. Tauc plots of (a) pure TiO_2 (b) TiN doped TiO_2 (N/TiO_2) (c) TiC doped TiO_2 (C/TiO_2) (d) TiS_2 doped TiO_2 (S/TiO_2) after calcination in air between 500 to 800 ^oC for the indirect band gap calculations.

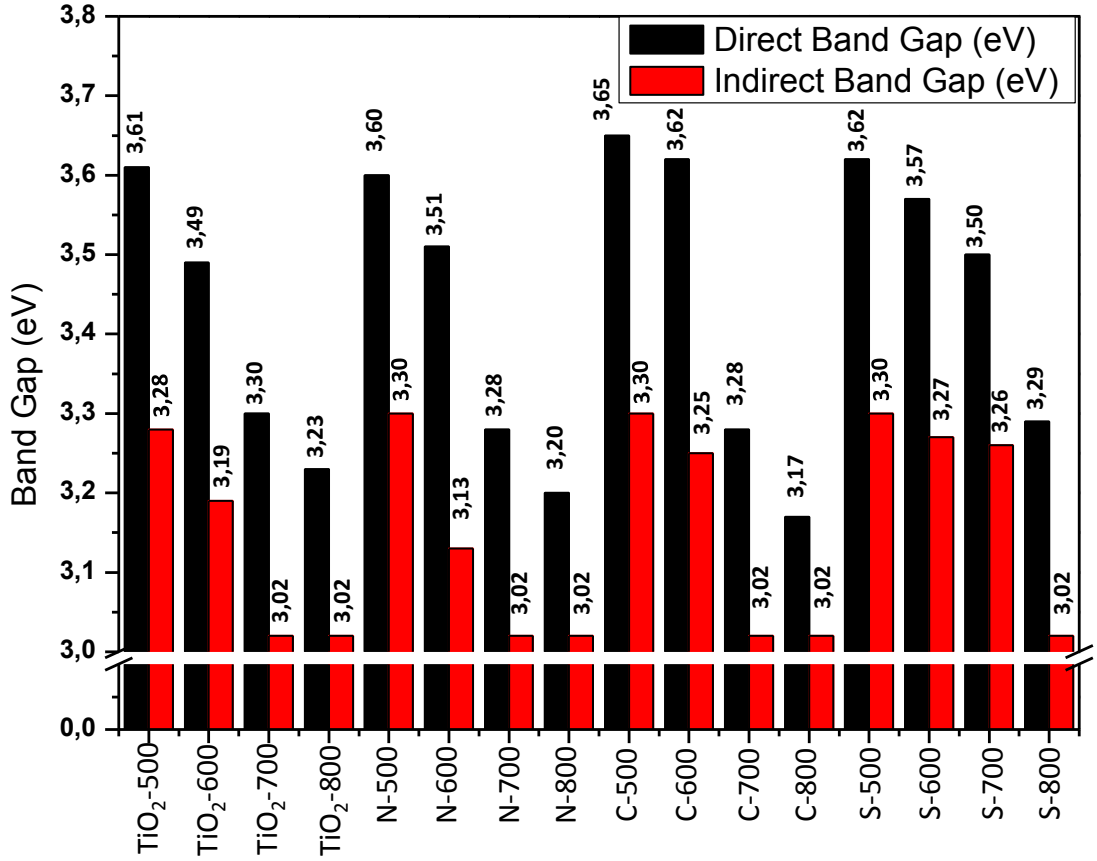

Figure 13. Calculated direct and indirect band gap values of pure TiO_2, TiN doped TiO_2 (N/TiO_2), TiC doped TiO_2 (C/TiO_2), TiS_2 doped TiO_2 (S/TiO_2) after calcination in air between 500 to 800 ^oC.

3.1.1.1 Raman Analysis

Figure 15 represents the Raman data for the thermally treated TiN, TiC and TiS_2. In panel (a), the evolution of TiO_2 crystalline phases in oxidized TiN can be observed upon calcination between 500-800^oC for 1h. Here, the Raman spectra are in accordance with the XRD data, showing crystalline anatase and rutile signals even at 500^oC. At 600^oC and 700^oC, rutile formation is clearly observed with the Raman signals at 447 and 612 cm^{-1} and at 800^oC, the crystalline phase becomes completely rutile.

In panels (b) and (c) of Figure 15, the thermal transformations of TiC and TiS_2 are illustrated. In general, current Raman spectra of the materials are consistent with the XRD data. However, the Raman measurements are more sensitive in monitoring the surface crystallization fraction compared to XRD data in the case for

TiN and TiC. For instance, in TiN and TiC calcined at 800°C, the Raman spectrum shows a significant proof of anatase phase while in XRD, diffraction lines of anatase phase are considerably low.

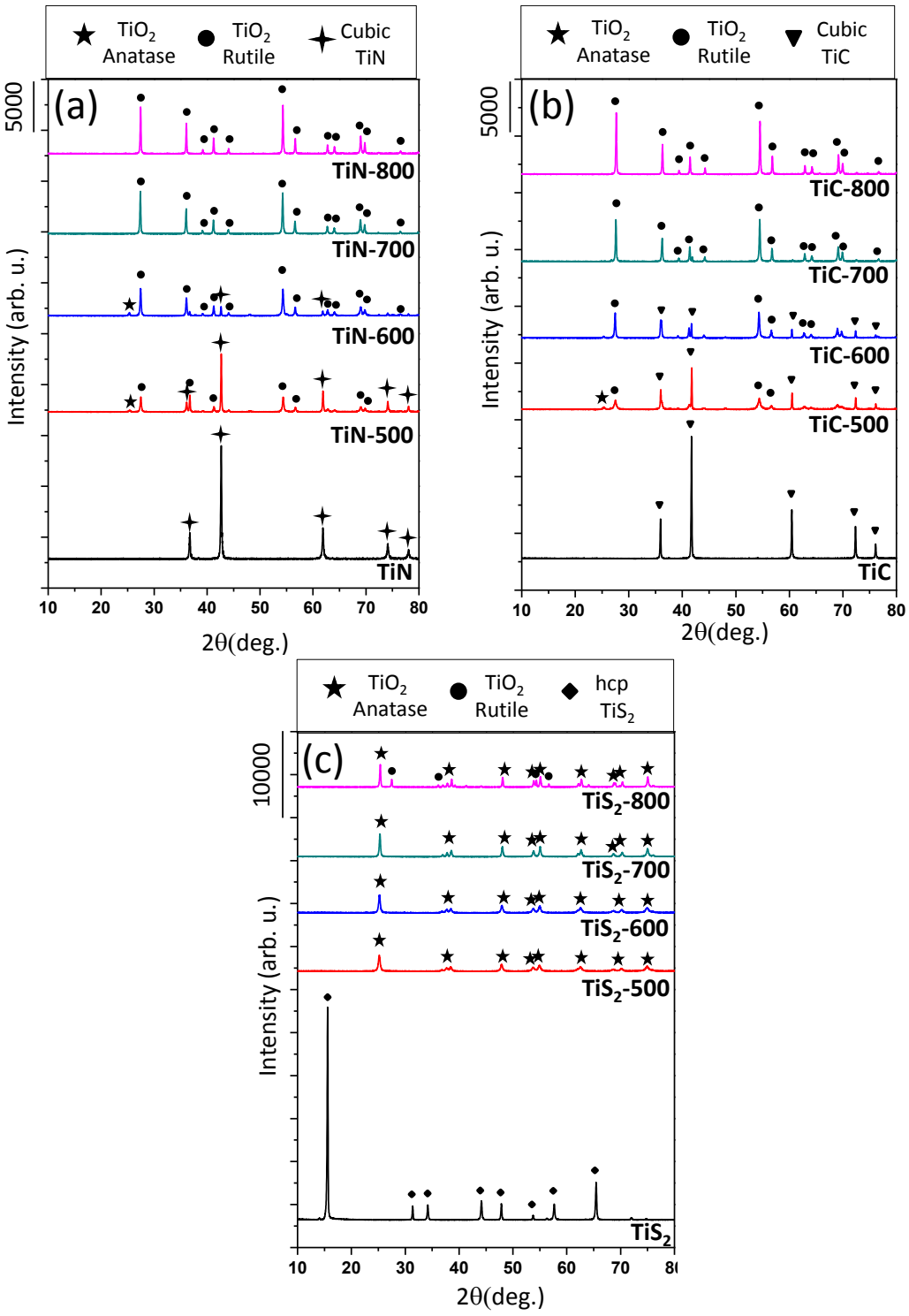

Figure 14. XRD patterns of (a) TiN, (b) TiC, (c) TiS_2 powders before (as is) and after calcination in air between 500 to 800 °C.

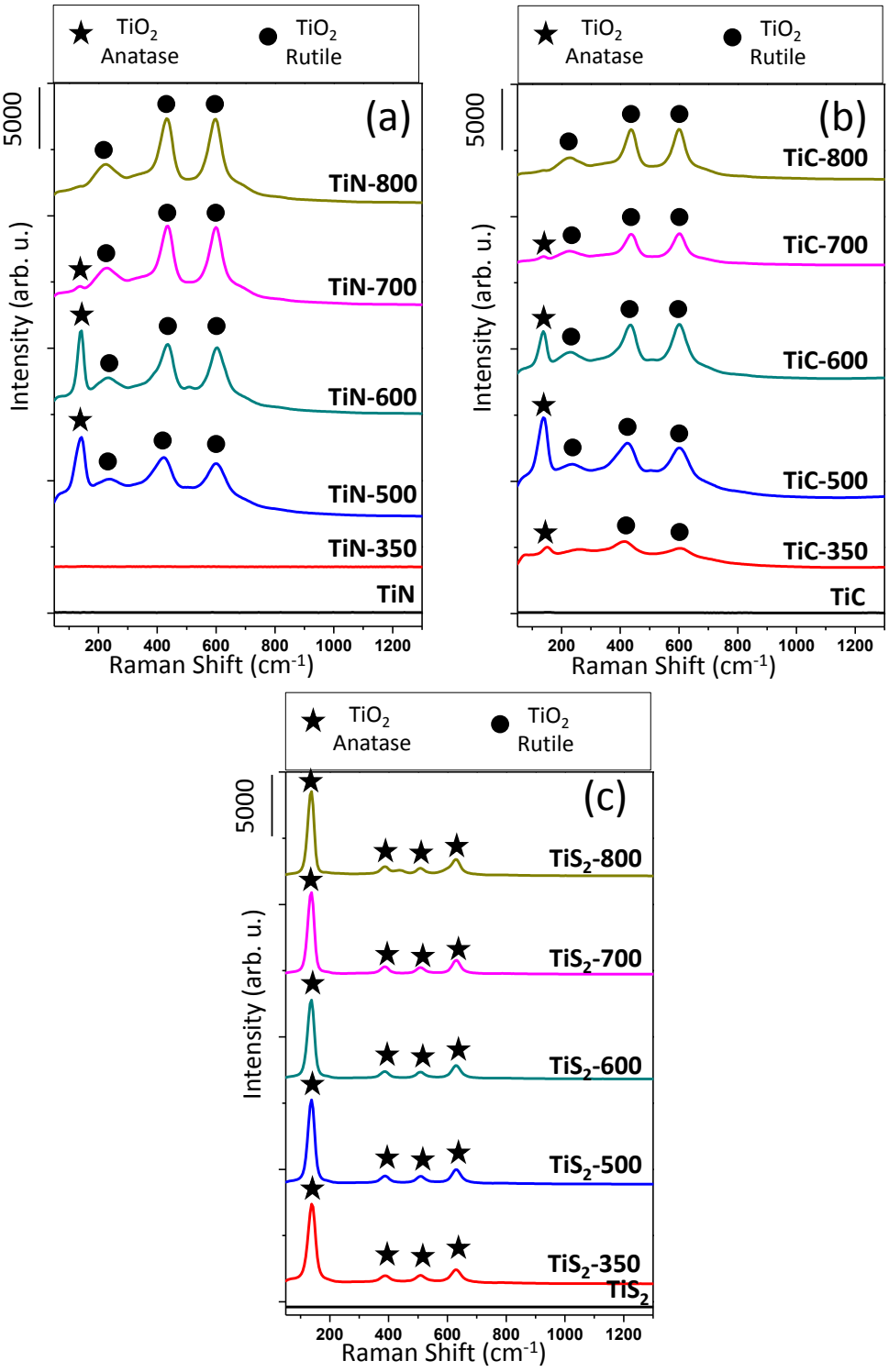

Figure 15. Raman spectra of (a) TiN (b) TiC (c) TiS_2 doped TiO_2 powders before (as is) and after calcination in air between 500 to 800 ^{o}C.

3.1.1.1 BET Analysis

Specific surface areas of TiN-500, TiC-500 and TiS_2-500 are found to be 6, 4.9 and 32.4 m^2/g respectively. Low SSAs for TiN and TiC powders annealed at 500^oC accounted for high rutile mass fraction. At 500 ^oC, TiS_2 is completely oxidized to TiO_2 with anatase form, therefore higher surface area than the other samples are expected.

3.1.1.1 UV-VIS Diffuse Reflectance Experiments

In order to estimate the band gap distance, UV-VIS DRS was employed. Figure 16 shows Kubelka-Munk transformed spectra of the thermally treated TiN, TiC and TiS_2. In panel (a) and (b) of Figure 16, it can be seen that thermally treated TiN and TiC samples don't show any change in visible light absorption with respect to calcination temperatures. However in Figure 16c, TiS_2 sample calcined at 800 ^oC shows red shift due to rutile formation in the spectrum.

The calculations of direct and indirect band gaps of the samples were done constructing Tauc plots. Figure 17 shows the Tauc plots of the thermally treated TiN, TiC and TiS_2 upon calcination between 500-800^oC for 1h for direct band gap calculations. Extrapolation of the linear portion of the plot gives direct band gaps values of 3.11, 3.14, 3.13 and 3.11 eV for the TiN-500, TiN-600, TiN-700 and TiN-800 respectively in Figure 17a. In Figure 17b, direct band gap values of TiC samples are found to be 3.13, 3.11, 3.11 and 3.10 eV, decreasing with increasing calcination temperatures. In Figure 17c, direct band gap values of TiS_2 samples are found to be 3.23, 3.36, 3.37 and 3.34 eV for the TiS_2-500, TiS_2-600, TiS_2-700, and TiS_2-800 respectively.

Figure 18 shows the Tauc plots of the thermally treated TiN, TiC and TiS_2 upon calcination between 500-800^oC for 1h for indirect band gap calculations. Extrapolation of the linear portion of the plot gives indirect band gaps values of 3.05, 3.03, 3.04 and 2.99 eV for the TiN-500, TiN-600, TiN-700 and TiN-800 respectively, as shown in Figure 18a. Indirect band gap values of TiC samples are found to be 3.06, 3.04, 3.00 and 2.98 eV, for the TiC-500, TiC-600, TiC-700 and TiC-800 respectively, as it can be seen in Figure 18b. In Figure 18c, indirect band

gap values of TiS_2samples are found to be 3.36, 3.19, 3.20 and 3.01 eV, for the TiS_2-500, TiS_2-600, TiS_2-700, and TiS_2-800 respectively.

Figure 19 summarizes the direct and indirect band gap values for samples discussed above.

3.1.1 Non-Metal Compound Doped Titania

3.1.1.1 XRD Experiments

Figure 20 illustrates the thermal behavior of pure TiO_2 calcined in air between 150-700^oC for 2 h. It is shown that crystalline titania begins to form very early at 350^oC with anatase diffraction pattern. At 500^oC, the anatase lines in the XRD pattern become much more apparent. When the sample is calcined at 600^oC, rutile begins to form. Finally, when the TiO_2 is heated up to 700^oC, the crystal structure becomes fully rutile.

In Figure 20 panel (b), the thermal behavior of boric acid added TiO_2 calcined in air between 150-700^oC for 2 h is shown. Unlike pure TiO_2, it is amorphous at 350^oC. At 500^oC, the anatase formation starts to occur but it is observable that average size of the anatase particles is very small by looking at the peak width. In addition to anatase structure, there is a little amount of boric acid (Sassolite mineral, JCPDS 30-0199) seen at 27,94^o. Surprisingly, even at high calcination temperatures, material keeps its anatase form and no sign of rutile is observed.

In Figure 20 panel (c), the thermal behavior of diethanolamine (DEA) added TiO_2 calcined in air between 150-700^oC for 2 h is shown. Similar to boron added TiO_2, material is amorphous at 350^oC. At 500^oC, the anatase formation starts to occur as well as the rutile formation. When the sample is calcined at 600^oC, the crystal structure becomes fully rutile and at 700^oC, rutile lines in the diffraction pattern become more intense.

In Figure 20 panel (d), the thermal behavior of triethylamine (TEA) added TiO_2 calcined in air between 150-700^oC for 2 h is shown. Similar to boron and DEA added TiO_2, material is amorphous at 350^oC. At 500^oC, the crystal structure is anatase but also a very little rutile peak is observed at 27^o. When the sample is

calcined at 600°C, the crystal structure becomes almost completely rutile with some anatase pattern and at 700°C, rutile lines in the diffraction pattern become much more intense.

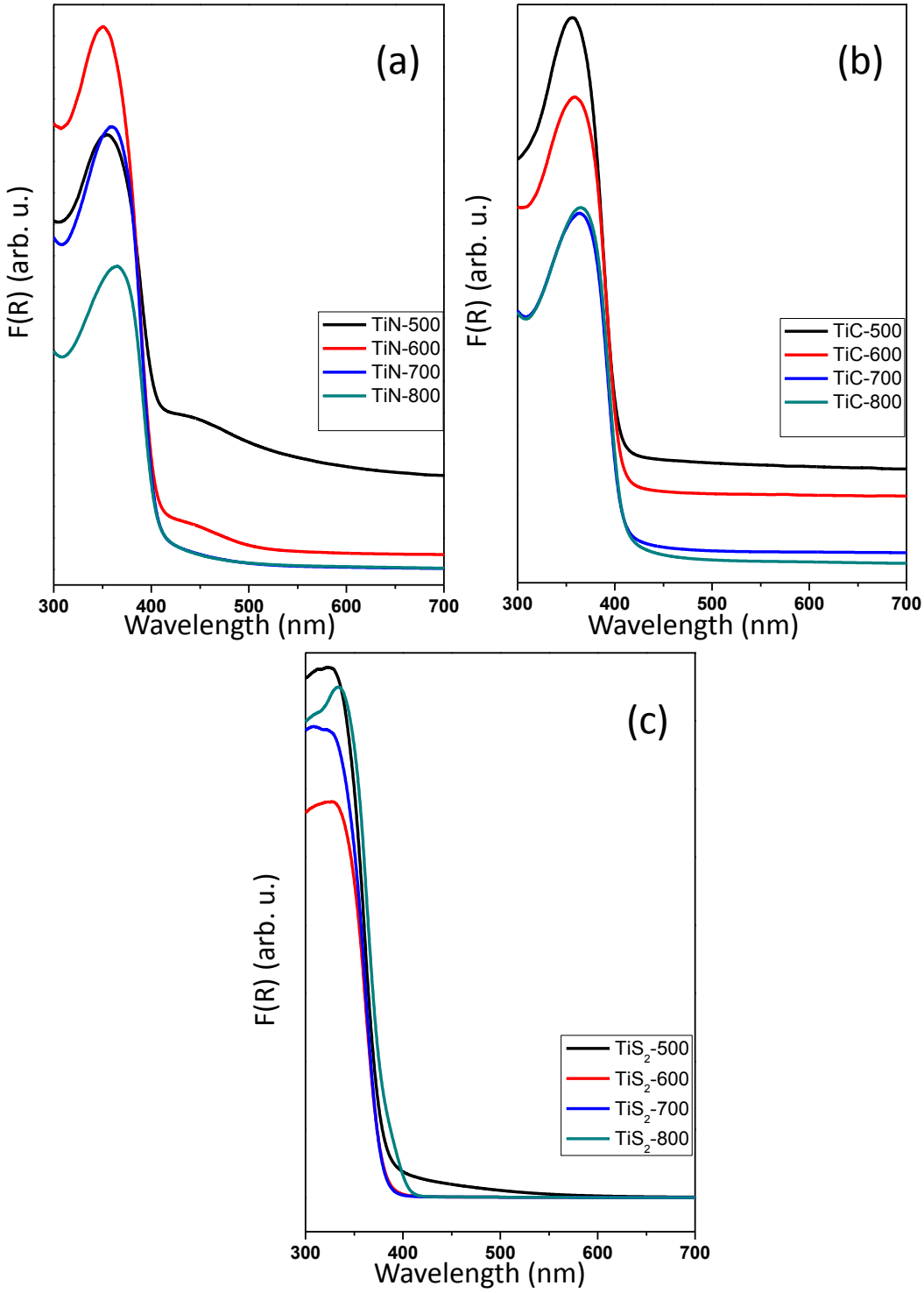

Figure 16. Kubelka-Munk transformed UV-VIS Diffuse Reflectance Spectra of (a) TiN (b) TiC (c) TiS_2 powders after calcination in air between 500 to 800 °C.

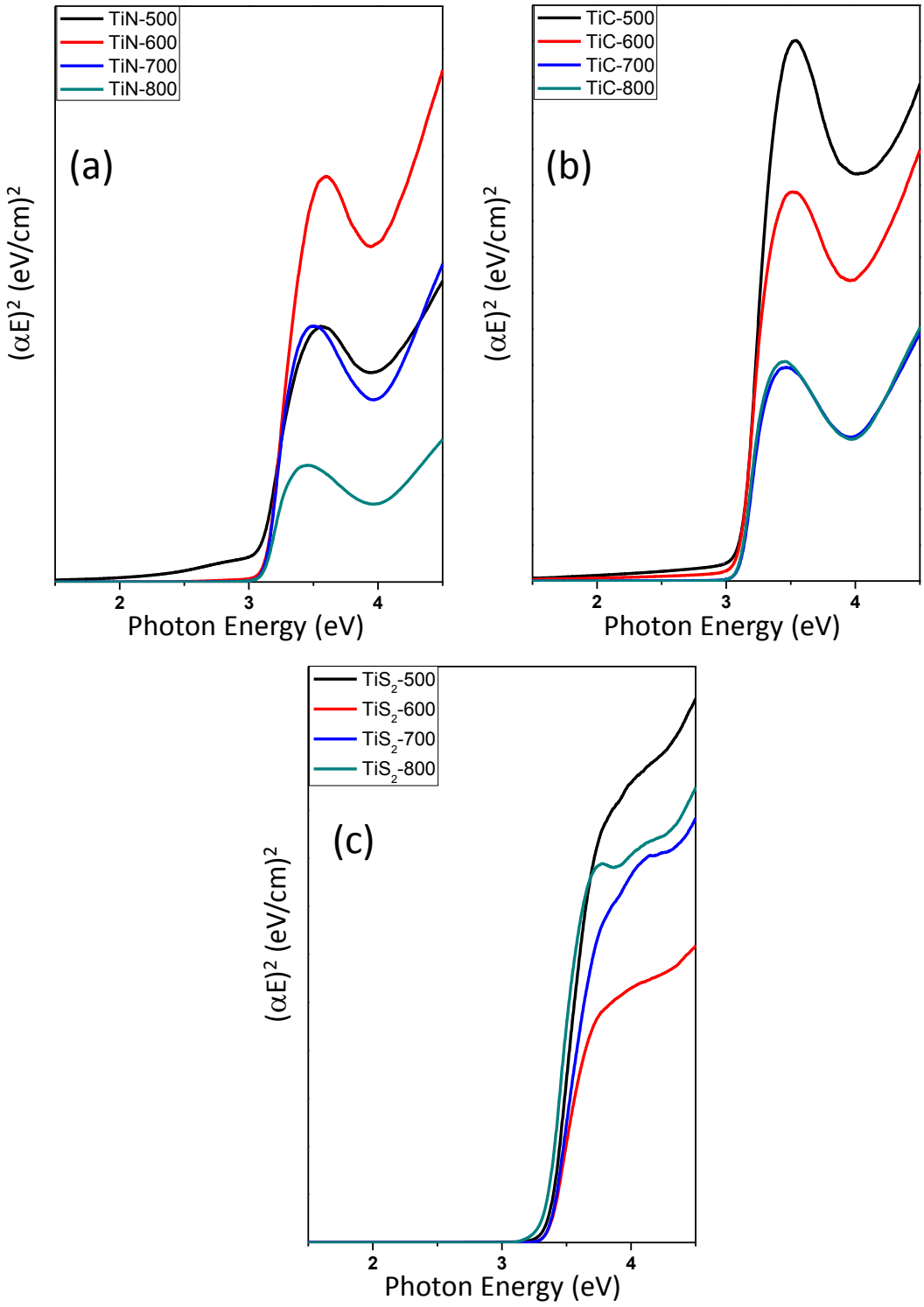

Figure 17. Tauc plots of (a) TiN (b) TiC (c) TiS_2 powders after calcination in air between 500 to 800 ^{o}C for the direct band gap calculations.

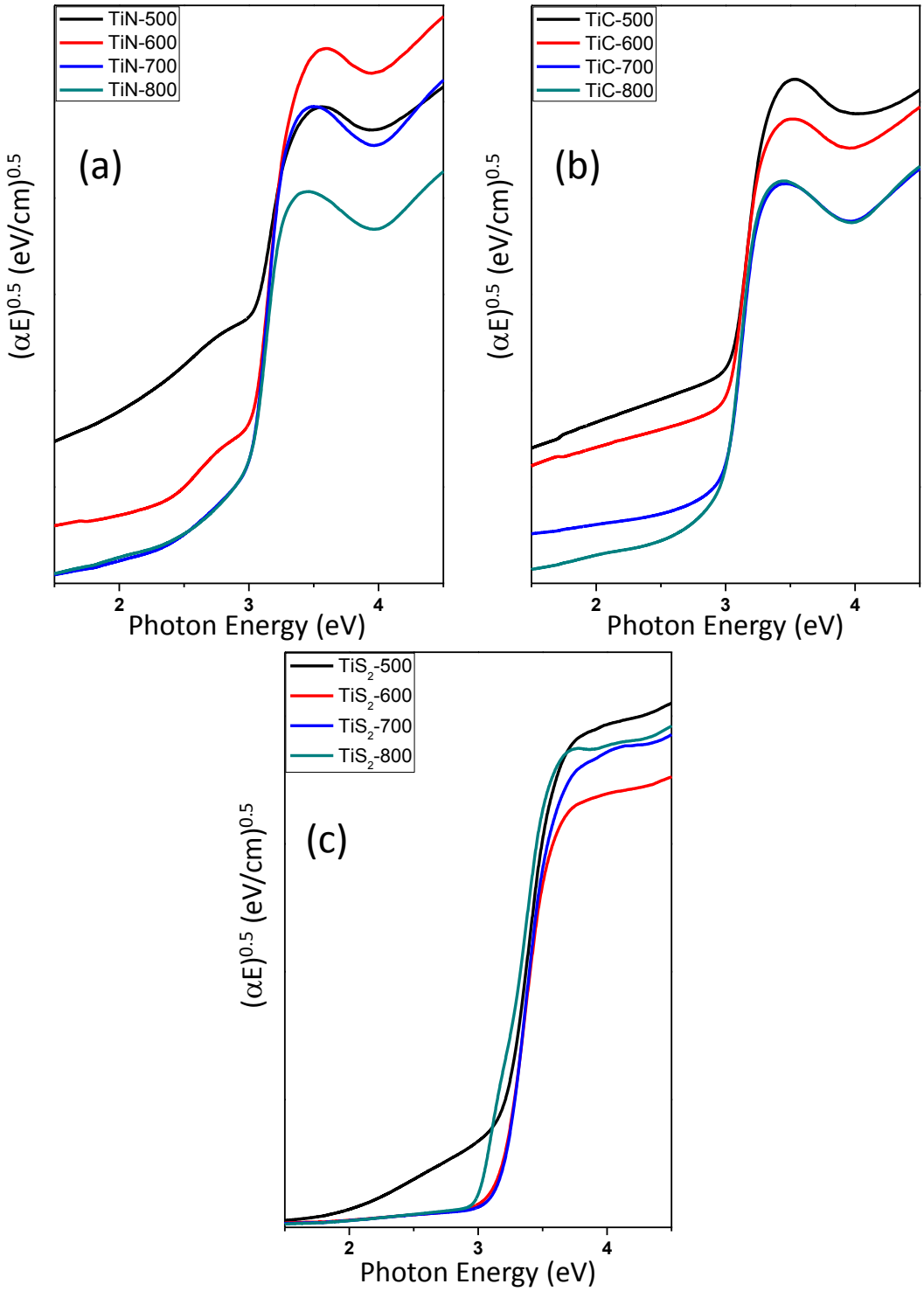

Figure 18. Tauc plots of (a) TiN (b) TiC (c) TiS_2 powders after calcination in air between 500 to 800 ^{o}C for the indirect band gap calculations.

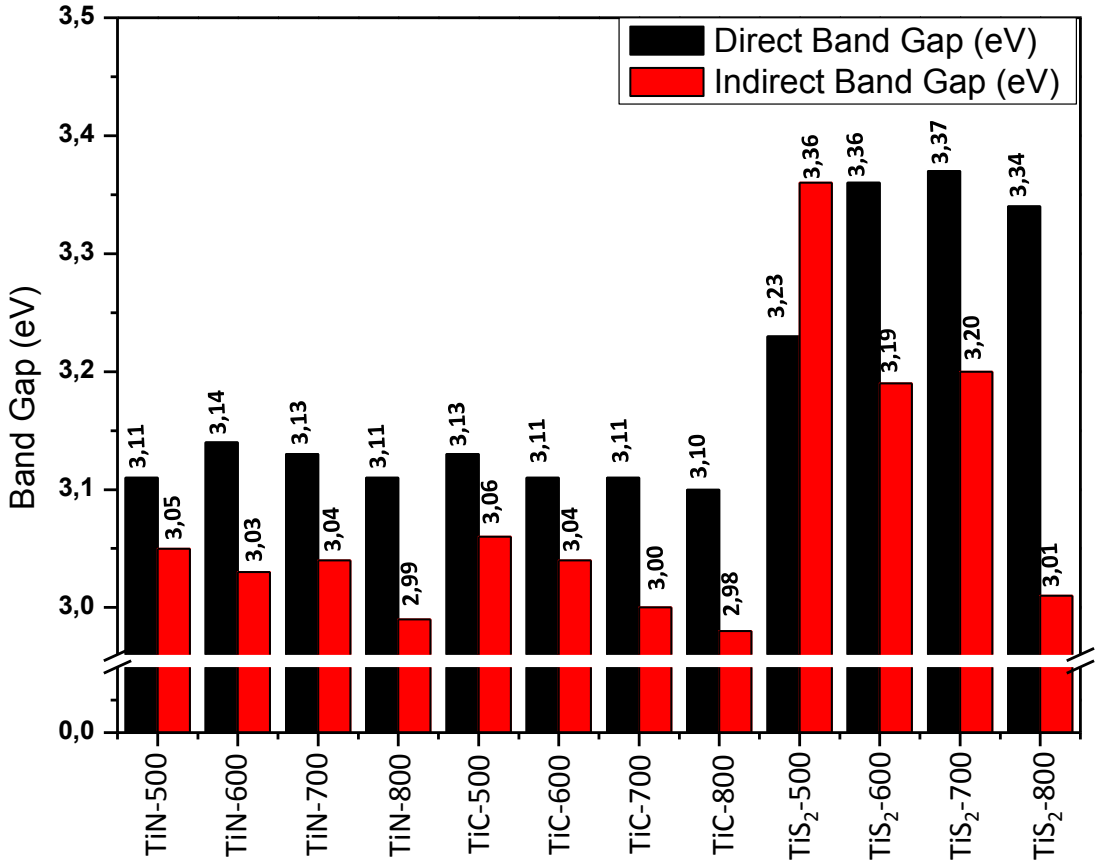

Figure 19. Calculated direct and indirect band gap values of TiN, TiC and TiS_2 powders after calcination in air between 500 to 800 ^oC.

Figure 21 illustrates the thermal behavior of thiourea added TiO_2 calcined in air between 150-700^oC for 2 h. It is shown that crystalline titania begins at 500^oC with anatase diffraction pattern. At 600^oC, the anatase lines in the XRD pattern become much more apparent with no sign of rutile. When the sample is calcined at 700^oC, almost half of the anatase crystal structure transforms into rutile.

In Figure 21 panel (b), the thermal behavior of urea added TiO_2 calcined in air between 150-700^oC for 2 h is shown. Similar to thiourea added TiO_2, it is amorphous at 350^oC. At 500^oC, the anatase formation starts to occur. At 600^oC, the anatase lines in the XRD pattern become much more apparent with a little rutile line present. When the sample is calcined at 700^oC, all of the anatase crystal structure transforms into rutile.

In Figure 21 panel (c), the thermal behavior of cyclohexanol added TiO_2 calcined in air between 150-700^oC for 2 h is shown. At 350^oC, material looks like amorphous but there is subtle formation of anatase crystal structure. At 500^oC, the

anatase formation is visible. At 600°C, the anatase lines in the XRD pattern become much more apparent with a little rutile line present. When the sample is calcined at 700°C, all of the anatase crystal structure transforms into rutile.

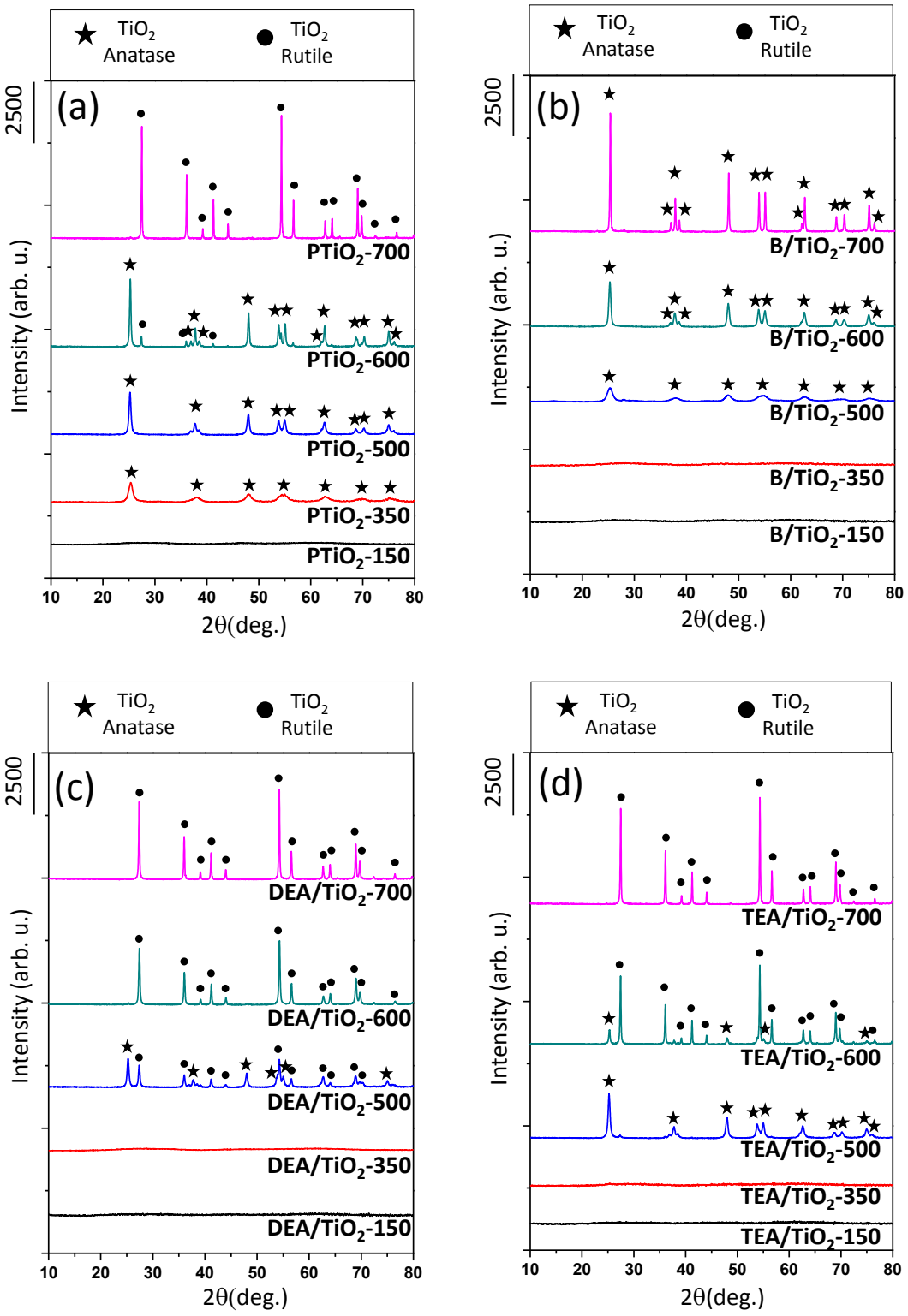

Figure 20. XRD patterns of (a) pure TiO_2 (b) B/TiO_2 (c) DEA/TiO_2 (d) TEA/TiO_2 after calcination in air between 150 to 700 °C.

For all of the cases above, it can be said that formation temperature of anatase crystal structure is shifted to a higher calcination temperature. Also, it is observed that boron atoms inhibit the phase transformation from anatase to rutile. This inhibition is also valid for thiourea case. While urea and cyclohexanol addition have almost no effect on phase transformation, TEA and DEA additions are observed to decrease the calcination temperature for anatase to rutile transformation.

Table 6 summarizes the anatase and rutile mass percentages of all the samples discussed above.

3.1.1.1 Raman Analysis

Figure 22 represents the Raman data for the thermally treated pure TiO_2, boric acid, DEA and TEA added titania. In panel (a), the evolution of TiO_2 crystalline phases in pure TiO_2 can be observed upon calcination between 500-700^oC for 2h. Here, the Raman spectra are in accordance with the XRD data, showing crystalline anatase at 500^oC. At 700^oC, rutile formation is clearly observed with the Raman signals at 236, 447 and 612 cm^{-1} and anatase phase is also seen at 144 cm^{-1}.

In panels (b), (c) and (d) of Figure 22, the thermal transformations of boric acid, DEA and TEA added titania are illustrated. In general, current Raman spectra of the materials are consistent with the XRD data. Although the Raman measurements are more sensitive in monitoring the surface crystallization fraction compared to XRD data in the case for pure titania, it is not the case for boric acid added titania. For instance, in pure titania calcined at 700^oC, the Raman spectrum shows a significant proof of anatase phase while in XRD, diffraction lines of anatase phase are considerably low. Boric acid added titania calcined at 500^oC shows no sign of anatase even though XRD tells us there is anatase phase forming up.

Figure 23 represents the Raman data for the thermally treated thiourea, urea and cyclohexanol added titania. In panel (a), the evolution of TiO_2 crystalline phases in thiourea added TiO_2 can be observed upon calcination between 500-700^oC for 2h. Here, the Raman spectra are in good agreement with the XRD data, showing crystalline anatase signals at 144, 399, 516 and 639 cm^{-1} calcined at 500^oC. At 700^oC, rutile formation is clearly observed with the Raman signals at 447 and 612 cm^{-1} in addition to anatase phase.

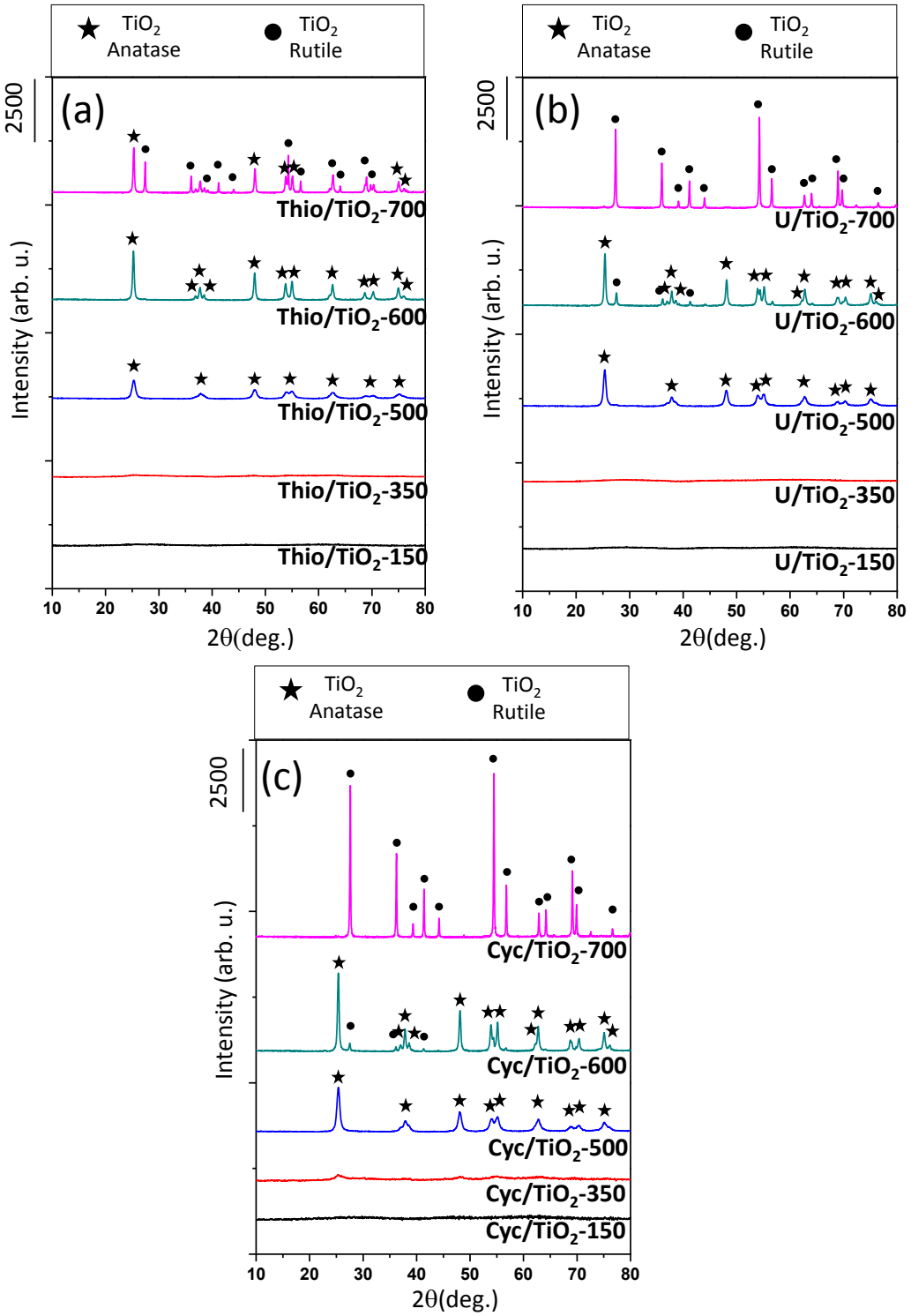

Figure 21. XRD patterns of (a) Thio/TiO_2 (b) U/TiO_2 (c) Cyc/TiO_2 after calcination in air between 150 to 700 ^{o}C.

Table 6. Calculated mass fraction percentages of anatase (A%) and rutile (R%) phases for pure TiO_2, B/TiO_2, DEA/TiO_2, TEA/TiO_2, Thio/TiO_2, U/TiO_2, Cyc/TiO_2

Sample	$PTiO_2$		B-TiO_2		DEA-TiO_2		TEA-TiO_2		Thio- TiO_2		U- TiO_2		Cyc- TiO_2	
T/ °C	A %	R %	A %	R %	A %	R %	A %	R %	A %	R %	A %	R %	A %	R %
350	100	-	-	-	-	-	-	-	-	-	-	-	-	-
500	100	-	100	-	50,83	49,17	100	-	100	-	100	-	100	-
600	83,72	16,28	100	-	-	100	14,36	85,64	100	-	76,02	23,98	88,42	11,58
700	-	100	100	-	-	100	-	100	53,6	46,4	-	100	-	100

In panels (b) and (c) of Figure 23, the thermal transformations of urea and cyclohexanol added titania are illustrated. In general, current Raman spectra of the materials are consistent with the XRD data.

3.1.1.1 BET Analysis

BET surface areas of the thermally treated pure titania and non metal compound doped samples were analyzed and the results are given in Table 7. With increasing calcination temperatures, the S_{BET} values decrease monotonically, showing that the samples are strongly affected by the thermal treatment. Smaller particle size of boric acid addition at 500 °C calcination temperature gives rise to higher SSA, compared to TEA which is also in anatase form but it has a sharper XRD line for anatase.

Table 7. BET Specific surface areas (in m^2/g) of the pure, B/TiO_2, DEA/TiO_2, TEA/TiO_2, Thio/TiO_2, U/TiO_2 and Cyc/TiO_2 samples calcined within 500-700°C.

Sample T/ °C	**$PTiO_2$**	**B-TiO_2**	**DEA-TiO_2**	**TEA-TiO_2**	**Thio-TiO_2**	**U-TiO_2**	**Cyc-TiO_2**

500	<2*	70	10	17	67	39	35
600	<2*	43	<2	<2	11	8	3
700	<2*	<2	-	-	-	-	-

* *Samples were measured twice; the reason could be ineffective degassing process*

3.1.1.1 UV-VIS Diffuse Reflectance Experiments

Figure 24 shows Kubelka-Munk transformed spectra of pure, boric acid, DEA and TEA doped TiO_2. Samples calcined at 150^oC (black spectrum) and 350^oC (red spectrum) are shown as inset due to inexplicable nature of them caused by amorphous structures and unburnt residual carbon. Pure TiO_2 calcined at 700^oC has a red shift towards visible range because of the rutile phase formation, clearly shown in Figure 24a. On the other hand, B-500 sample has a continuous absorption tail to the visible range, indicating that this material is definitely doped with boron atoms which formed impurity band above the valence band and can be possibly a visible light active photocatalyst that can be seen in Figure 24b. Upon calcination at higher temperatures however, this tail disappears. In Figure 24c, it can be seen that DEA has almost no effect on absorption edges at different temperatures. Rutile phase presence at 600^oC and 700^oC is understandable from the shift towards higher wavelengths for TEA doped samples, shown in Figure 24d.

Figure 25 shows Kubelka-Munk transformed spectra of thiourea, urea and cyclohexanol doped TiO_2. In Figure 25a, a red shift due to rutile formation at 700^oC is observed for thiurea doped sample. U-500 sample has a similar tail like B-500, also indicating U-500 can be a candidate visible light active photocatalyst, that can be seen in Figure 25b. Cyc-500, shown in Figure 25c, also has a visible light tail that disappears with increasing calcination temperature.

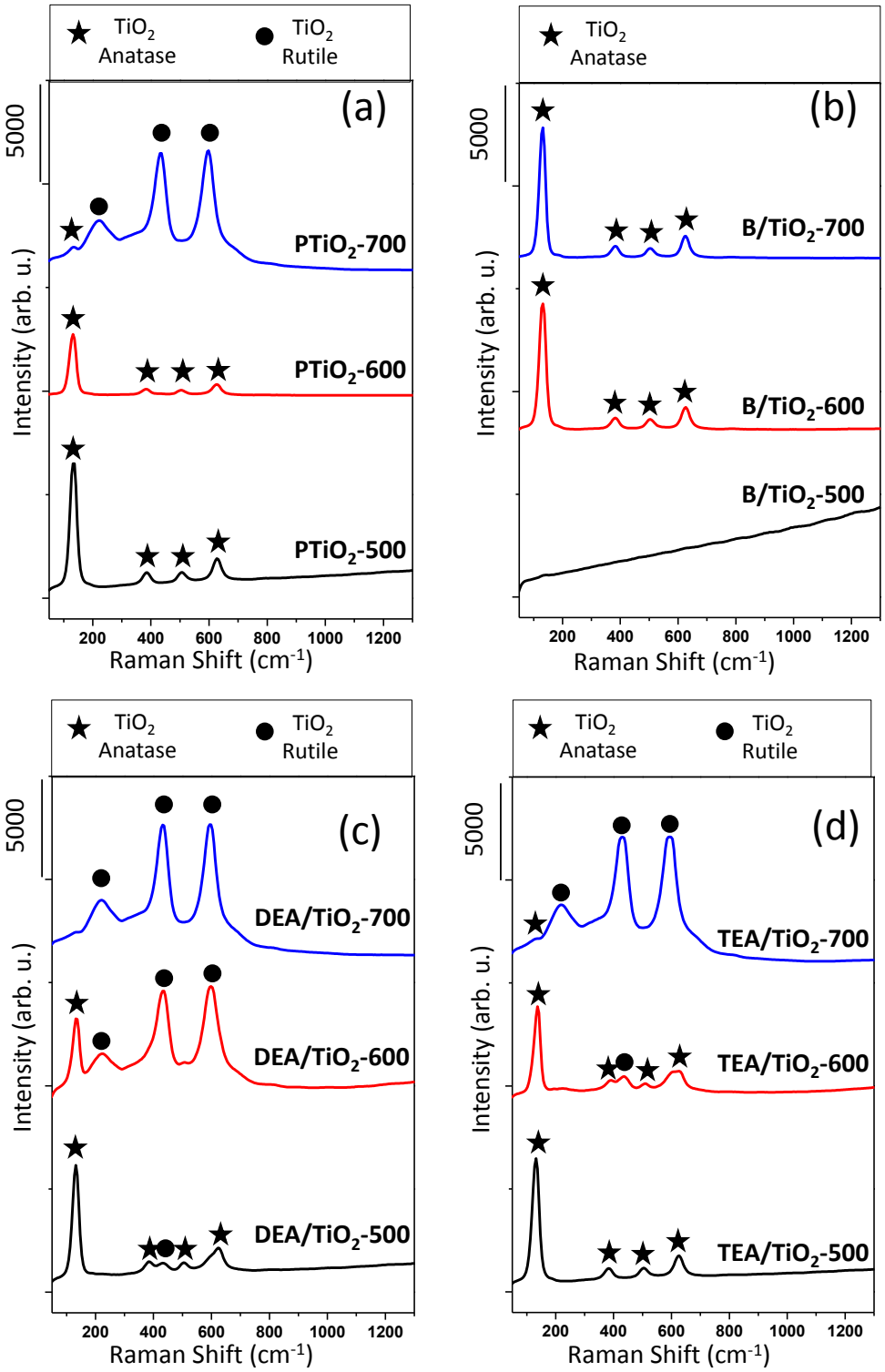

Figure 22. Raman spectra of (a) pure TiO_2 (b) B/TiO_2 (c) DEA/TiO_2 (d) TEA/TiO_2 after calcination in air between 500 to 700 ^oC.

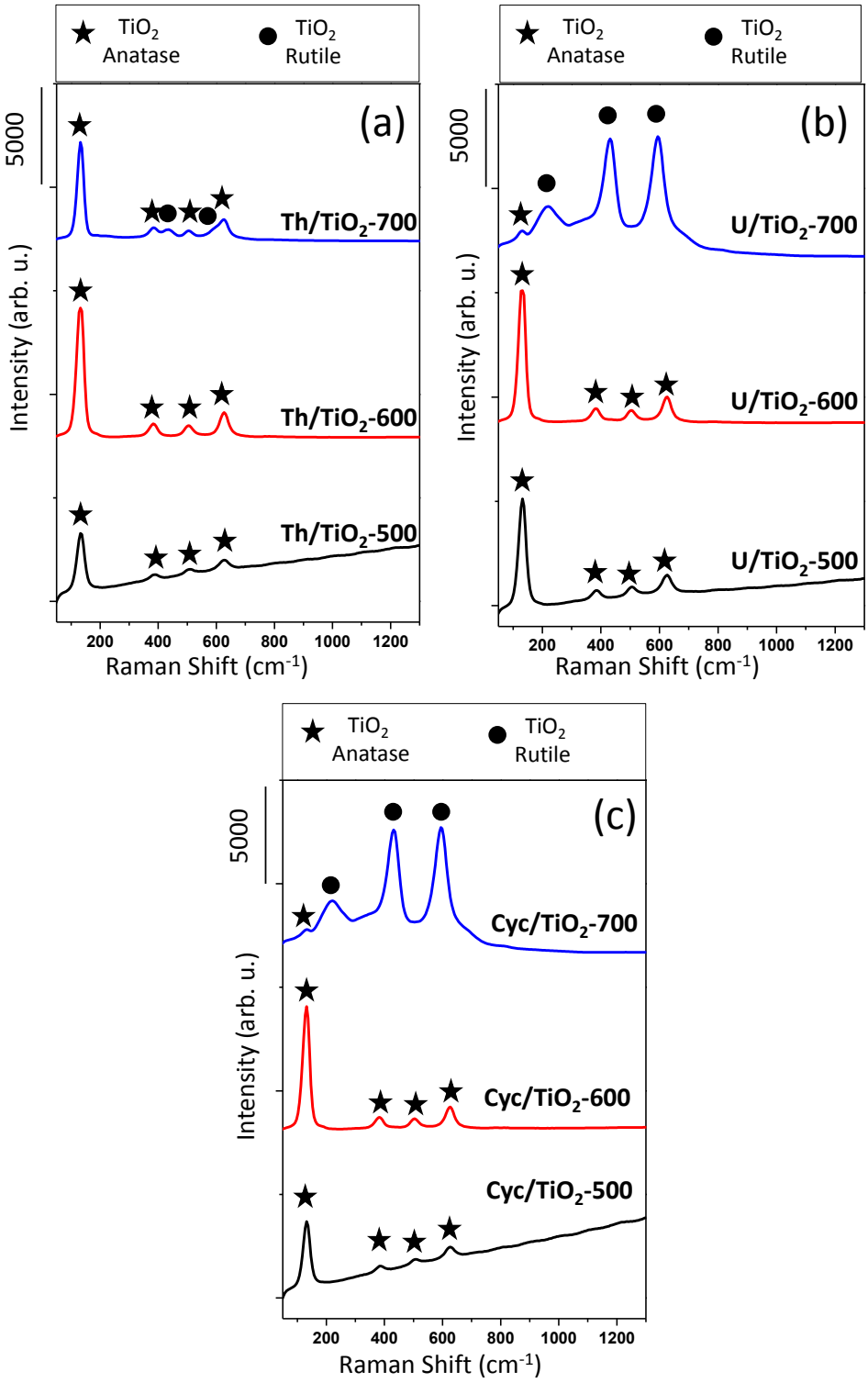

Figure 23. Raman spectra of (a) Thio/TiO_2 (b) U/TiO_2 (c) Cyc/TiO_2 after calcination in air between 500 to 700 ^{o}C.

The calculations of direct and indirect band gaps of the samples were done constructing Tauc plots. Figure 26 shows the Tauc plots of the thermally treated pure, boric acid, DEA and TEA doped TiO_2 upon calcination between 500-700^oC for 2h for direct band gap calculations. In Figure 26a, extrapolation of the linear portion of the plot gives direct band gaps values of 3.29, 3.25, and 3.08 eV for the $PTiO_2$-500, $PTiO_2$-600, and $PTiO_2$-700 respectively. Direct band gap values of B- TiO_2 samples are found to be 3.31, 3.32, and 3.37 eV, directly proportional with the calcination temperatures, shown in Figure 26b. In Figure 26c, direct band gap values of DEA-TiO_2 samples are found to be 3.07, 3.05, and 3.07 eV for DEA-500, DEA-600, DEA-700, respectively. Finally in Figure 26d, direct band gap values of TEA doped titania samples are calculated to be 3.21, 3.06 and 3.07 eV for TEA-500, TEA-600, TEA-700, respectively.

Figure 27 shows the Tauc plots of the thermally treated thiourea, urea and cyclohexanol doped TiO_2 upon calcination between 500-700^oC for 2h for direct band gap calculations. Shown in Figure 27a, calculated direct band gaps values are 3.31, 3.24, and 3.24 eV for the Thio-500, Thio-600, and Thio-700 respectively. In Figure 27b, direct band gap values of U-TiO_2 samples are found to be 3.26, 3.25, and 3.07 eV, decreasing with the increasing calcination temperatures. Direct band gap values of Cyc-TiO_2 samples are found to be 3.20, 3.25, and 3.07 eV for Cyc-500, Cyc-600, Cyc-700, respectively, shown in Figure 27c.

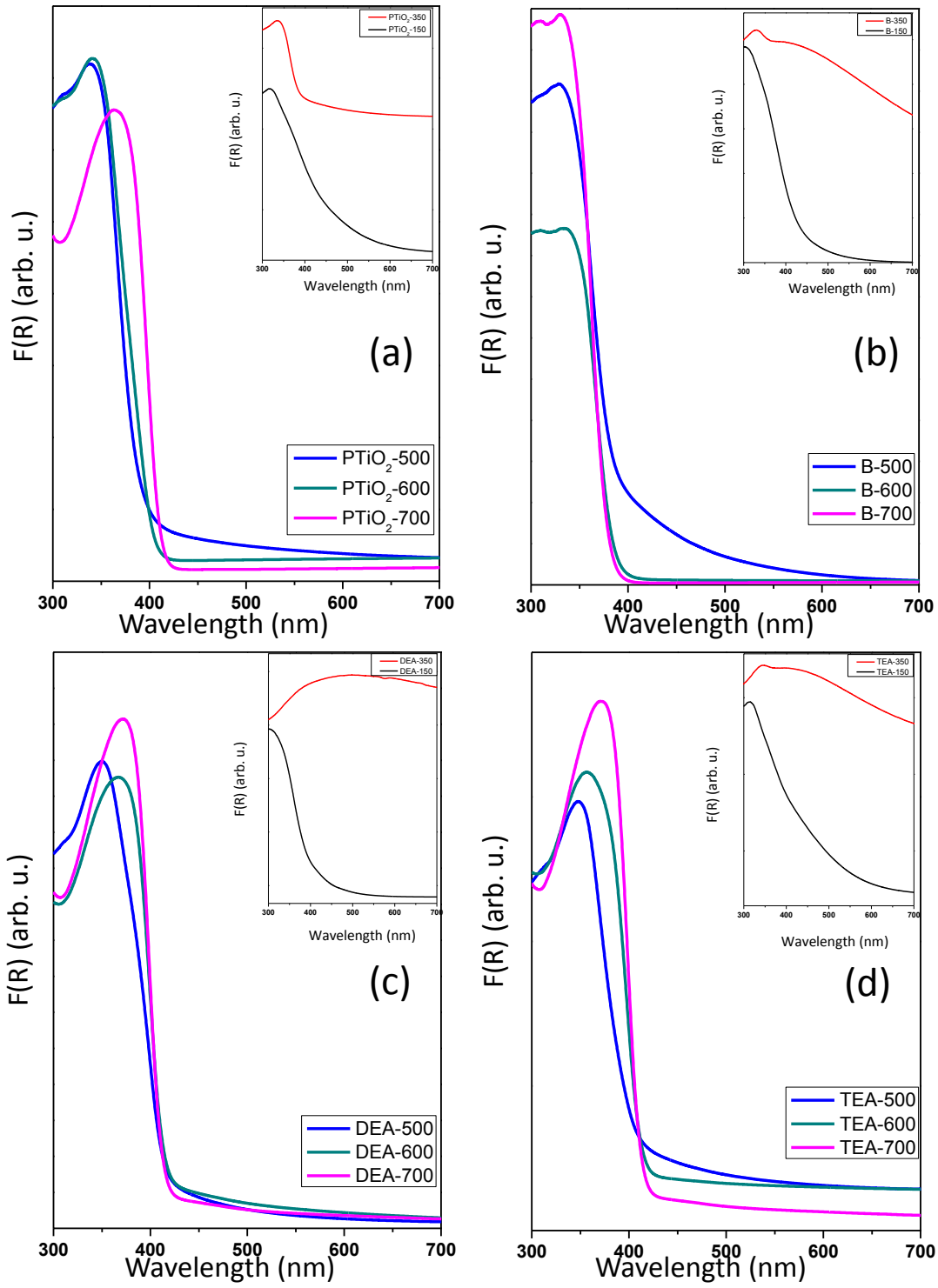

Figure 24. Kubelka-Munk transformed UV-VIS Diffuse Reflectance Spectra of (a) pure TiO_2 (b) B/TiO_2 (c) DEA/TiO_2 (d) TEA/TiO_2 after calcination in air between 150 to 700 ^oC.Insets: Kubelka-Munk transformed UV-VIS Diffuse Reflectance Spectra of the samples calcined at 150 ^oC (lower black spectra) and 350 ^oC (upper red spectra)

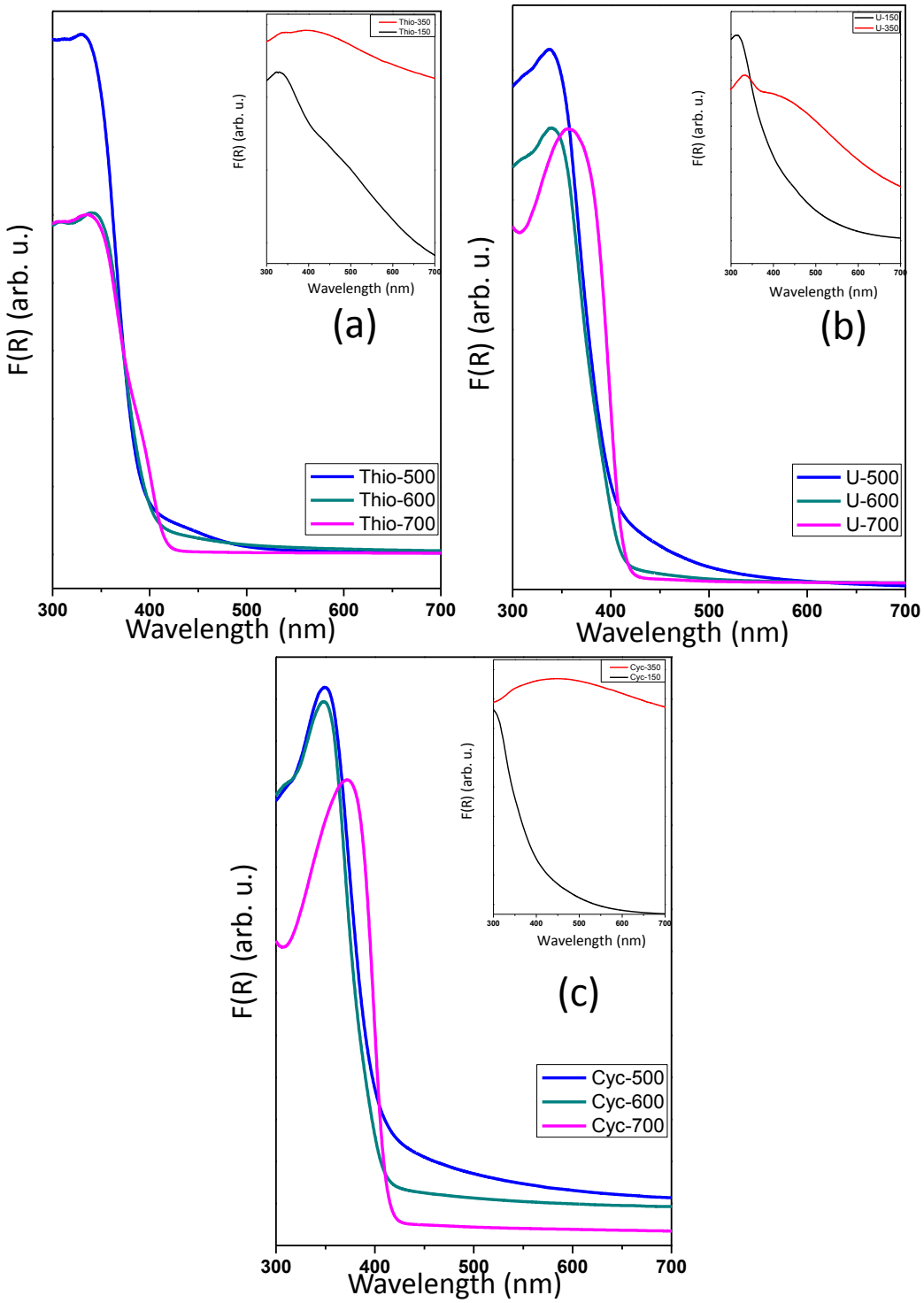

Figure 25. Kubelka-Munk transformed UV-VIS Diffuse Reflectance Spectra of (a) Thio/TiO_2 (b) U/TiO_2 (c) Cyc/TiO_2 after calcination in air between 150 to 700 ^oC. Insets: Kubelka-Munk transformed UV-VIS Diffuse Reflectance Spectra of the samples calcined at 150 ^oC (lower black spectra) and 350 ^oC (upper red spectra)

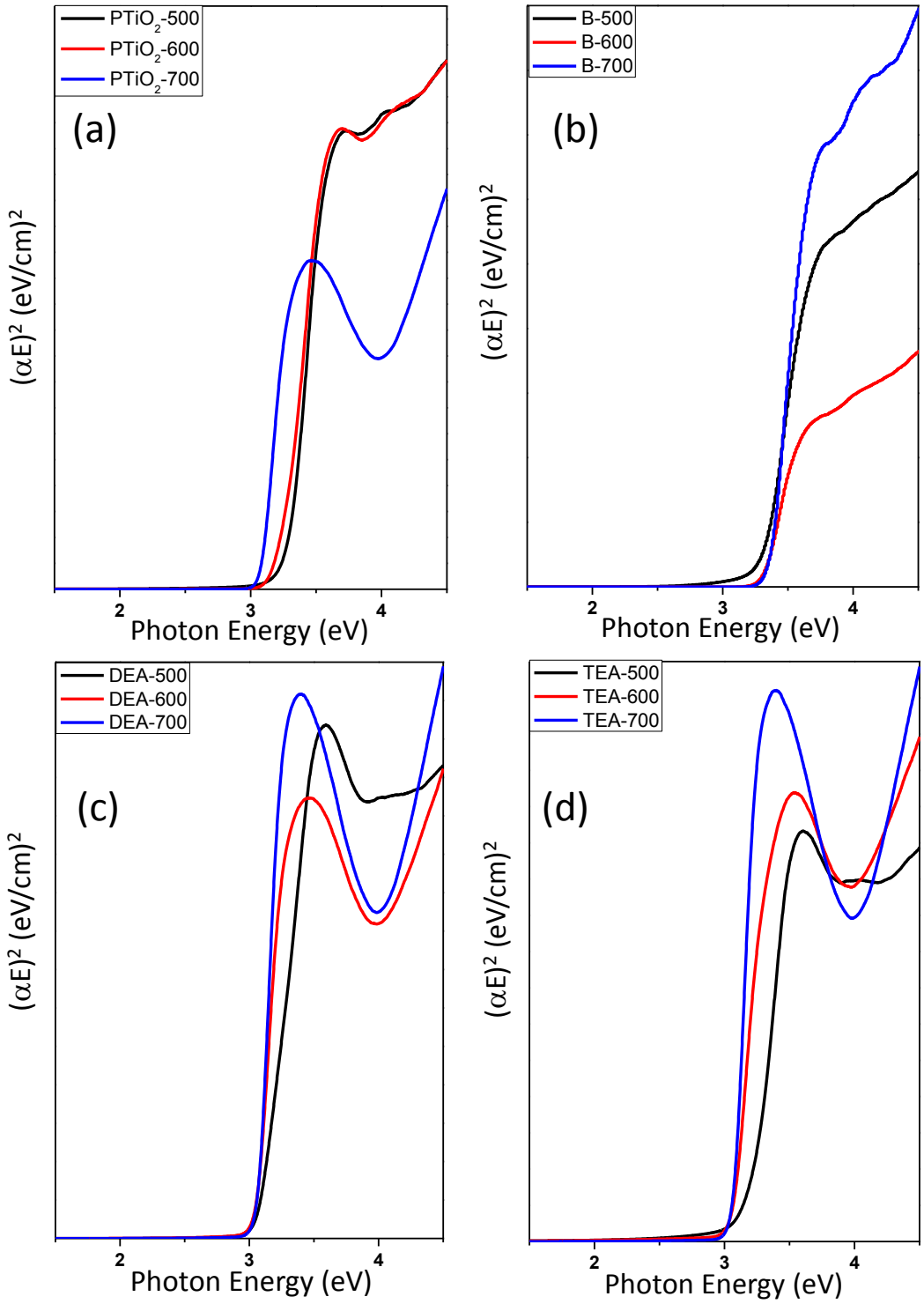

Figure 26. Tauc plots of (a) pure TiO_2 (b) B/TiO_2 (c) DEA/TiO_2 (d) TEA/TiO_2 after calcination in air between 500 to 700 ^oC for the direct band gap calculations.

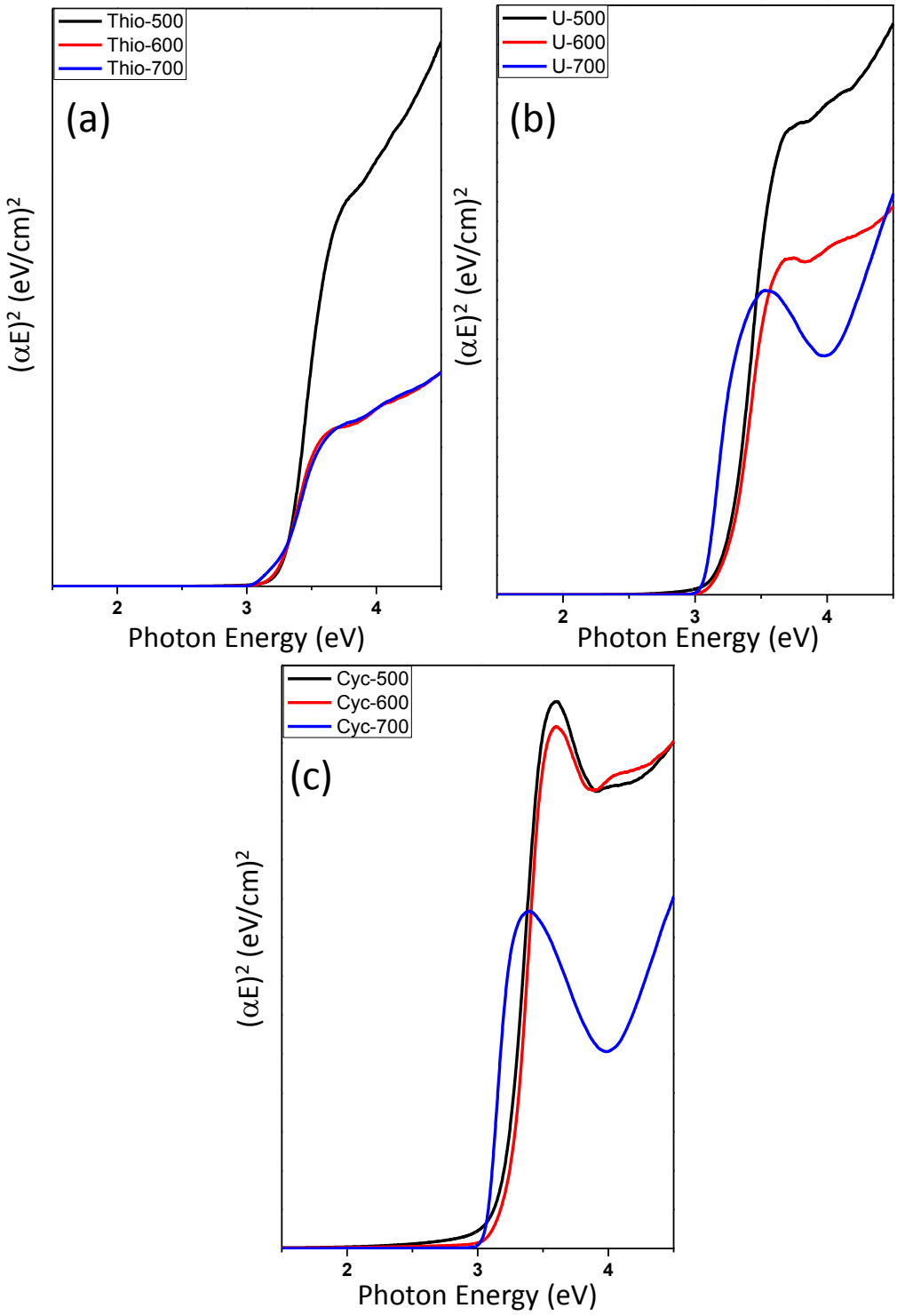

Figure 27. Tauc plots of of (a) Thio/TiO_2 (b) U/TiO_2 (c) Cyc/TiO_2 after calcination in air between 500 to 700 ^oC for the direct band gap calculations.

Figure 28 shows the Tauc plots of the thermally treated pure, boric acid, DEA and TEA doped TiO_2 upon calcination between 500-700^oC for 2h for indirect band

gap calculations. In Figure 28a, indirect band gap values are calculated to be 3.10, 3.03, and 2.97 eV for the $PTiO_2$-500, $PTiO_2$-600, and $PTiO_2$-700 respectively. Indirect band gap values of B-TiO_2 samples are found to be 3.23, 3.14, and 3.17 eV, for B-500, B-600, B-700, respectively, shown in Figure 28b. Although the calculated indirect band gap value is 3.23 eV for B-500, this sample has low band gap domains causing absorption in the visible range. In Figure 28c, indirect band gap values of DEA-TiO_2 samples are found to be 2.90, 2.88, and 2.91 eV for DEA-500, DEA-600, DEA-700, respectively. Ananpattarachai et al. also observed similar low indirect band gap values for DEA doped titania prepared via sol-gel route [147]. Finally in Figure 28d, indirect band gap values of TEA doped titania samples are calculated to be 2.75, 2.85 and 2.90 eV for TEA-500, TEA-600, TEA-700, respectively. Todorova et al. reported also low band gap value for TEA doped sol-gel titania and attributed it to simultaneous N-,C-doping achieved by the modification. They also found out that sample did not exhibit any photocatalytic activity under visible light despite its high absorbance in the entire visible part of the spectrum and this finding was ascribed to the large amount of residual carbon revealed by XPS analysis [148].

Figure 29 shows the Tauc plots of the thermally treated treated thiourea, urea and cyclohexanol doped TiO_2 upon calcination between 500-700^oC for 2h for indirect band gap calculations. In Figure 29a, extrapolation of the linear portion of the plot gives indirect band gaps values of 3.01, 3.00, and 2.92 eV for the Thio-500, Thio-600, and Thio-700 respectively. In Figure 29b, indirect band gap values of U-TiO_2 samples are found to be 3.08, 2.95, and 2.96 eV, for U-500, U-600, U-700, respectively. In Figure 29c, indirect band gap values of Cyc-TiO_2 samples are found to be 3.02, 3.03, and 2.98 eV for Cyc-500, Cyc-600, Cyc-700, respectively.

Figure 30 summarizes the direct and indirect band gap values for samples discussed above.

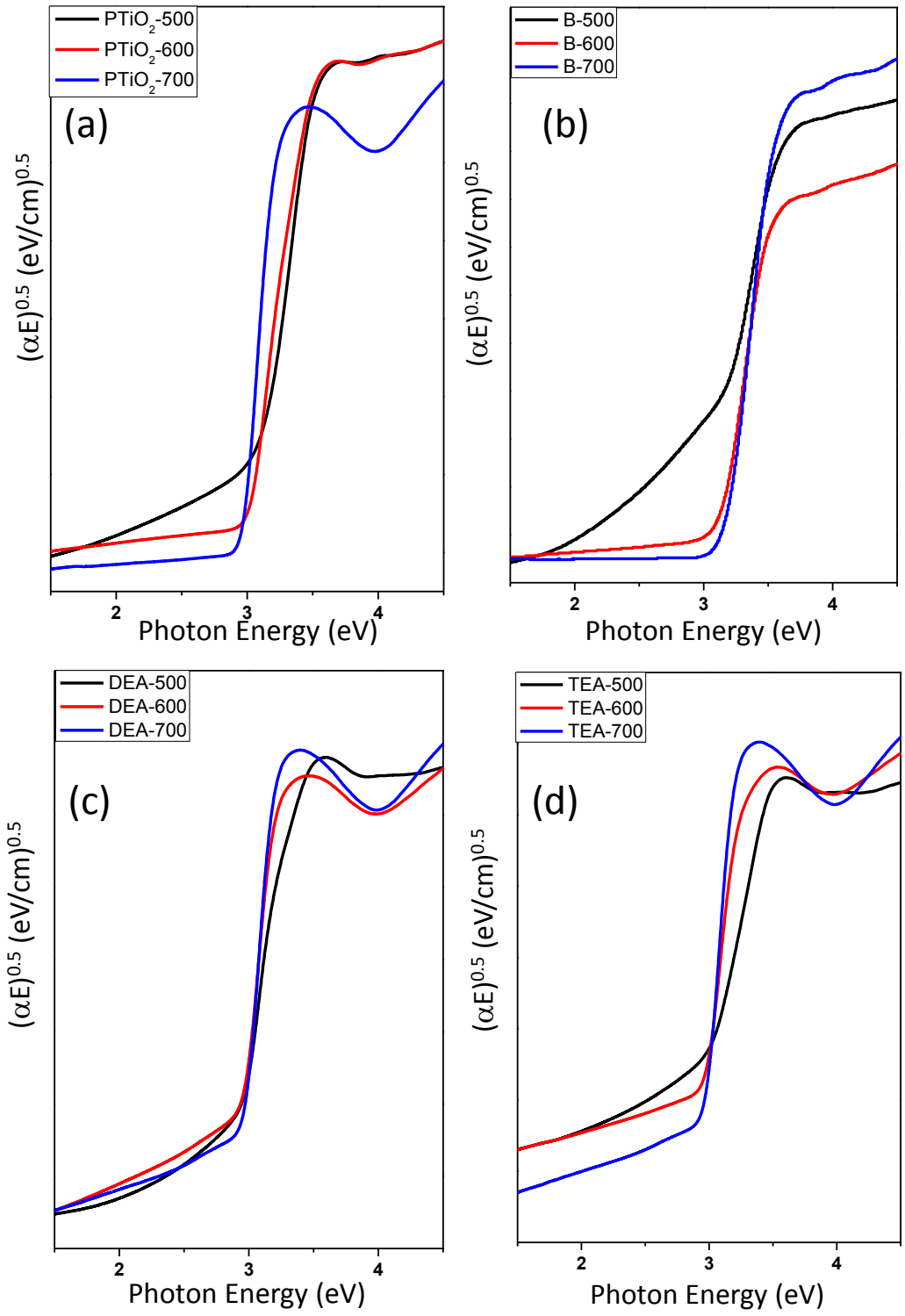

Figure 28. Tauc plots of (a) pure TiO_2 (b) B/TiO_2 (c) DEA/TiO_2 (d) TEA/TiO_2 after calcination in air between 500 to 700 ^{o}C for the indirect band gap calculations.

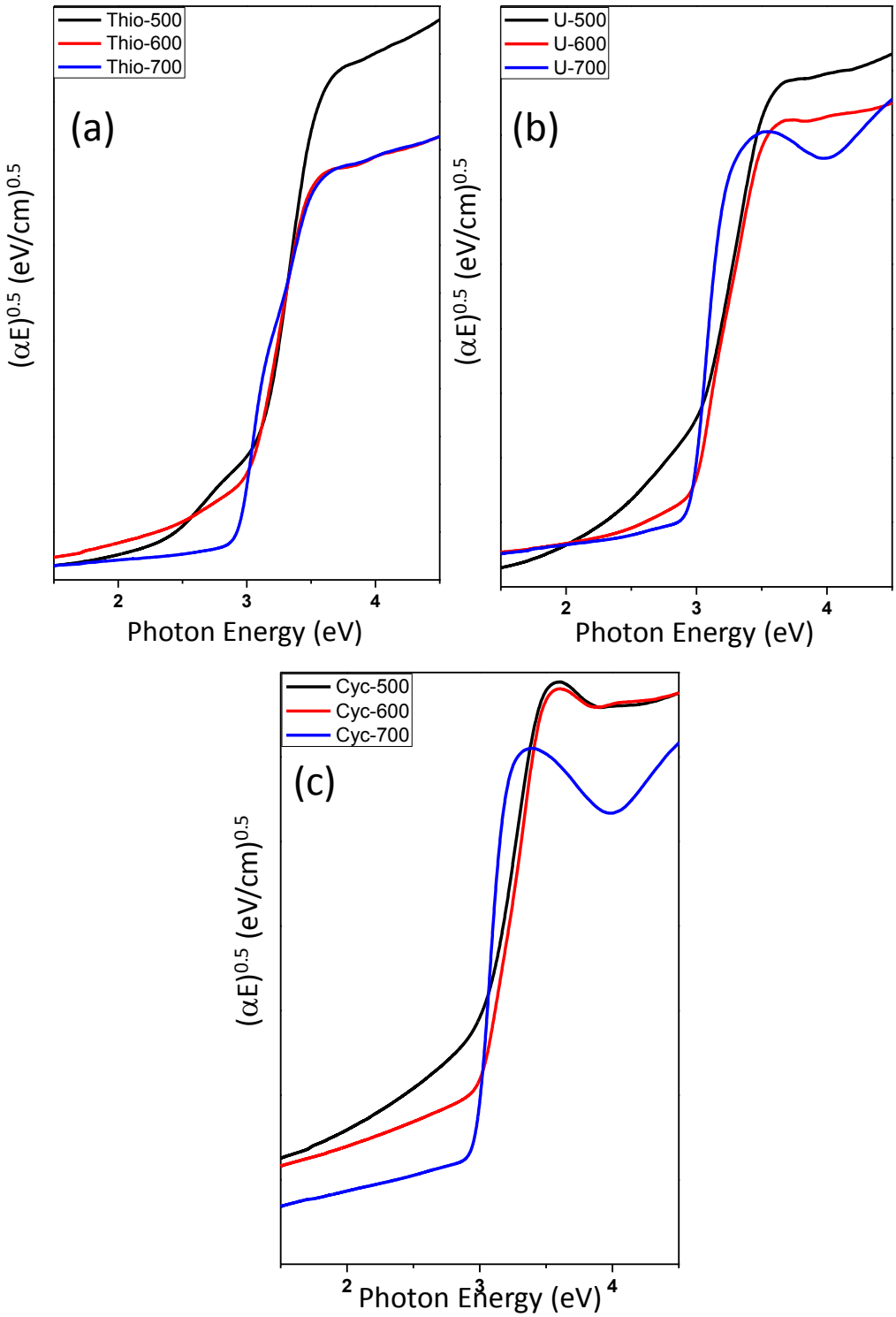

Figure 29. Tauc plots of of (a) Thio/TiO_2 (b) U/TiO_2 (c) Cyc/TiO_2 after calcination in air between 500 to 700 ^{o}C for the indirect band gap calculations.

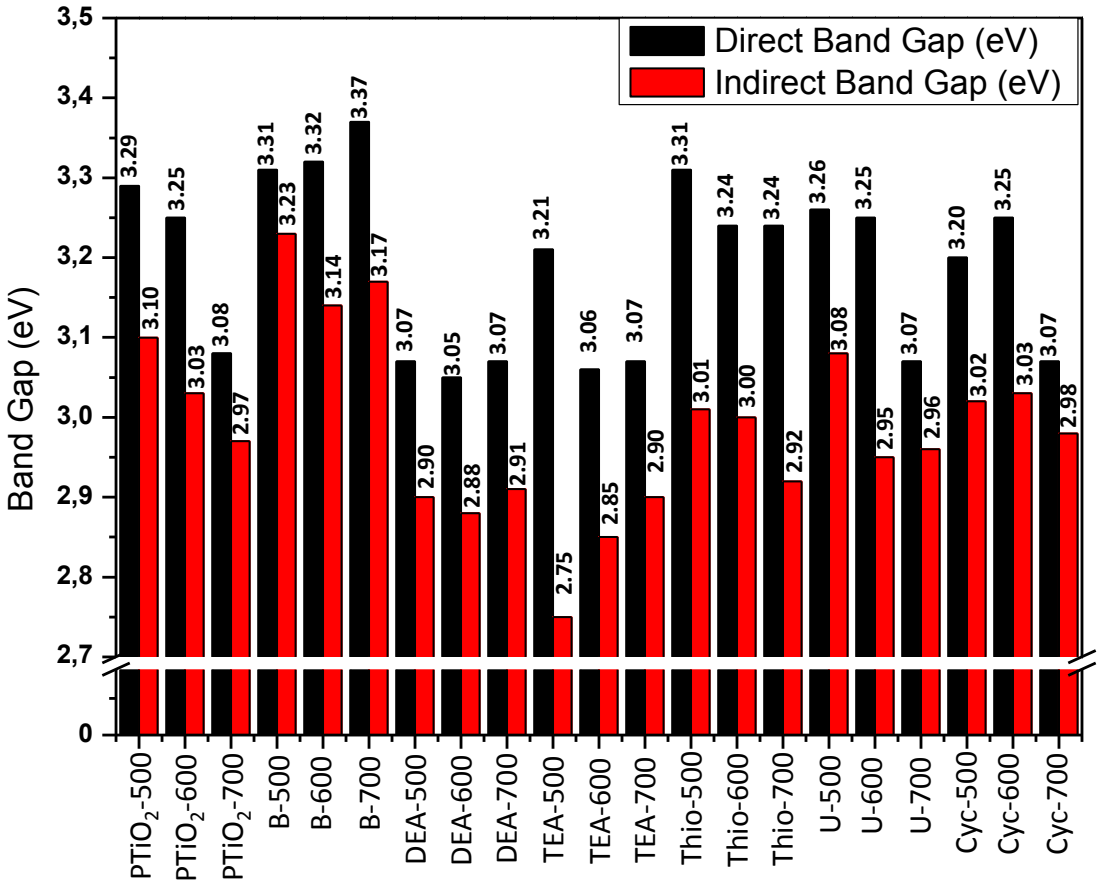

Figure 30. Calculated direct and indirect band gap values of pure TiO_2, B/TiO_2, DEA/TiO_2, TEA/TiO_2, $Thio/TiO_2$, U/TiO_2, Cyc/TiO_2 after calcination in air between 500 to 700 ^oC.

3.2 Photocatalytic Activity Measurements

The photocatalytic activity of the materials was investigated using the degradation of an organic pollutant (Rhodamine B) in liquid phase under visible light illumination.

3.2.1 Construction of Calibration Curves

A calibration curve was used to determine the concentration of an unknown sample solution. The curve was constructed by measuring the concentration and absorbance of several prepared solutions, called calibration standards. To be able to follow the degradation patterns of photocatalysts, it is crucial to prepare a good

calibration curve with different concentrations of Rhodamine B dye. The stock solution (40 mg/L) was prepared by dissolving 10 mg of Rhodamine B dye in 250 mL of deionized water and 22 different concentrations of Rh B solution are prepared. In Figure 31a, UV-VIS absorption spectra of different calibration solutions with varying concentrations are given. These absorbance values at 553 nm are used to construct the calibration curve in Figure 31b, giving a linear plot of absorbance versus concentration with R^2 = 0,9997. By determining the mathematical form of this calibration curve, concentration of a degraded Rh B solution with photocatalyst at a specific time is easily calculated.

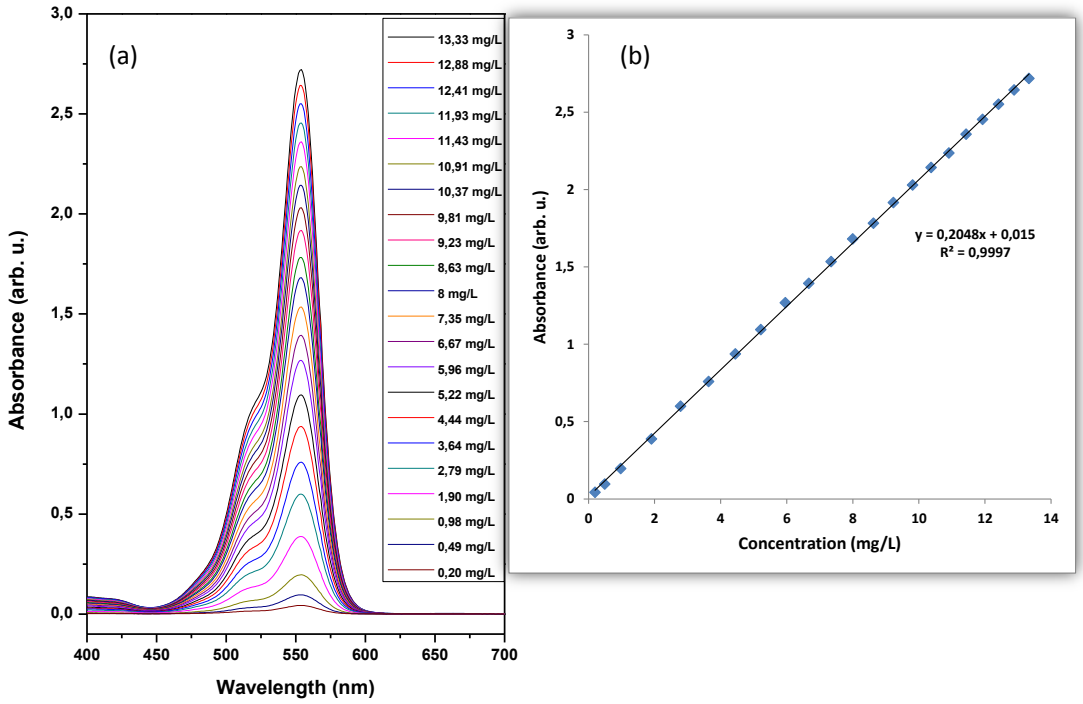

Figure 31. (a) UV-VIS spectra of Rh B solutions with different concentrations (b) calibration curve constructed from part(a) using Beer-Lambert Law.

3.2.2 Photosensitization and Photolysis (Self-Degradation) of Rhodamine B Dye

In order to understand the true photocatalytic activity of a photocatalyst in liquid phase experiments where a dye is used as an exemplary pollutant, one should choose a non-degradable, stable dye that is unaffected by the light source.

Figure 32a shows the UV-VIS spectra of 10 mg/L Rh B degradation in 320 minutes of visible light illumination in the absence of any photocatalyst. In Figure 32b, it can be seen that only 22% of the dye is degraded after 320 minutes of illumination. This percentage may seem high, but it is observed that the best photocatalysts completely degrade the dye in the first 110 minutes at which Rh B self-photolysis is only 5%. Therefore, it is concluded that Rhodamine B dye is sufficiently stable in visible range for the catalysts families used in the current work. This result is also in agreement with many research groups confirming that Rhodamine B dye has a very low self degradation percentage under visible light for about 100 minutes of illumination [149], [150].

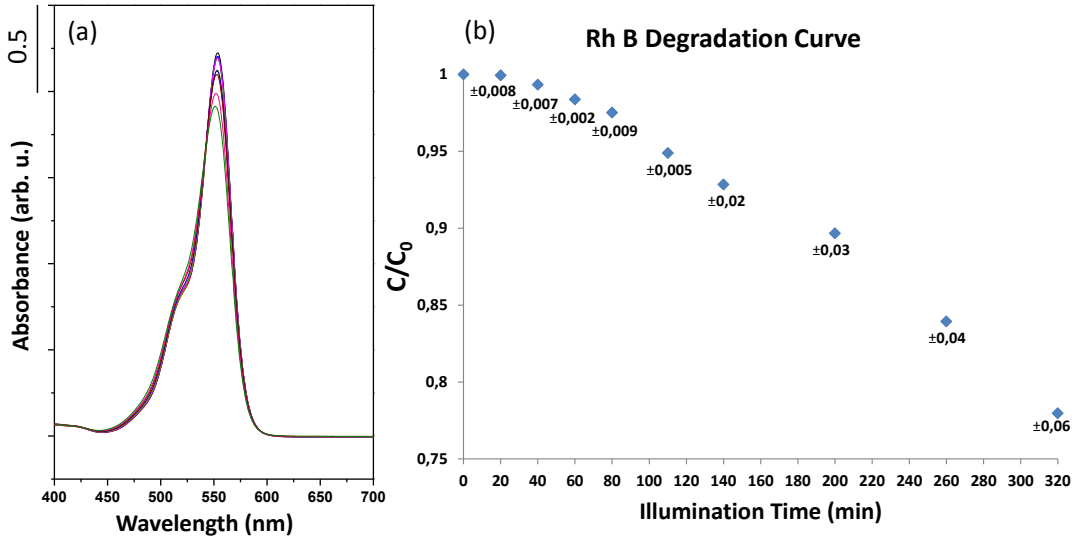

Figure 32. (a) UV-VIS spectral changes of 10 mg/L Rh B solution without any catalyst under visible light over 320 minutes of illumination (b) C/C_0 vs time graph of (a) with standard deviation values.

Another process that should be considered is photosensitized mechanism of the dye. It is well-known that Rhodamine B dye can absorb the visible light in the range 460-600 nm, as it is seen in Figure 32a. Namely in that region, Rhodamine B absorbs the incident photon flux, then the photogenerated electrons are transferred to the excited state of the dye owing to the intramolecular $\pi -> \pi^*$ transition. The photoelectrons of the excited state are immediately injected into the conduction band of the titania forming oxygen radicals that lead to the mineralization of the dye [150]. However, photocatalytic degradation process is the predominant process among them

as Fu et al. [150] suggests, since photosensitization process can only occur when λ>470 nm. In addition, strong adsorption of the dye to the titania surface is desired for fast and efficient injection, but in our study, an average of 1% of loss in the concentration of Rh B solution in the presence of prepared catalysts after one hour of dark mixing was observed. However, this loss is higher in the case of P25, probably implying that photosensitization mechanism may contribute highly to the degradation process.

3.2.3 Control Experiments Using Degussa P25 Commercial Benchmark Photocatalyst

In all of the photocatalytic activity tests, commercially available Degussa P25 mixed phase titania was utilized as the benchmark (i.e. control experiment). In Figure 33, UV-VIS absorption spectra of 10 mg/L Rh B degradation with P25 catalyst are shown. Early studies on the Rhodamine B photodegradation mechanism showed that hypsochromic shift (blue shift; change of spectral band position to a shorter wavelength) of the absorbance peak observed during degradation process was caused by stepwise de-ethylation of Rhodamine B (Figure 34) [151], [152]. The fully de-ethylation of Rh B is complete when the major peak is shifted to 504-506 nm [150]. The changes of absorbance and the shift of the absorption wavelength during the photocatalytic degradation of Rhodamine B under VIS-light illumination can be clearly seen in Figure 33, which indicates that the diminution of the absorbance was simultaneous with the hypsochromic shift in the maximum absorbance. The attenuation of absorbance was mainly related to the destruction of the Rhodamine B chromogen.

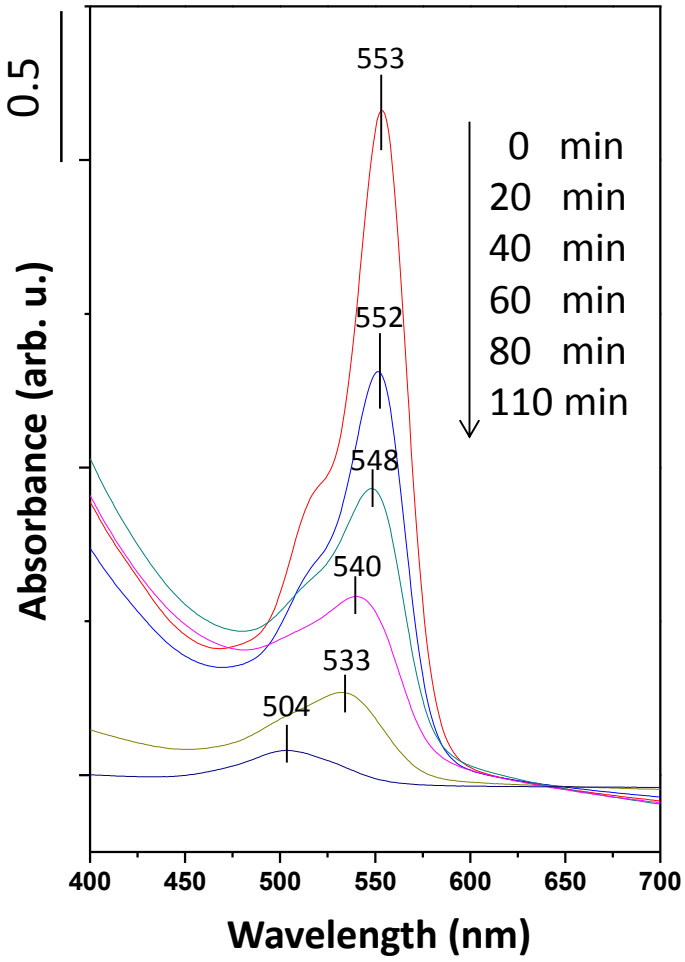

Figure 33. UV-VIS spectral changes of 10 mg/L Rh B solution in the presence of 50 mg Degussa P25 catalyst under visible light.

Although the designed system for photocatalytic activity tests has 10 different reaction cells, only 4 of them, namely B1, B2, C2 and D2 were decided to be used. Figure 35a shows the C/C_0 vs time graph of Rh B degradation curve in the presence of Degussa P25. Initial adsorption of the dye on Degussa P25 photocatalyst surface was around 3%. Rhodamine B solution was completely degraded in 110 minutes under visible light illumination. Figure 35b shows pseudo first order kinetics of the degradation. The determined reaction rate constants (k) were 0.0275, 0.0312, 0.0333 and 0.0253 min^{-1}, respectively, for B1, B2, C2 and D2 cells. These reaction rate constants give an average first order rate constant of 0.02765 min^{-1} for the degradation of Rh B in the presence of Degussa P25.

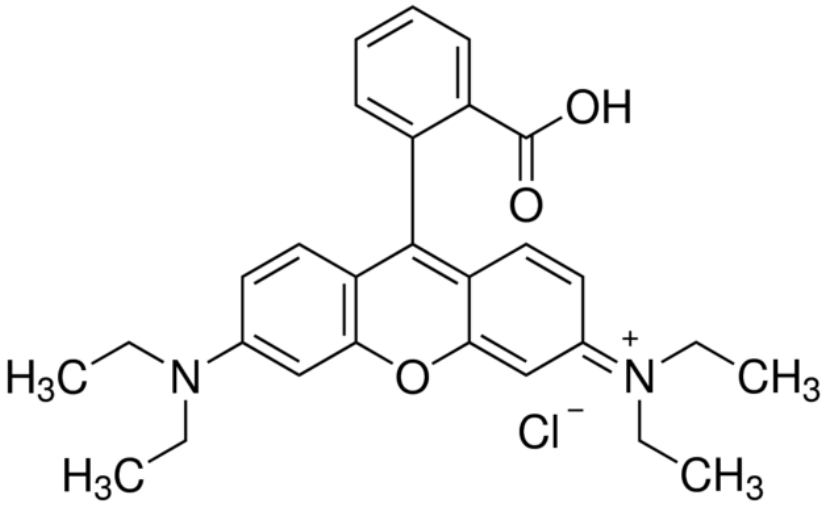

Figure 34. Structure of Rhodamine B dye.

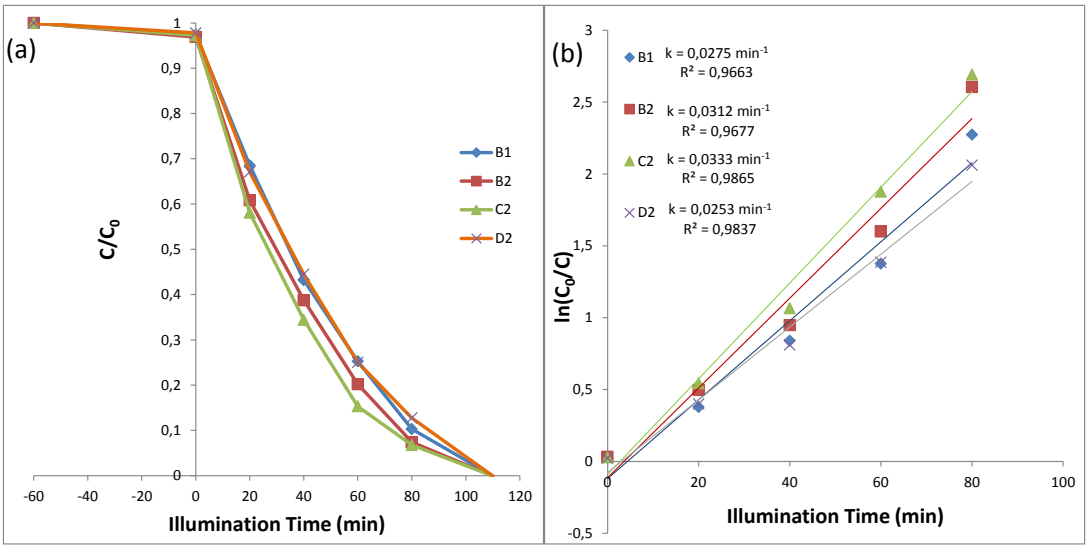

Figure 35. (a) Photodegradation curves of 10 mg/L Rh B solution in the presence of 50 mg Degussa P25 catalyst under visible light on different reaction cells (b) First-order reaction rate calculations of part(a).

3.2.4 TiN, TiC and TiS_2 Doped Titania

Figure 36a illustrates the C/C_0 vs time graphs of Rh B degradation in the presence of pure TiO_2 synthesized and calcined in air between 500-800^oC for 1 h. In Figure 35b, pseudo first order rate constants are shown. At 500^oC, sample shows the highest degradation rate constant of 0.0195 min^{-1}, compared to other calcination temperatures. Magnitude of this large rate constant is presumably related to the high

surface area of the sample which is 97 m^2/g. As the surface area diminishes to 17 m^2/g at 600°C, so does the rate constant to 0.0148 min^{-1}. TiO_2-700 shows the lowest rate constant among all. High rutile formation at 800°C compensates the low surface area in reaction rate constant, therefore the reaction constant that is 0.0144 min^{-1} is as high as TiO_2-600's.

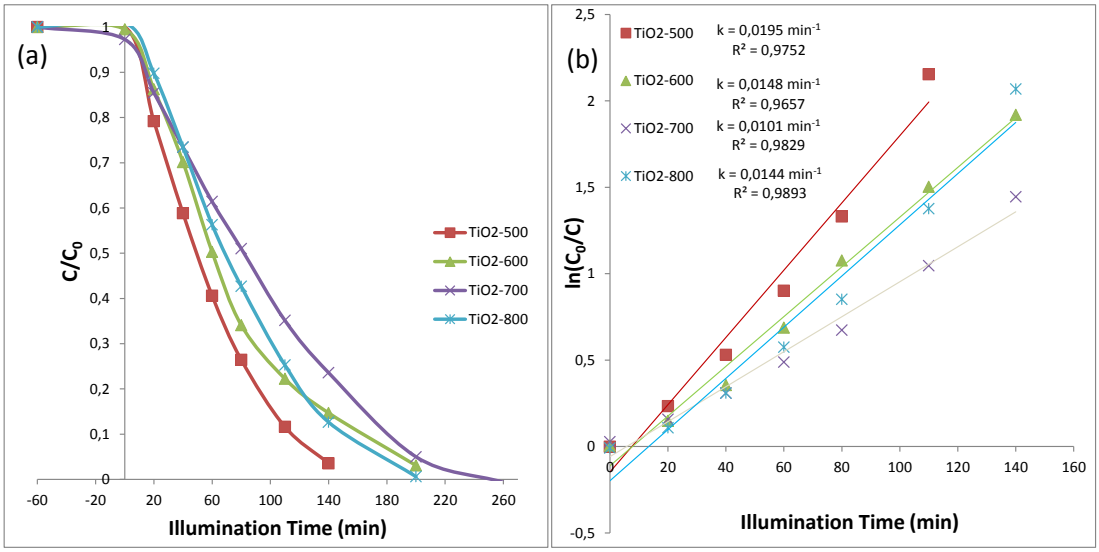

Figure 36. (a) Photodegradation curves of 10 mg/L Rh B solution in the presence of 50 mg pure titania catalysts synthesized and calcined at 500 to 800 °C, under visible light. (b) First-order reaction rate constant calculations for the data given in panel (a).

Figure 37a illustrates the C/C_0 vs time graphs of Rh B degradation in the presence of N/TiO_2 synthesized and calcined in air between 450-800°C for 1 h and in panel (b) pseudo first order rate constants are shown. N/TiO_2-500 has completely degraded Rh B in 110 minutes, c.a. 30 min earlier than the TiO_2-500 and with a higher rate constant compared to Degussa P25. Although the surface area is 25 m^2/g smaller compared to TiO_2-500, N/TiO_2-500 showed a high rate constant of 0.0345 min^{-1}, which is related to the effect of N dopant atoms incorporated in titania lattice. As the calcination temperature increases, surface area and anatase mass fraction decrease, lattice becomes more compact and impurity nitrogen atoms may leave the solid, as a result the rate constant diminishes to 0.0121 min^{-1}.

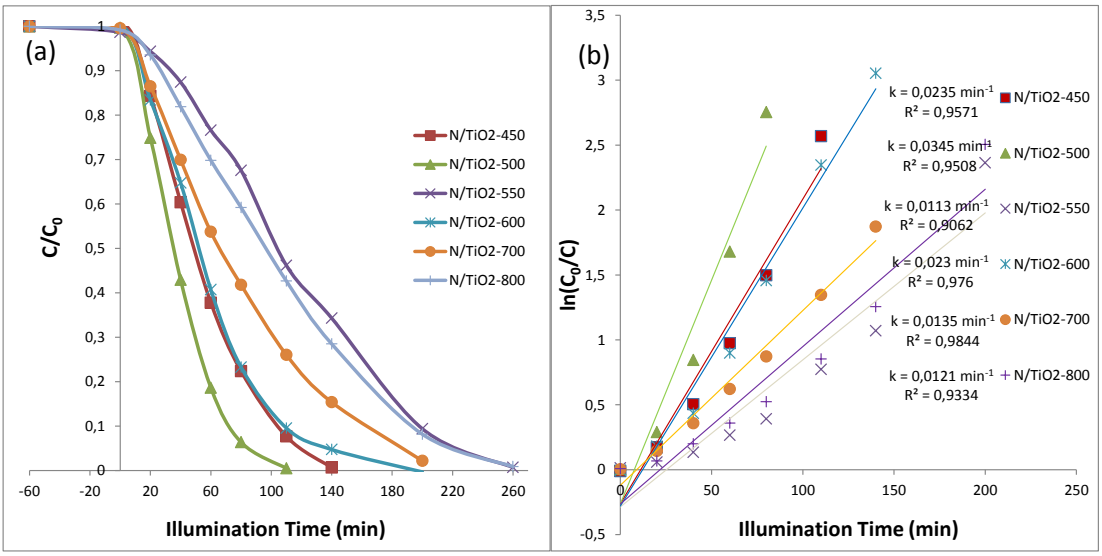

Figure 37. (a) Photodegradation curves of 10 mg/L Rh B solution in the presence of 50 mg N/TiO_2 catalysts synthesized and calcined at 450 to 800 ^oC, under visible light. (b) First-order reaction rate constant calculations of part (a).

Figure 38a illustrates the C/C_0 vs time graphs of Rh B degradation in the presence of C/TiO_2 synthesized and calcined in air between 450-800^oC for 1 h and in panel (b) pseudo first order rates are shown. Both samples calcined at 450 and 500^oC degraded Rh B in 140 minutes, same as the undoped case, but since TiO_2-500 fits better to logarithmic degradation curve compared to TiC doped one, the rate constants of C/TiO_2-450 and C/TiO_2-500 are lower (0,0158 min^{-1}) than TiO_2-500's (0.0196 min^{-1}). Although C/TiO_2-600 clears the dye solution in 200 min, the rate constant is the highest among TiC doped samples which is 0.0169 min^{-1}. In this case it can be said that the highest degradation rate is achieved by the mixture of relatively high surface area (56 m^2/g) and crystal structure having high anatase-low rutile mass fractions (90.48% A, 9.52% R).

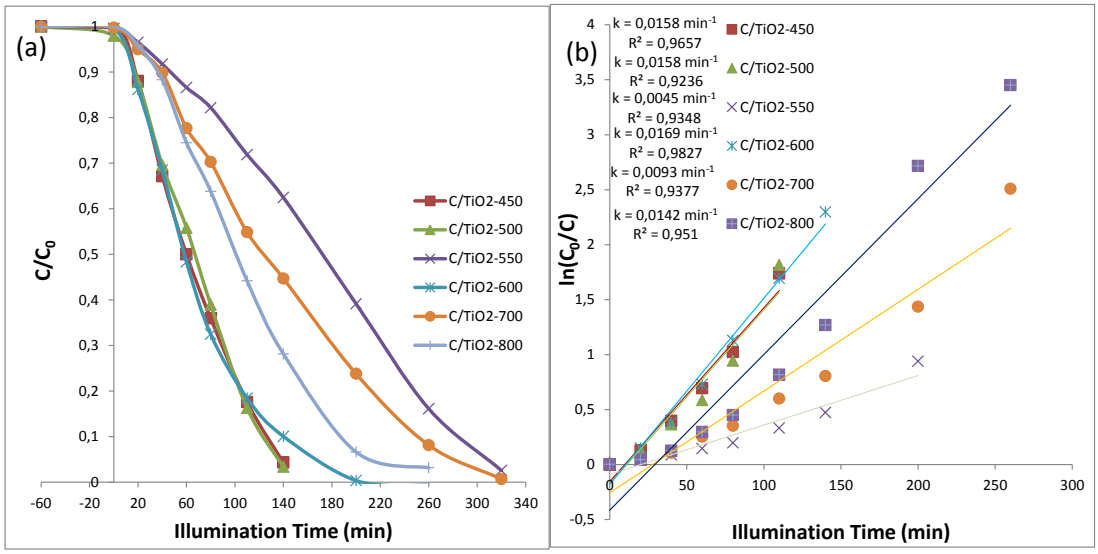

Figure 38. (a) Photodegradation curves of 10 mg/L Rh B solution in the presence of 50 mg C/TiO_2 catalysts synthesized and calcined at 450 to 800 ^oC, under visible light. (b) First-order reaction rate constant calculations of part(a).

Figure 39a illustrates the C/C_0 vs time graphs of Rh B degradation in the presence of S/TiO_2 synthesized and calcined in air between 450-800^oC for 1 h and in panel (b) pseudo first order rate constants are shown. As for the S doped TiO_2, the highest rate constant is 0.0144 min^{-1}, quite low even compared to the undoped case. Even though S/TiO_2-500 has the highest surface area among all the doped and undoped samples, it is surprising that the sample has a relatively low rate constant of 0.0103 min^{-1}. Therefore it is concluded that sulfur doping may not be efficient for this synthesis protocol.

Figure 40 illustrates the relationship between rate constants and calcination temperatures for all the samples discussed above.

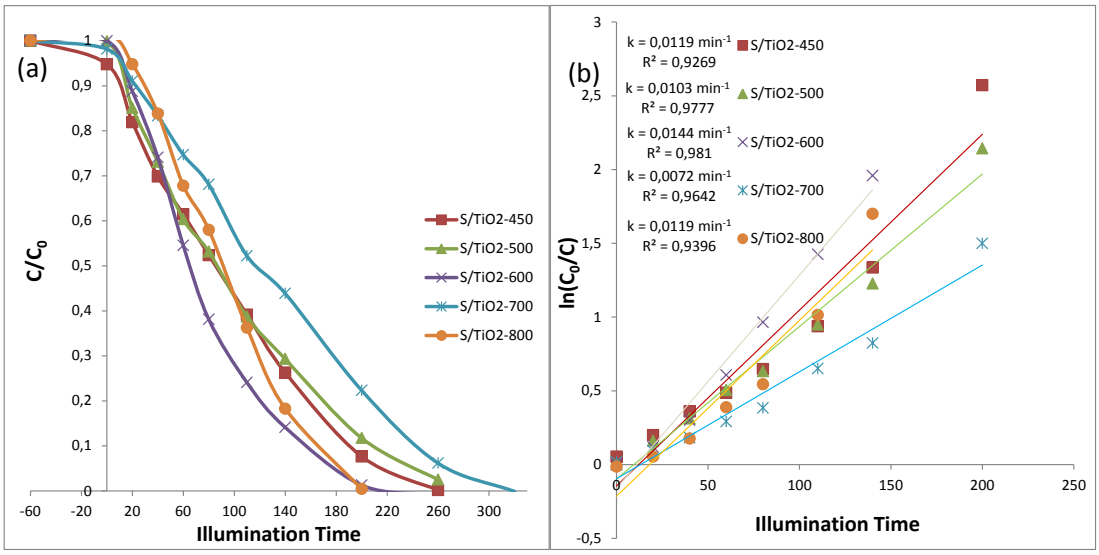

Figure 39. (a) Photodegradation curves of 10 mg/L Rh B solution in the presence of 50 mg S/TiO_2 catalysts synthesized and calcined at 450 to 800 ^oC, under visible light (b) First-order reaction rate constant calculations of part(a).

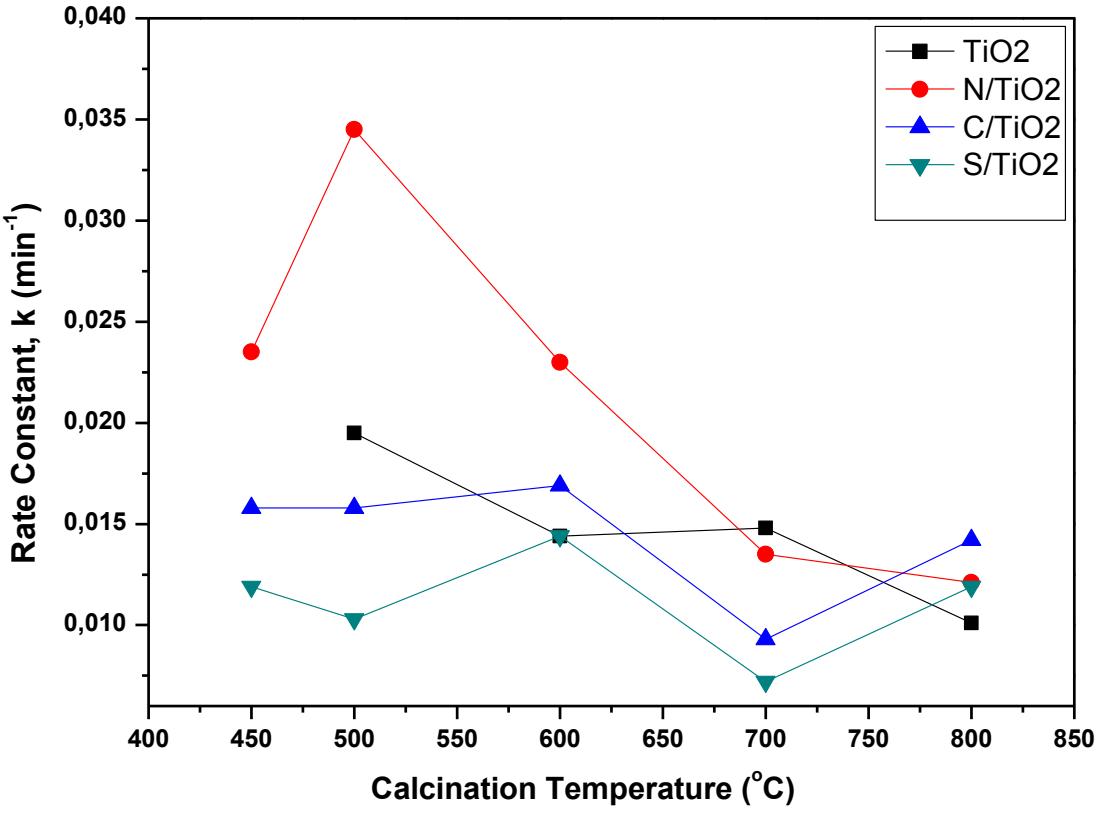

Figure 40. Graph relating calcination temperatures to photocatalytic RhB degradation rate constants for pure TiO_2, TiN doped TiO_2 (N/TiO_2), TiC doped TiO_2 (C/TiO_2), TiS_2 doped TiO_2 (S/TiO_2)

3.1.1 Partial Oxidation of TiN, TiC and TiS_2 By Annealing

Figure 41a illustrates the C/C_0 vs time graphs of Rh B degradation in the presence of commercially available TiN powder calcined in air between 350-800^oC for 1 h and in panel (b) pseudo first order rate constants are shown. Best working sample is TiN-600, which is a mixture of rutile TiO_2 and unoxidized TiN powder and it has a 0,0110 min^{-1} reaction rate constant. As the calcination temperature is increased to 700 ^oC, TiN is completely oxidized to rutile TiO_2 and the reaction rate constant is decreased to 0.0042 min^{-1}.

Figure 42a illustrates the C/C_0 vs time graphs of Rh B degradation in the presence of commercially available TiC powder calcined in air between 350-800^oC for 1 h and in panel (b) pseudo first order rate constants are shown. Best working sample is TiC-500, which is a mixture of rutile TiO_2 and unoxidized TiC powder and it has a 0.0119 min^{-1} reaction rate constant. As the calcination temperature increases, TiC is also completely oxidized to rutile TiO_2 and the reaction rate constant drastically decreases.

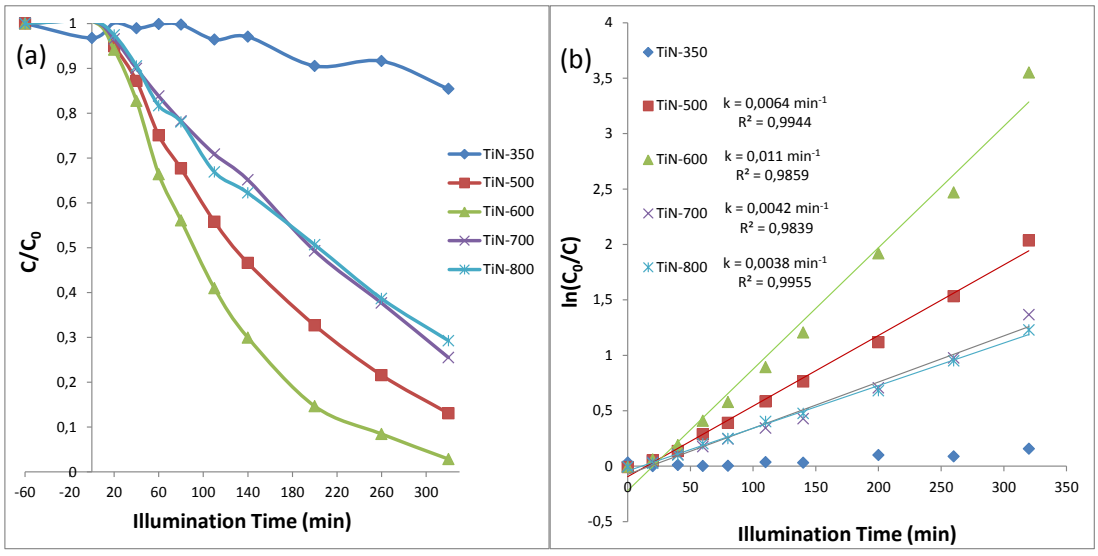

Figure 41. (a) Photodegradation curves of 10 mg/L Rh B solution in the presence of 50 mg TiN powders calcined at 350 to 800 ^oC, under visible light. (b) First-order reaction rate constant calculations of part(a).

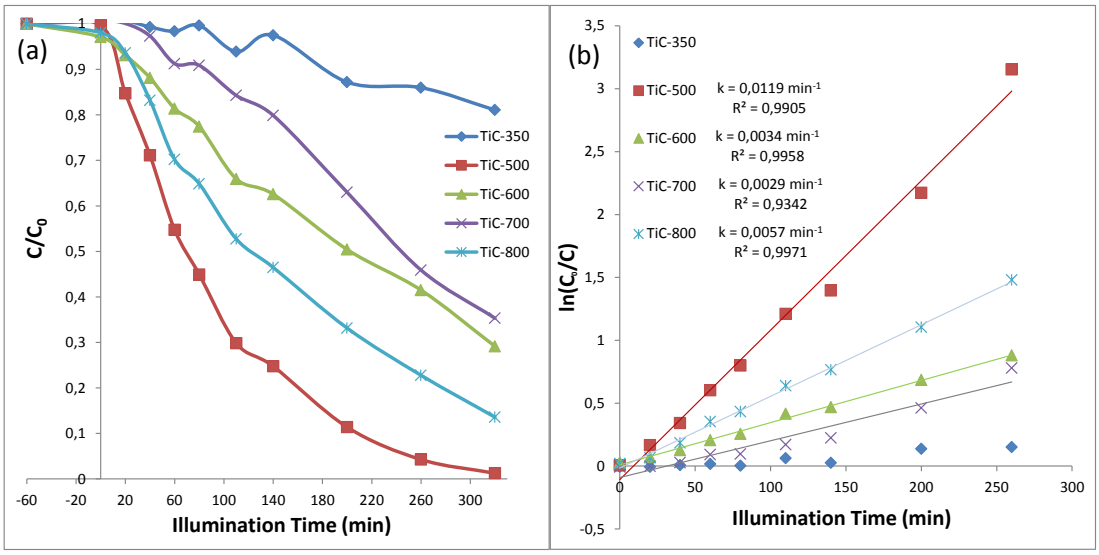

Figure 42. (a) Photodegradation curves of 10 mg/L Rh B solution in the presence of 50 mg TiC powders calcined at 350 to 800 ^{o}C, under visible light. (b) First-order reaction rate constant calculations of part(a).

Figure 43a illustrates the C/C_0 vs time graphs of Rh B degradation in the presence of commercially available TiS_2 powder calcined in air between 350-800^{o}C for 1 h and in panel (b) pseudo first order rate constants are shown. Up to 800 ^{o}C, reaction rate constant does not change. Best working sample is TiS_2-800 with a reaction constant of 0.0134 min^{-1}, which is a mixture of anatase and rutile TiO_2.

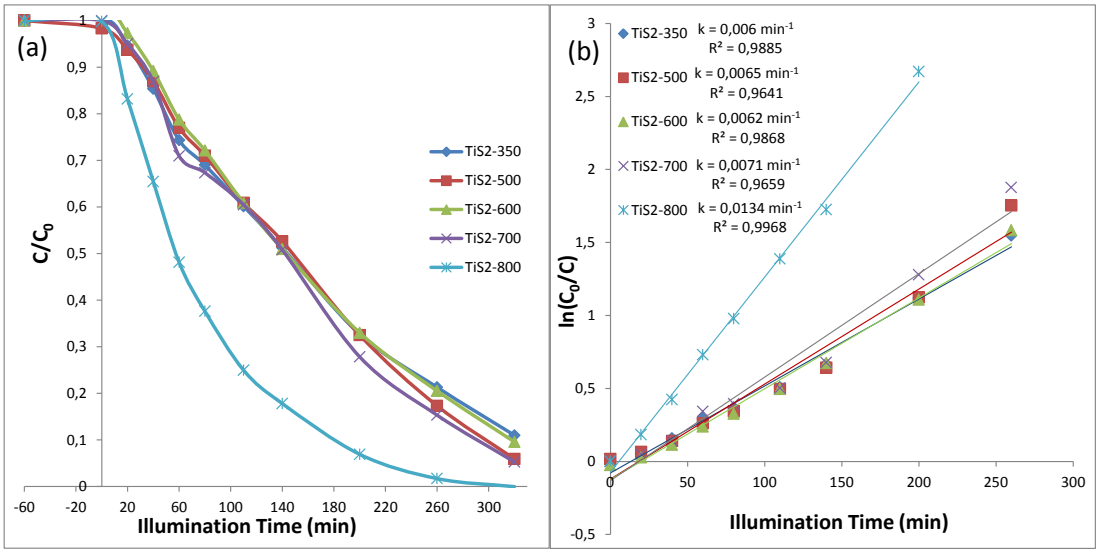

Figure 43. (a) Photodegradation curves of 10 mg/L Rh B solution in the presence of 50 mg TiS_2 powders calcined at 350 to 800 ^{o}C, under visible light. (b) First-order reaction rate constant calculations of part(a).

In summary, annealed powders are not as good as sol gel prepared doped samples in liquid phase degradation of Rh B even though the calculated indirect band gaps are closer to the visible range.

3.1.2 Non-Metal Compound Doped Titania

Figure 44a illustrates the C/C_0 vs time graphs of Rh B degradation in the presence of pure TiO_2 synthesized and calcined in air between 150-700^oC for 2 h and in panel (b) pseudo first order rate constants are shown. At 600^oC, sample shows the lowest degradation rate constant of 0.0034 min^{-1}, compared to other calcination temperatures. Titania synthesized via this synthesis protocol has a very low surface area, therefore the degradation rates are very low for most of the samples. The best working one is $PTiO_2$-350, which is in anatase form.

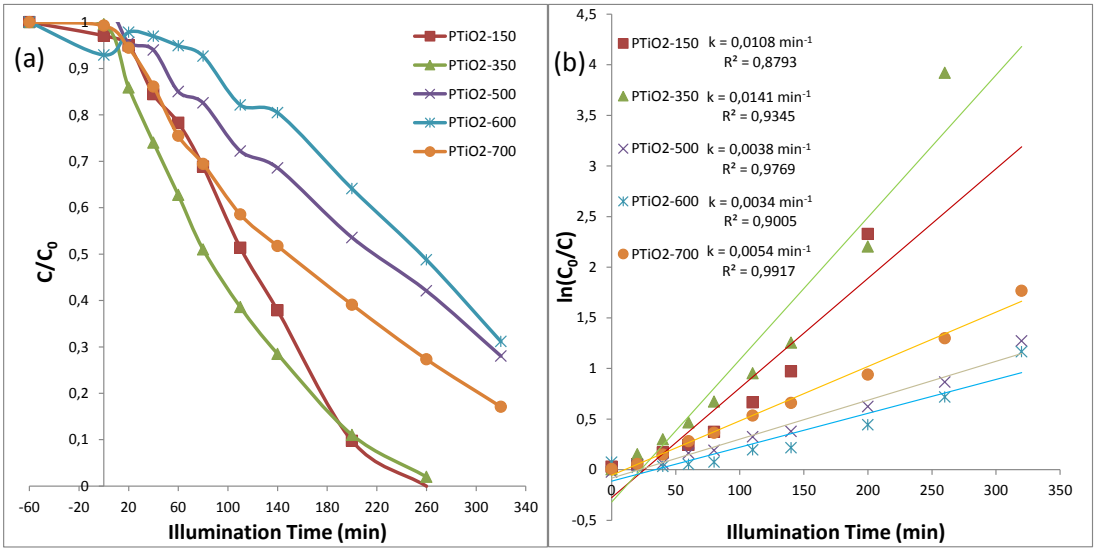

Figure 44. (a) Photodegradation curves of 10 mg/L Rh B solution in the presence of 50 mg $PTiO_2$ catalysts synthesized and calcined at 150 to 700 ^oC, under visible light. (b) First-order reaction rate constant calculations of part(a).

Figure 45a illustrates the C/C_0 vs time graphs of Rh B degradation in the presence of B-TiO_2 synthesized and calcined in air between 150-700^oC for 2 h and in panel (b) pseudo first order rate constants are shown. At 500^oC, sample shows the highest degradation rate constant of 0.0437 min^{-1}, compared to other calcination temperatures and sample groups. B-TiO_2 degrades the dye completely in 80 min, half an hour earlier than P25 and with a rate constant almost twice as big as P25. One

possible explanation for this high activity can be attributed to the high specific surface area (70 m^2/g) caused by small crystallite size that can be observed in XRD pattern. Crystallite growth is hindered due to high level of boron impurity atoms confirmed with sassolite peak in XRD pattern. Small crystal size may also affect the average indirect band gap calculations, giving a very high indirect band gap for that sample due to quantum size effect.

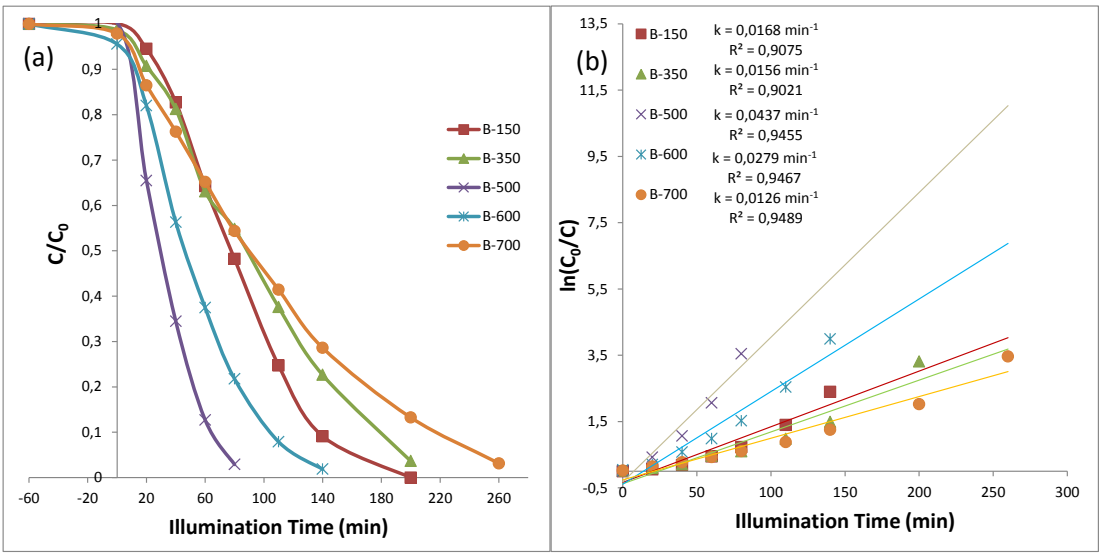

Figure 45. (a) Photodegradation curves of 10 mg/L Rh B solution in the presence of 50 mg B/TiO_2 catalysts synthesized and calcined at 150 to 700 ^oC, under visible light (b) First-order reaction rate constant calculations of part(a).

Figure 46a illustrates the C/C_0 vs time graphs of Rh B degradation in the presence of DEA-TiO_2 synthesized and calcined in air between 150-700^oC for 2 h and in panel (b) pseudo first order rates are shown. At 500^oC, sample shows the highest degradation rate constant of 0.0162 min^{-1}, compared to other calcination temperatures. DEA-TiO_2 does not seem to enhance the activity as boron addition does.

Figure 47a illustrates the C/C_0 vs time graphs of Rh B degradation in the presence of TEA-TiO_2 synthesized and calcined in air between 150-700^oC for 2 h and in panel (b) pseudo first order rate constants are shown. At 500^oC, sample shows the highest degradation rate constant of 0.0237 min^{-1}, compared to other calcination temperatures. Although it is not as effective as boron addition, TEA addition is increased the activity compared to the undoped titania.

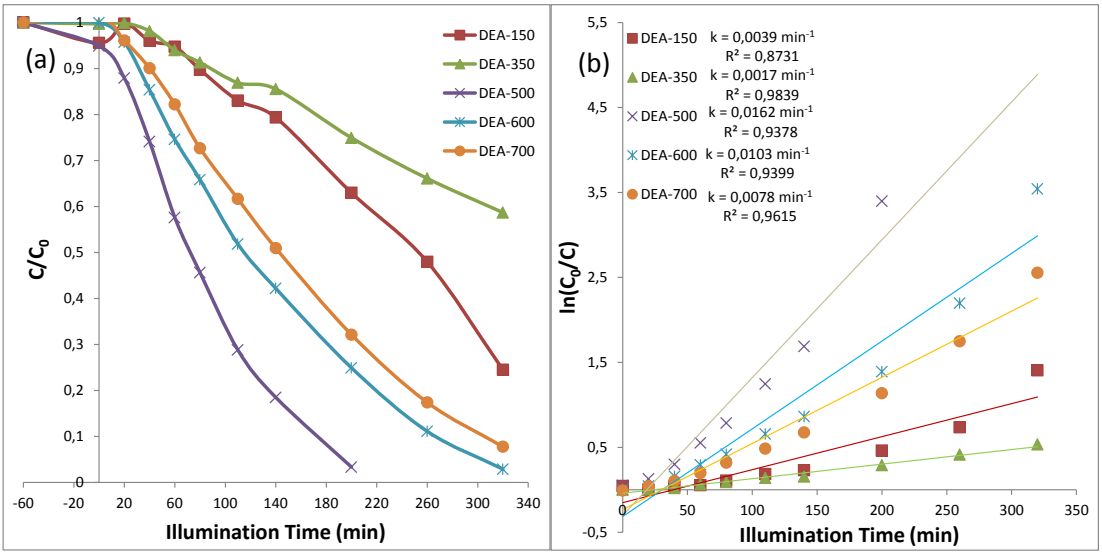

Figure 46. (a) Photodegradation curves of 10 mg/L Rh B solution in the presence of 50 mg DEA/TiO_2 catalysts synthesized and calcined at 150 to 700 ^oC, under visible light. (b) First-order reaction rate constant calculations of part(a).

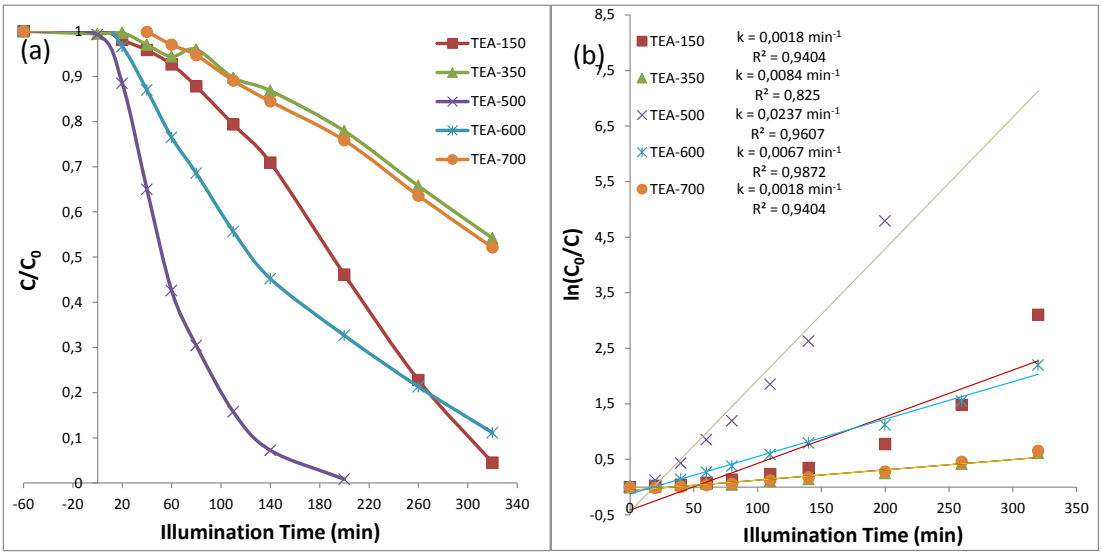

Figure 47. (a) Photodegradation curves of 10 mg/L Rh B solution in the presence of 50 mg TEA/TiO_2 catalysts synthesized and calcined at 150 to 700 ^oC, under visible light. (b) First-order reaction rate constant calculations of part(a).

Figure 48a illustrates the C/C_0 vs time graphs of Rh B degradation in the presence of Thio-TiO_2 synthesized and calcined in air between 150-700^oC for 2 h and in panel (b) pseudo first order rate constants are shown. At 500^oC, sample shows the

highest degradation rate constant of 0.0245 min^{-1}, compared to other calcination temperatures. Similar to other dopant compounds, thiourea has increased the activity, and it follows the pattern that the best working sample is calcined at 500 ^{o}C.

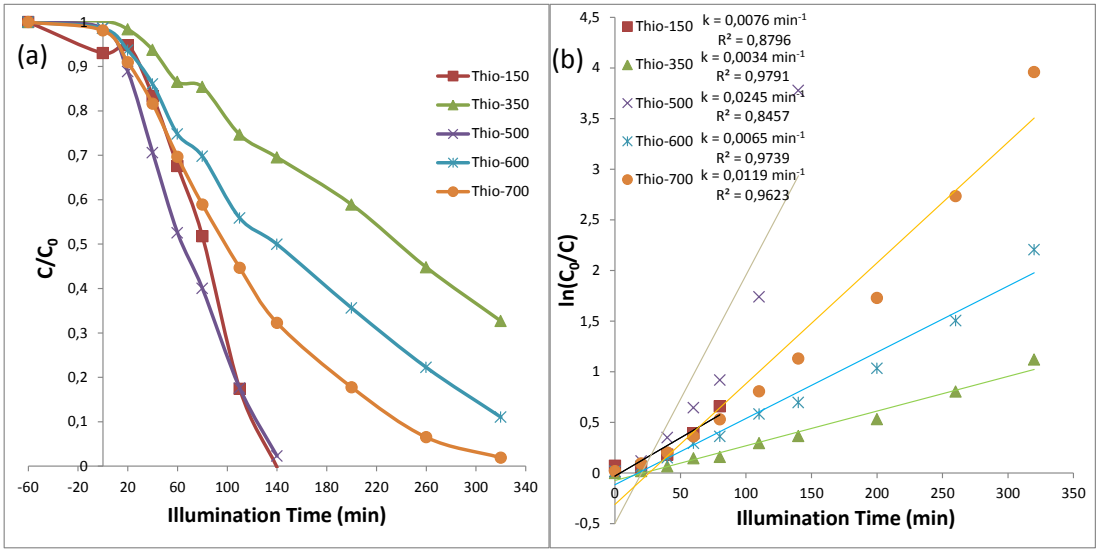

Figure 48. (a) Photodegradation curves of 10 mg/L Rh B solution in the presence of 50 mg Thio/TiO_2 catalysts synthesized and calcined at 150 to 700 ^{o}C, under visible light (b) First-order reaction rate constant calculations of part(a).

Figure 49a illustrates the C/C_0 vs time graphs of Rh B degradation in the presence of U-TiO_2 synthesized and calcined in air between 150-700^{o}C for 2 h and in panel (b) pseudo first order rate constants are shown. At 600^{o}C, sample shows the highest degradation rate constant of 0.0173 min^{-1}, compared to other calcination temperatures. Urea addition does not enhance the activity that much but it still is a better titania catalyst compared to the undoped titania prepared with the same procedure.

Lastly, figure 50a illustrates the C/C_0 vs time graphs of Rh B degradation in the presence of Cyc-TiO_2 synthesized and calcined in air between 150-700^{o}C for 2 h and in panel (b) pseudo first order rate constants are shown. At 600^{o}C, sample shows the highest degradation rate of 0.0135 min^{-1}, compared to other calcination temperatures. Cyclohexanol addition is the worst by far compared to doped titania prepared in this group.

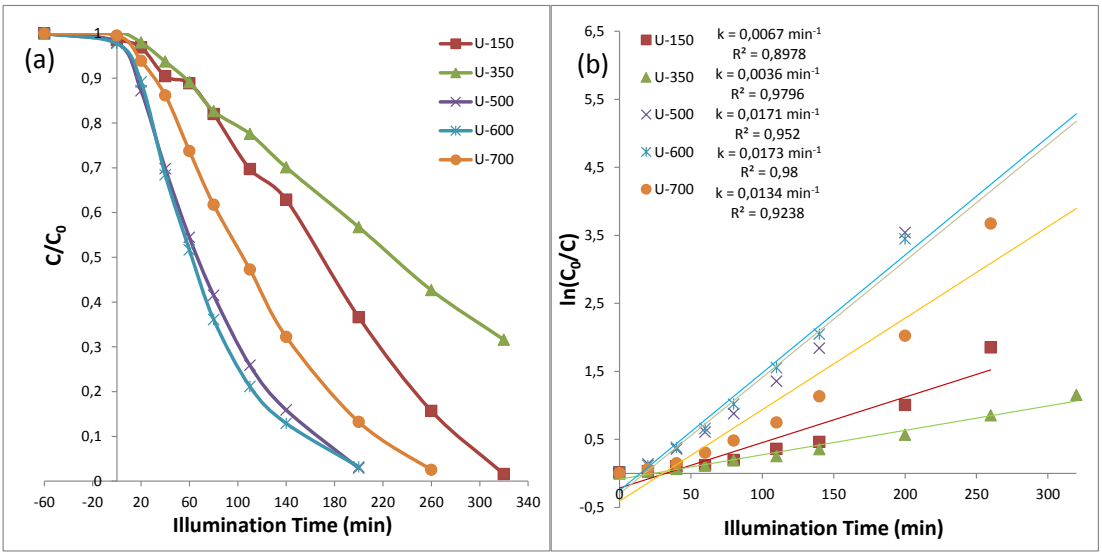

Figure 49. (a) Photodegradation curves of 10 mg/L Rh B solution in the presence of 50 mg U/TiO_2 catalysts synthesized and calcined at 150 to 700 ^oC, under visible light. (b) First-order reaction rate constant calculations of part(a).

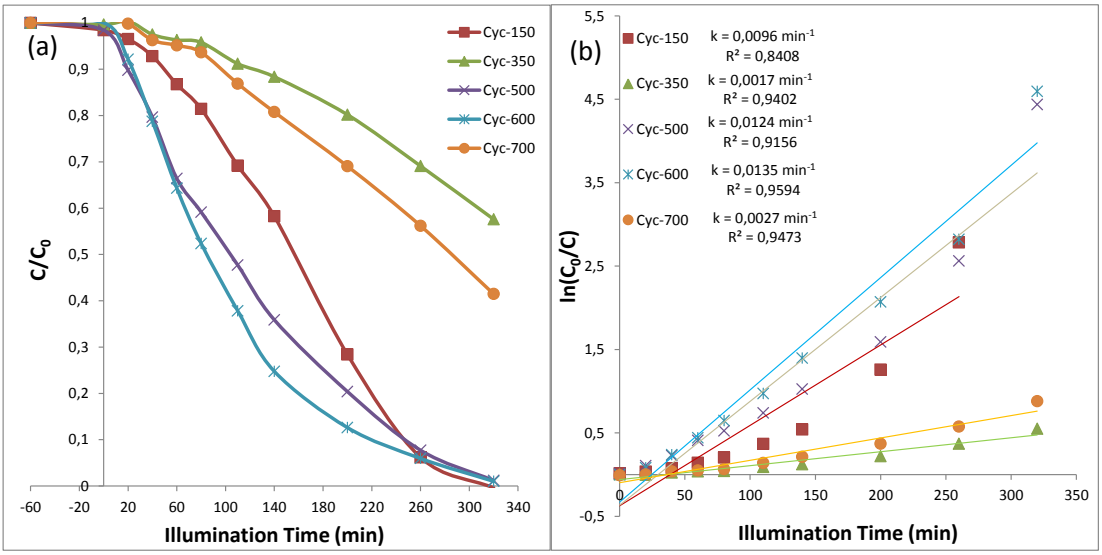

Figure 50. (a) Photodegradation curves of 10 mg/L Rh B solution in the presence of 50 mg Cyc/TiO_2 catalysts synthesized and calcined at 150 to 700 ^oC, under visible light. (b) First-order reaction rate constant calculations of part(a).

In summary, photocatalytic activity of all of the non-metal compound added titania is increased compared to the unmodified sol gel titania due to impurity effect. These impurity states acted as trap states for electron and holes, reducing their recombination rate and therefore increased the utilization of visible illumination.

Although “doping” may not have been effectively taken place, undoubtfully, addition of impurity atoms have increased the photocatalytic activity, especially in boric acid case.

Figure 51 illustrates the relationship between rate constants and calcination temperatures for the samples discussed in the current section.

Finally, Figure 52 shows the performances of the best catalysts that have been investigated in the current work in comparison to the Degussa P25 commercial benchmark catalyst.

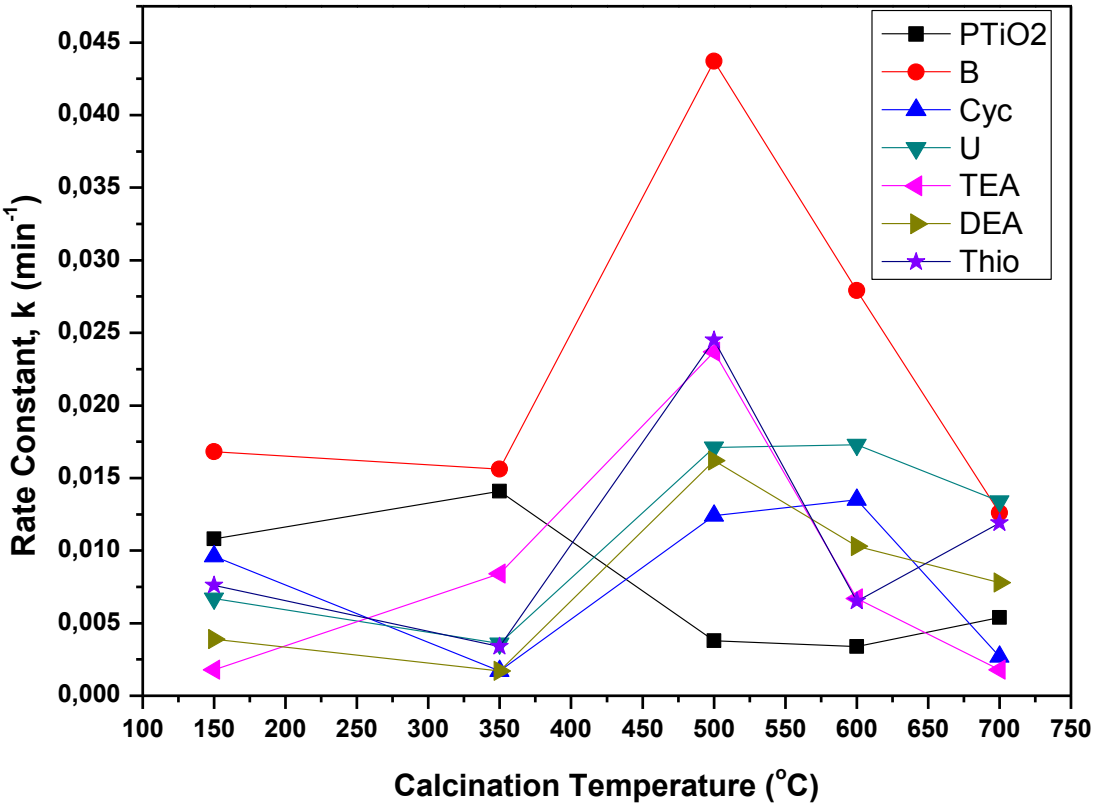

Figure 51. Graph relating calcination temperatures to rate constants for pure TiO_2, B/TiO_2, DEA/TiO_2, TEA/TiO_2, $Thio/TiO_2$, U/TiO_2, Cyc/TiO_2

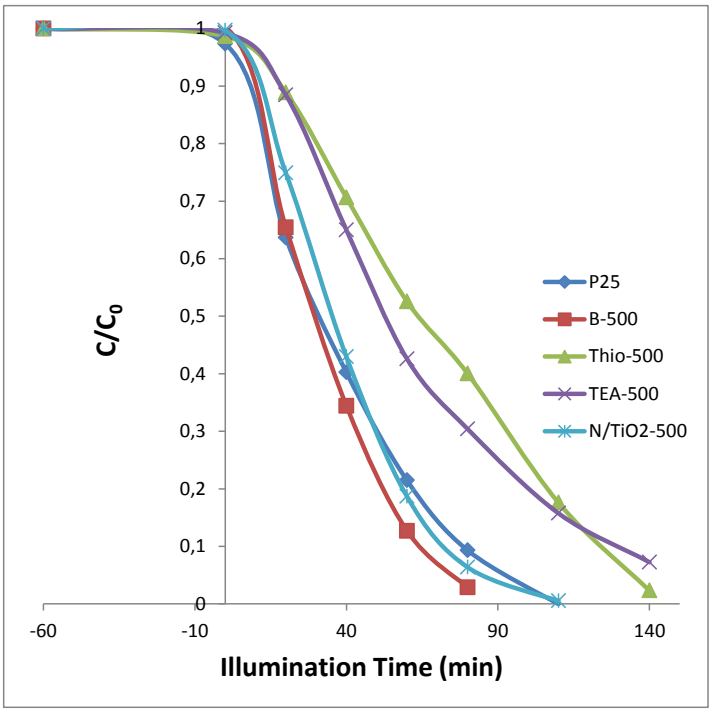

Figure 52. Photodegradation curves of Rh B solution in the presence of the best catalytic materials used in the current study as compared to Degussa P25 commercial benchmark.

4. CONCLUSIONS

In this thesis, a variety of non-metal compound addition to sol-gel synthesis protocol of titanium dioxide has been investigated for the purpose of preparing visible active titanium dioxide powders. This study has been a preliminary work to design a simple, sol-gel synthesis route for the preparation of visible active titanium dioxide to be used in combination with previously designed UV-active titanium dioxide based photocatalytic systems in an attempt to create tandem systems that will harvest both visible and UV light for air purification. Consequently, two different sets of samples were prepared and investigated:

A) The first set of samples was prepared by a sol-gel route with the addition of non metallic compounds of Titanium which are Titanium nitride (TiN), Titanium carbide (TiC) and Titanium Sulfide (TiS_2). Synthesized materials were calcined in air for 1 hour, at different temperatures between 500-800^{o}C. Dopant non-metal atom to titanium mol ratio was kept at 0.1:1 and the syntesized powders were

characterized by XRD, Raman Spectroscopy, BET, UV-VIS DR Spectroscopy to investigate the effect of calcination temperature, surface area and band gap on photocatalytic activity. Besides sol-gel, these commercial powders that were used as dopants, were annealed in open air to prepare partially oxidized titanium materials.

B) Secondly, inexpensive sources of non-metal compounds such as boric acid, diethanolamine (DEA), triethylamine (TEA), thiourea, urea and cyclohexanol were added in a different sol gel synthesis route. Dopant compound to titanium dioxide mol ratio was kept at 0.5:1. Synthesized materials were calcined in air for 2 hours, at different temperatures between 150-700^{o}C. Same characterization methods were used to investigate the same parameters on photocatalytic activity.

Photocatalytic activity measurements were done in liquid phase for the degradation of an organic contaminant, Rhodamine B dye, in a custom-designed VIS-illuminated reaction cells in ambient conditions. Photocatalytic performance of all samples were compared with that of a commercially available Degussa P25 TiO_2 benchmark catalyst.

In the light of the structural characterizations of these samples, it can be concluded that, addition of impurity atoms shifted the anatase to rutile transformation to higher calcination temperatures. Also in the presence of a high concentration of boric acid, sassolite presence in the photocatalyst structure has been detected, which is known to be a grain growth inhibitor. BET analysis showed that photocatalyticaly active materials also typically reveal high surface area values. Indirect band gap calculations showed that band gap values are indirectly proportional to the calcination temperatures. Active materials were also found to reveal high indirect band gap values while materials with low indirect band gap values were found to be inactive. It has been shown that visible light activity of the proposed materials depends on many parameters such as oxygen vacancies that were introduced during doping, particle size and anatase-rutile ratio.

Particularly, two promising visible-light active photocatalytic materials, namely B-500 and N/TiO_2-500 were synthesized, characterized and photocatalytically tested. These systems revealed comparable or better photocatalytic performance compared to Degussa P25 commercial benchmark in the photodegradation of Rh B under Visible illumination. As a future work, the influence of the doping amount will be investigated. Furthermore, these promising VIS-active photocatalysts obtained in the current combinatorial study will be also tested in the photocatalytic gas phase NO_x oxidation and storage systems in tandem with the previously designed UV-active NO_x oxidation and storage photocatalysts.

5. REFERENCES

[1] a Fujishima, X. Zhang, and D. Tryk, "TiO2 photocatalysis and related surface phenomena," *Surf. Sci. Rep.*, vol. 63, no. 12, pp. 515–582, Dec. 2008.

[2] C. F. Goodeve and J. A. Kitchener, "The mechanism of photosensitisation by solids," *Trans. Faraday Soc.*, vol. 34, pp. 902–908, 1938.

[3] S. Kato and F. Mashio, "Abtr. Book Annu. Meet." Chemical Society of Japan, 1956.

[4] T. Ochiai and A. Fujishima, "Photoelectrochemical properties of TiO2 photocatalyst and its applications for environmental purification," *J. Photochem. Photobiol. C Photochem. Rev.*, vol. 13, no. 4, pp. 247–262, Dec. 2012.

[5] S. N. Frank and A. J. Bard, "Heterogeneous photocatalytic oxidation of cyanide ion in aqueous solutions at titanium dioxide powder," *J. Am. Chem. Soc.*, vol. 99, no. 1, pp. 303–304, 1977.

[6] S. N. Frank and A. J. Bard, "Heterogeneous photocatalytic oxidation of cyanide and sulfite in aqueous solutions at semiconductor powders," *J. Phys. Chem.*, vol. 81, no. 15, pp. 1484–1488, 1977.

[7] C.-Y. Hsiao, C.-L. Lee, and D. F. Ollis, "Heterogeneous photocatalysis: Degradation of dilute solutions of dichloromethane (CH< sub> 2</sub> Cl< sub> 2</sub>), chloroform (CHCl< sub> 3</sub>), and carbon tetrachloride (CCl< sub> 4</sub>) with illuminated TiO< sub> 2</sub> photocatalyst," *J. Catal.*, vol. 82, no. 2, pp. 418–423, 1983.

[8] A. L. Pruden and D. F. Ollis, “Photoassisted heterogeneous catalysis: the degradation of trichloroethylene in water,” *J. Catal.*, vol. 82, no. 2, pp. 404–417, 1983.

[9] B. O’regan and M. Grfitzeli, “A low-cost, high-efficiency solar cell based on dye-sensitized,” *Nature*, vol. 353, pp. 737–740, 1991.

[10] R. Wang, K. Hashimoto, A. Fujishima, M. Chikuni, E. Kojima, A. Kitamura, M. Shimohigoshi, and T. Watanabe, “Light-induced amphiphilic surfaces,” *Nature*, vol. 388, pp. 431–432, 1997.

[11] S. Y. Lee and S. J. Park, “TiO2 photocatalyst for water treatment applications,” *J. Ind. Eng. Chem.*, vol. 19, no. 6, pp. 1761–1769, Nov. 2013.

[12] K. Maeda and K. Domen, “New non-oxide photocatalysts designed for overall water splitting under visible light,” *J. Phys. Chem. C*, vol. 111, no. 22, pp. 7851–7861, 2007.

[13] F. E. Osterloh, “Inorganic materials as catalysts for photochemical splitting of water,” *Chem. Mater.*, vol. 20, no. 1, pp. 35–54, 2007.

[14] A. Kudo and Y. Miseki, “Heterogeneous photocatalyst materials for water splitting.,” *Chem. Soc. Rev.*, vol. 38, no. 1, pp. 253–78, Jan. 2009.

[15] G. Liu, L. Wang, H. G. Yang, H.-M. Cheng, and G. Q. (Max) Lu, “Titania-based photocatalysts—crystal growth, doping and heterostructuring,” *J. Mater. Chem.*, vol. 20, no. 5, p. 831, 2010.

[16] X. Chen, S. Shen, L. Guo, and S. S. Mao, “Semiconductor-based photocatalytic hydrogen generation.,” *Chem. Rev.*, vol. 110, no. 11, pp. 6503–70, Nov. 2010.

[17] K. Maeda and K. Domen, “Photocatalytic Water Splitting: Recent Progress and Future Challenges,” *J. Phys. Chem. Lett.*, vol. 1, no. 18, pp. 2655–2661, Sep. 2010.

[18] K. Maeda, “Photocatalytic water splitting using semiconductor particles: History and recent developments,” *J. Photochem. Photobiol. C Photochem. Rev.*, vol. 12, no. 4, pp. 237–268, Dec. 2011.

[19] W. Y. Teoh, J. a. Scott, and R. Amal, “Progress in Heterogeneous Photocatalysis: From Classical Radical Chemistry to Engineering Nanomaterials and Solar Reactors,” *J. Phys. Chem. Lett.*, vol. 3, no. 5, pp. 629–639, Mar. 2012.

[20] H. Tong, S. Ouyang, Y. Bi, N. Umezawa, M. Oshikiri, and J. Ye, “Nano-photocatalytic materials: possibilities and challenges.,” *Adv. Mater.*, vol. 24, no. 2, pp. 229–51, Jan. 2012.

[21] Y. Qu and X. Duan, “Progress, challenge and perspective of heterogeneous photocatalysts.,” *Chem. Soc. Rev.*, vol. 42, no. 7, pp. 2568–80, Apr. 2013.

[22] H. G. Yang, C. H. Sun, S. Z. Qiao, J. Zou, G. Liu, S. C. Smith, H. M. Cheng, and G. Q. Lu, “Anatase TiO2 single crystals with a large percentage of reactive facets.,” *Nature*, vol. 453, no. 7195, pp. 638–41, May 2008.

[23] G. Liu, J. C. Yu, G. Q. M. Lu, and H.-M. Cheng, “Crystal facet engineering of semiconductor photocatalysts: motivations, advances and unique properties.,” *Chem. Commun. (Camb).*, vol. 47, no. 24, pp. 6763–83, Jun. 2011.

[24] P. D. Tran, L. H. Wong, J. Barber, and J. S. C. Loo, “Recent advances in hybrid photocatalysts for solar fuel production,” *Energy Environ. Sci.*, vol. 5, no. 3, p. 5902, 2012.

[25] A. J. Cowan and J. R. Durrant, “Long-lived charge separated states in nanostructured semiconductor photoelectrodes for the production of solar fuels.,” *Chem. Soc. Rev.*, vol. 42, no. 6, pp. 2281–93, Mar. 2013.

[26] A. Ramakrishnan, S. Neubert, B. Mei, J. Strunk, L. Wang, M. Bledowski, M. Muhler, and R. Beranek, “Enhanced performance of surface-modified TiO2 photocatalysts prepared via a visible-light photosynthetic route.,” *Chem. Commun. (Camb).*, vol. 48, no. 68, pp. 8556–8, Sep. 2012.

[27] C. X. Kronawitter, L. Vayssieres, S. Shen, L. Guo, D. a. Wheeler, J. Z. Zhang, B. R. Antoun, and S. S. Mao, “A perspective on solar-driven water splitting with all-oxide hetero-nanostructures,” *Energy Environ. Sci.*, vol. 4, no. 10, p. 3889, 2011.

[28] W. Choi, A. Termin, and M. R. Hoffmann, “The Role of Metal Ion Dopants in Quantum-Sized TiO2: Correlation between Photoreactivity and Charge Carrier Recombination Dynamics,” *J. Phys. Chem.*, vol. 98, no. 51, pp. 13669–13679, Dec. 1994.

[29] J. Z. Bloh, R. Dillert, and D. W. Bahnemann, “Designing Optimal Metal-Doped Photocatalysts: Correlation between Photocatalytic Activity, Doping Ratio, and Particle Size,” *J. Phys. Chem. C*, vol. 116, no. 48, pp. 25558–25562, Dec. 2012.

[30] R. Asahi, T. Morikawa, T. Ohwaki, K. Aoki, and Y. Taga, “Visible-light photocatalysis in nitrogen-doped titanium oxides.,” *Science*, vol. 293, no. 5528, pp. 269–71, Jul. 2001.

[31] P. Wang, B. Huang, Y. Dai, and M.-H. Whangbo, “Plasmonic photocatalysts: harvesting visible light with noble metal nanoparticles.,” *Phys. Chem. Chem. Phys.*, vol. 14, no. 28, pp. 9813–25, Jul. 2012.

[32] W. Hou and S. B. Cronin, “A Review of Surface Plasmon Resonance-Enhanced Photocatalysis,” *Adv. Funct. Mater.*, vol. 23, no. 13, pp. 1612–1619, Apr. 2013.

[33] O. Carp, C. L. Huisman, and a. Reller, “Photoinduced reactivity of titanium dioxide,” *Prog. Solid State Chem.*, vol. 32, no. 1–2, pp. 33–177, 2004.

[34] Y. Hu, H.-L. Tsai, and C.-L. Huang, “Effect of brookite phase on the anatase–rutile transition in titania nanoparticles,” *J. Eur. Ceram. Soc.*, vol. 23, no. 5, pp. 691–696, Apr. 2003.

[35] Y. Shao, D. Tang, J. Sun, Y. Lee, and W. Xiong, “Lattice deformation and phase transformation from nano-scale anatase to nano-scale rutile TiO< sub> 2</sub> prepared by a sol-gel technique,” *China particuology*, vol. 2, no. 3, pp. 119–123, 2004.

[36] X. Chen and S. S. Mao, “Titanium dioxide nanomaterials: synthesis, properties, modifications, and applications.,” *Chem. Rev.*, vol. 107, no. 7, pp. 2891–959, Jul. 2007.

[37] A. Wisitsoraat, A. Tuantranont, E. Comini, G. Sberveglieri, and W. Wlodarski, “Characterization of n-type and p-type semiconductor gas sensors based on NiO< sub> x</sub> doped TiO< sub> 2</sub> thin films,” *Thin Solid Films*, vol. 517, no. 8, pp. 2775–2780, 2009.

[38] R. Asahi, Y. Taga, W. Mannstadt, and A. J. Freeman, “Electronic and optical properties of anatase TiO 2,” *Phys. Rev. B*, vol. 61, no. 11, p. 7459, 2000.

[39] N. Hosaka, T. Sekiya, M. Fujisawa, C. Satokob, and S. Kurita, “UV Reflection Spectra of Anatase TiOz,” vol. 78, pp. 75–78, 1996.

[40] L. Kavan, M. Gra, S. E. Gilbert, C. Klemenz, and H. J. Scheel, “Electrochemical and Photoelectrochemical Investigation of Single-Crystal Anatase,” vol. 650, no. 16, pp. 6716–6723, 1996.

[41] A. Amtout and R. Leonelli, “Optical properties of rutile near its fundamental band gap,” *Phys. Rev. B*, vol. 51, no. 11, p. 6842, 1995.

[42] K. M. Glassford and J. R. Chelikowsky, “Structural and electronic properties of titanium dioxide,” *Phys. Rev. B*, vol. 46, no. 3, p. 1284, 1992.

[43] J. Pascual, J. Camassel, and H. Mathieu, “Fine structure in the intrinsic absorption edge of Ti O 2,” *Phys. Rev. B*, vol. 18, no. 10, p. 5606, 1978.

[44] M. Koelsch, S. Cassaignon, C. Ta Thanh Minh, J.-F. Guillemoles, and J.-P. Jolivet, “Electrochemical comparative study of titania (anatase, brookite and rutile) nanoparticles synthesized in aqueous medium,” *Thin Solid Films*, vol. 451, pp. 86–92, 2004.

[45] J.-G. Li, T. Ishigaki, and X. Sun, “Anatase, Brookite, and Rutile Nanocrystals via Redox Reactions under Mild Hydrothermal Conditions: Phase-Selective Synthesis and Physicochemical Properties,” *J. Phys. Chem. C*, vol. 111, no. 13, pp. 4969–4976, Apr. 2007.

[46] D. Reyes-Coronado, G. Rodriguez-Gattorno, M. E. Espinosa-Pesqueira, C. Cab, R. De Coss, and G. Oskam, “Phase-pure TiO2 nanoparticles: anatase, brookite and rutile,” *Nanotechnology*, vol. 19, no. 14, p. 145605, 2008.

[47] M. R. Hoffmann, S. T. Martin, W. Choi, and D. W. Bahnemann, “Environmental applications of semiconductor photocatalysis,” *Chem. Rev.*, vol. 95, no. 1, pp. 69–96, 1995.

[48] Y. Wang, Y. Huang, W. Ho, L. Zhang, Z. Zou, and S. Lee, “Biomolecule-controlled hydrothermal synthesis of C–N–S-tridoped TiO< sub> 2</sub> nanocrystalline photocatalysts for NO removal under simulated solar light irradiation,” *J. Hazard. Mater.*, vol. 169, no. 1, pp. 77–87, 2009.

[49] C. Su, C.-M. Tseng, L.-F. Chen, B.-H. You, B.-C. Hsu, and S.-S. Chen, “Sol–hydrothermal preparation and photocatalysis of titanium dioxide,” *Thin Solid Films*, vol. 498, no. 1, pp. 259–265, 2006.

[50] M. R. Ranade, a Navrotsky, H. Z. Zhang, J. F. Banfield, S. H. Elder, a Zaban, P. H. Borse, S. K. Kulkarni, G. S. Doran, and H. J. Whitfield, “Energetics of nanocrystalline TiO2.,” *Proc. Natl. Acad. Sci. U. S. A.*, vol. 99 Suppl 2, pp. 6476–81, Apr. 2002.

[51] J. Wang, A. K. Mishra, Q. Zhao, and L. Huang, “Size effect on thermal stability of nanocrystalline anatase TiO2,” *J. Phys. D. Appl. Phys.*, vol. 46, no. 25, p. 255303, 2013.

[52] H. Zhang and J. F. Banfield, “Understanding polymorphic phase transformation behavior during growth of nanocrystalline aggregates: insights from TiO2,” *J. Phys. Chem. B*, vol. 104, no. 15, pp. 3481–3487, 2000.

[53] R. D. Shannon and J. A. Pask, “Kinetics of the Anatase-Rutile Transformation,” *J. Am. Ceram. Soc.*, vol. 48, no. 8, pp. 391–398, 1965.

[54] C. N. R. Rao, “Kinetics and thermodynamics of the crystal structure transformation of spectroscopically pure anatase to rutile,” *Can. J. Chem.*, vol. 39, no. 3, pp. 498–500, 1961.

[55] J. C. Jamieson, B. Olinger, F. Dachille, P. Y. Simons, and R. Roy, “PRESSURE-TEMPERATURE STUDIES OF ANATASE, BROOKITE RUTILE AND TIO2 (II)-A DISCUSSION,” *American Mineralogist*, vol. 54, no. 9–10. MINERALOGICAL SOC AMER 1015 EIGHTEENTH ST, NW SUITE 601, WASHINGTON, DC 20036, p. 1477, 1969.

[56] D. J. Reidy, J. D. Holmes, and M. A. Morris, “The critical size mechanism for the anatase to rutile transformation in TiO< sub> 2</sub> and doped-TiO< sub> 2</sub>,” *J. Eur. Ceram. Soc.*, vol. 26, no. 9, pp. 1527–1534, 2006.

[57] S. Riyas, G. Krishnan, and P. N. M. Das, “Anatase–rutile transformation in doped titania under argon and hydrogen atmospheres,” *Adv. Appl. Ceram.*, vol. 106, no. 5, pp. 255–264, 2007.

[58] R. Janes, L. J. Knightley, and C. J. Harding, “Structural and spectroscopic studies of iron (III) doped titania powders prepared by sol-gel synthesis and hydrothermal processing,” *Dye. Pigment.*, vol. 62, no. 3, pp. 199–212, 2004.

[59] M. Batzill, E. H. Morales, and U. Diebold, “Influence of nitrogen doping on the defect formation and surface properties of TiO 2 rutile and anatase,” *Phys. Rev. Lett.*, vol. 96, no. 2, p. 26103, 2006.

[60] T. Ihara, M. Miyoshi, Y. Iriyama, O. Matsumoto, and S. Sugihara, “Visible-light-active titanium oxide photocatalyst realized by an oxygen-deficient structure and by nitrogen doping,” *Appl. Catal. B Environ.*, vol. 42, no. 4, pp. 403–409, 2003.

[61] D. A. H. Hanaor and C. C. Sorrell, “Review of the anatase to rutile phase transformation,” *J. Mater. Sci.*, vol. 46, no. 4, pp. 855–874, 2011.

[62] D. Chen, D. Yang, Q. Wang, and Z. Jiang, “Effects of boron doping on photocatalytic activity and microstructure of titanium dioxide nanoparticles,” *Ind. Eng. Chem. Res.*, vol. 45, no. 12, pp. 4110–4116, 2006.

[63] B. Grzmil, M. Glen, B. Kic, and K. Lubkowski, “Preparation and characterization of single-modified TiO2 for pigmentary applications,” *Ind. Eng. Chem. Res.*, vol. 50, no. 11, pp. 6535–6542, 2011.

[64] A. Mills and S. Le Hunte, “An overview of semiconductor photocatalysis,” *J. Photochem. Photobiol. A Chem.*, vol. 108, no. 1, pp. 1–35, 1997.

[65] P. Suppan, *Chemistry and light*. Royal Society of Chemistry, 1994.

[66] M. Pelaez, N. T. Nolan, S. C. Pillai, M. K. Seery, P. Falaras, A. G. Kontos, P. S. M. Dunlop, J. W. J. Hamilton, J. A. Byrne, K. O’Shea, M. H. Entezari, and D. D. Dionysiou, “A review on the visible light active titanium dioxide photocatalysts for environmental applications,” *Appl. Catal. B Environ.*, vol. 125, pp. 331–349, Aug. 2012.

[67] A. Testino, I. R. Bellobono, V. Buscaglia, C. Canevali, M. D’Arienzo, S. Polizzi, R. Scotti, and F. Morazzoni, “Optimizing the photocatalytic properties of hydrothermal TiO2 by the control of phase composition and particle morphology. A systematic approach,” *J. Am. Chem. Soc.*, vol. 129, no. 12, pp. 3564–3575, 2007.

[68] T. Tachikawa, M. Fujitsuka, and T. Majima, “Mechanistic insight into the TiO2 photocatalytic reactions: design of new photocatalysts,” *J. Phys. Chem. C*, vol. 111, no. 14, pp. 5259–5275, 2007.

[69] P. . Cozzoli, R. Comparelli, E. Fanizza, M. . Curri, and A. Agostiano, “Photocatalytic activity of organic-capped anatase TiO2 nanocrystals in homogeneous organic solutions,” *Mater. Sci. Eng. C*, vol. 23, no. 6–8, pp. 707–713, Dec. 2003.

[70] E. R. Carraway, A. J. Hoffman, and M. R. Hoffmann, “Photocatalytic oxidation of organic acids on quantum-sized semiconductor colloids,” *Environ. Sci. Technol.*, vol. 28, no. 5, pp. 786–793, 1994.

[71] F. Mahdavi, T. C. Bruton, and Y. Li, “Photoinduced reduction of nitro compounds on semiconductor particles,” *J. Org. Chem.*, vol. 58, no. 3, pp. 744–746, 1993.

[72] J. Liqiang, Q. Yichun, W. Baiqi, L. Shudan, J. Baojiang, Y. Libin, F. Wei, F. Honggang, and S. Jiazhong, “Review of photoluminescence performance of nano-sized semiconductor materials and its relationships with photocatalytic activity,” *Sol. Energy Mater. Sol. Cells*, vol. 90, no. 12, pp. 1773–1787, Jul. 2006.

[73] W. Choi, A. Termin, and M. R. Hoffmann, “The role of metal ion dopants in quantum-sized TiO2: correlation between photoreactivity and charge carrier recombination dynamics,” *J. Phys. Chem.*, vol. 98, no. 51, pp. 13669–13679, 1994.

[74] J. Soria, J. C. Conesa, V. Augugliaro, L. Palmisano, M. Schiavello, and A. Sclafani, “Dinitrogen photoreduction to ammonia over titanium dioxide powders doped with ferric ions,” *J. Phys. Chem.*, vol. 95, no. 1, pp. 274–282, 1991.

[75] J. C. Yu, J. Yu, W. Ho, Z. Jiang, and L. Zhang, “Effects of F-doping on the photocatalytic activity and microstructures of nanocrystalline TiO2 powders,” *Chem. Mater.*, vol. 14, no. 9, pp. 3808–3816, 2002.

[76] Y. R. Do, W. Lee, K. Dwight, and A. Wold, “The Effect of WO< sub> 3</sub> on the Photocatalytic Activity of TiO< sub> 2</sub>,” *J. Solid State Chem.*, vol. 108, no. 1, pp. 198–201, 1994.

[77] J. Engweiler, J. Harf, and A. Baiker, “WO< sub> x</sub>/TiO< sub> 2</sub> Catalysts Prepared by Grafting of Tungsten Alkoxides: Morphological Properties and Catalytic Behavior in the Selective Reduction of NO by NH< sub> 3</sub>,” *J. Catal.*, vol. 159, no. 2, pp. 259–269, 1996.

[78] K. Vinodgopal and P. V Kamat, “Enhanced rates of photocatalytic degradation of an azo dye using SnO2/TiO2 coupled semiconductor thin films,” *Environ. Sci. Technol.*, vol. 29, no. 3, pp. 841–845, 1995.

[79] A. J. Maira, K. L. Yeung, C. Y. Lee, P. L. Yue, and C. K. Chan, “Size Effects in Gas-Phase Photo-oxidation of Trichloroethylene Using Nanometer-Sized TiO< sub> 2</sub> Catalysts,” *J. Catal.*, vol. 192, no. 1, pp. 185–196, 2000.

[80] Z. Xu, J. Shang, C. Liu, C. Kang, H. Guo, and Y. Du, “The preparation and characterization of TiO< sub> 2</sub> ultrafine particles,” *Mater. Sci. Eng. B*, vol. 63, no. 3, pp. 211–214, 1999.

[81] C. A. Emilio, M. I. Litter, M. Kunst, M. Bouchard, and C. Colbeau-Justin, “Phenol photodegradation on platinized-TiO2 photocatalysts related to charge-carrier dynamics,” *Langmuir*, vol. 22, no. 8, pp. 3606–3613, 2006.

[82] N. Serpone, “Relative photonic efficiencies and quantum yields in heterogeneous photocatalysis,” *J. Photochem. Photobiol. A Chem.*, vol. 104, no. 1, pp. 1–12, 1997.

[83] N. Serpone, D. Lawless, and R. Khairutdinov, “Size effects on the photophysical properties of colloidal anatase TiO2 particles: size quantization versus direct transitions in this indirect semiconductor?,” *J. Phys. Chem.*, vol. 99, no. 45, pp. 16646–16654, 1995.

[84] B. Neppolian, H. C. Choi, S. Sakthivel, B. Arabindoo, and V. Murugesan, “Solar/UV-induced photocatalytic degradation of three commercial textile dyes,” *J. Hazard. Mater.*, vol. 89, no. 2, pp. 303–317, 2002.

[85] M. Anpo and M. Takeuchi, “The design and development of highly reactive titanium oxide photocatalysts operating under visible light irradiation,” *J. Catal.*, vol. 216, no. 1, pp. 505–516, 2003.

[86] M. Shen, Z. Wu, H. Huang, Y. Du, Z. Zou, and P. Yang, “Carbon-doped anatase TiO< sub> 2</sub> obtained from TiC for photocatalysis under visible light irradiation,” *Mater. Lett.*, vol. 60, no. 5, pp. 693–697, 2006.

[87] W. Ren, Z. Ai, F. Jia, L. Zhang, X. Fan, and Z. Zou, “Low temperature preparation and visible light photocatalytic activity of mesoporous carbon-doped crystalline TiO< sub> 2</sub>,” *Appl. Catal. B Environ.*, vol. 69, no. 3, pp. 138–144, 2007.

[88] L. Mai, C. Huang, D. Wang, Z. Zhang, and Y. Wang, “Effect of C doping on the structural and optical properties of sol–gel TiO< sub> 2</sub> thin films,” *Appl. Surf. Sci.*, vol. 255, no. 22, pp. 9285–9289, 2009.

[89] M.-S. Wong, S.-W. Hsu, K. K. Rao, and C. P. Kumar, “Influence of crystallinity and carbon content on visible light photocatalysis of carbon doped titania thin films,” *J. Mol. Catal. A Chem.*, vol. 279, no. 1, pp. 20–26, Jan. 2008.

[90] H. Wang and J. P. Lewis, “Second-generation photocatalytic materials: anion-doped TiO 2,” *J. Phys. Condens. Matter*, vol. 18, no. 2, pp. 421–434, Jan. 2006.

[91] F. Peng, L. Cai, H. Yu, H. Wang, and J. Yang, “Synthesis and characterization of substitutional and interstitial nitrogen-doped titanium dioxides with visible light photocatalytic activity,” *J. Solid State Chem.*, vol. 181, no. 1, pp. 130–136, Jan. 2008.

[92] M.-S. Wong, H. Pang Chou, and T.-S. Yang, “Reactively sputtered N-doped titanium oxide films as visible-light photocatalyst,” *Thin Solid Films*, vol. 494, no. 1–2, pp. 244–249, Jan. 2006.

[93] Y. Ao, J. Xu, D. Fu, and C. Yuan, “A simple method to prepare N-doped titania hollow spheres with high photocatalytic activity under visible light.,” *J. Hazard. Mater.*, vol. 167, no. 1–3, pp. 413–7, Aug. 2009.

[94] J. Zhang, Y. Wang, Z. Jin, Z. Wu, and Z. Zhang, “Visible-light photocatalytic behavior of two different N-doped TiO2,” *Appl. Surf. Sci.*, vol. 254, no. 15, pp. 4462–4466, May 2008.

[95] W.-K. Jo and J.-T. Kim, “Application of visible-light photocatalysis with nitrogen-doped or unmodified titanium dioxide for control of indoor-level volatile organic compounds.,” *J. Hazard. Mater.*, vol. 164, no. 1, pp. 360–6, May 2009.

[96] A. Trenczek-Zajac, K. Kowalski, K. Zakrzewska, and M. Radecka, “Nitrogen-doped titanium dioxide—Characterization of structural and optical properties,” *Mater. Res. Bull.*, vol. 44, no. 7, pp. 1547–1552, Jul. 2009.

[97] B. F. Abramović, D. V. Šojić, V. B. Anderluh, N. D. Abazović, and M. I. Čomor, “Nitrogen-doped TiO2 suspensions in photocatalytic degradation of mecoprop and (4-chloro-2-methylphenoxy)acetic acid herbicides using various light sources,” *Desalination*, vol. 244, no. 1–3, pp. 293–302, Aug. 2009.

[98] Z. Zhang, J. B. M. Goodall, D. J. Morgan, S. Brown, R. J. H. Clark, J. C. Knowles, N. J. Mordan, J. R. G. Evans, A. F. Carley, M. Bowker, and J. A. Darr, “Photocatalytic activities of N-doped nano-titanias and titanium nitride,” *J. Eur. Ceram. Soc.*, vol. 29, no. 11, pp. 2343–2353, Aug. 2009.

[99] T. Lindgren, J. M. Mwabora, E. Avendaño, J. Jonsson, A. Hoel, C.-G. Granqvist, and S.-E. Lindquist, “Photoelectrochemical and Optical Properties of Nitrogen Doped Titanium Dioxide Films Prepared by Reactive DC Magnetron Sputtering,” *J. Phys. Chem. B*, vol. 107, no. 24, pp. 5709–5716, May 2003.

[100] H. Irie, Y. Watanabe, and K. Hashimoto, “Nitrogen-Concentration Dependence on Photocatalytic Activity of TiO2-xNx Powders,” *J. Phys. Chem. B*, vol. 107, no. 23, pp. 5483–5486, May 2003.

[101] M.-C. Yang, T.-S. Yang, and M.-S. Wong, “Nitrogen-doped titanium oxide films as visible light photocatalyst by vapor deposition,” *Thin Solid Films*, vol. 469–470, pp. 1–5, Dec. 2004.

[102] T. Umebayashi, T. Yamaki, H. Itoh, and K. Asai, “Band gap narrowing of titanium dioxide by sulfur doping,” *Appl. Phys. Lett.*, vol. 81, no. 3, p. 454, 2002.

[103] T. Umebayashi, T. Yamaki, S. Yamamoto, a. Miyashita, S. Tanaka, T. Sumita, and K. Asai, “Sulfur-doping of rutile-titanium dioxide by ion implantation: Photocurrent spectroscopy and first-principles band calculation studies,” *J. Appl. Phys.*, vol. 93, no. 9, p. 5156, 2003.

[104] H. Tian, J. Ma, K. Li, and J. Li, “Hydrothermal synthesis of S-doped TiO2 nanoparticles and their photocatalytic ability for degradation of methyl orange,” *Ceram. Int.*, vol. 35, no. 3, pp. 1289–1292, Apr. 2009.

[105] Y. Liu, J. Liu, Y. Lin, Y. Zhang, and Y. Wei, “Simple fabrication and photocatalytic activity of S-doped TiO2 under low power LED visible light irradiation,” *Ceram. Int.*, vol. 35, no. 8, pp. 3061–3065, Dec. 2009.

[106] M. Hamadanian, a. Reisi-Vanani, and a. Majedi, “Preparation and characterization of S-doped TiO2 nanoparticles, effect of calcination temperature and evaluation of photocatalytic activity,” *Mater. Chem. Phys.*, vol. 116, no. 2–3, pp. 376–382, Aug. 2009.

[107] X. Xue, Y. Wang, and H. Yang, “Preparation and characterization of boron-doped titania nano-materials with antibacterial activity,” *Appl. Surf. Sci.*, vol. 264, pp. 94–99, Jan. 2013.

[108] H. Tian, F. Xin, X. Tan, and W. Han, “High Lithium Electroactivity of Boron-doped Hierarchical Rutile Submicrospheres TiO 2,” no. 1, pp. 3–4, 2014.

[109] A. Zaleska, E. Grabowska, J. W. Sobczak, M. Gazda, and J. Hupka, “Photocatalytic activity of boron-modified TiO2 under visible light: The effect of boron content, calcination temperature and TiO2 matrix,” *Appl. Catal. B Environ.*, vol. 89, no. 3–4, pp. 469–475, Jul. 2009.

[110] H. Tian, L. Hu, C. Zhang, S. Chen, J. Sheng, L. Mo, W. Liu, and S. Dai, “Enhanced photovoltaic performance of dye-sensitized solar cells using a highly crystallized mesoporous TiO2 electrode modified by boron doping,” *J. Mater. Chem.*, vol. 21, no. 3, p. 863, 2011.

[111] A. Zaleska, J. W. Sobczak, E. Grabowska, and J. Hupka, “Preparation and photocatalytic activity of boron-modified TiO2 under UV and visible light,” *Appl. Catal. B Environ.*, vol. 78, no. 1–2, pp. 92–100, Jan. 2008.

[112] W. Zhang, B. Yang, and J. Chen, “Effects of Calcination Temperature on Preparation of Boron-Doped TiO2 by Sol-Gel Method,” *Int. J. Photoenergy*, vol. 2012, pp. 1–8, 2012.

[113] E. Grabowska, J. Reszczy??ska, and A. Zaleska, “Mechanism of phenol photodegradation in the presence of pure and modified-TiO2: A review,” *Water Res.*, vol. 46, no. 17, pp. 5453–5471, Nov. 2012.

[114] N. Serpone, “Is the Band Gap of Pristine TiO2 Narrowed by Anion- and Cation-Doping of Titanium Dioxide in Second-Generation Photocatalysts?,” *J. Phys. Chem. B*, vol. 110, no. 48, pp. 24287–24293, Nov. 2006.

[115] C. Di Valentin, G. Pacchioni, A. Selloni, S. Livraghi, and E. Giamello, “Characterization of Paramagnetic Species in N-Doped TiO2 Powders by EPR Spectroscopy and DFT Calculations,” *J. Phys. Chem. B*, vol. 109, no. 23, pp. 11414–11419, May 2005.

[116] R. Nakamura, T. Tanaka, and Y. Nakato, “Mechanism for Visible Light Responses in Anodic Photocurrents at N-Doped TiO 2 Film Electrodes,” *J. Phys. Chem. B*, vol. 108, no. 30, pp. 10617–10620, Jul. 2004.

[117] S. U. M. Khan, M. Al-Shahry, and W. B. Ingler, “Efficient photochemical water splitting by a chemically modified n-TiO2.,” *Science*, vol. 297, no. 5590, pp. 2243–5, Sep. 2002.

[118] Y. Choi, T. Umebayashi, and M. Yoshikawa, “Fabrication and characterization of C-doped anatase TiO2 photocatalysts,” *J. Mater. Sci.*, vol. 39, no. 5, pp. 1837–1839, 2004.

[119] H. Irie, Y. Watanabe, and K. Hashimoto, “Carbon-doped Anatase TiO₂ Powders as a Visible-light Sensitive Photocatalyst,” *Chem. Lett.*, vol. 32, no. 8, pp. 772–773, 2003.

[120] S.-W. Hsu, T.-S. Yang, T.-K. Chen, and M.-S. Wong, “Ion-assisted electron-beam evaporation of carbon-doped titanium oxide films as visible-light photocatalyst,” *Thin Solid Films*, vol. 515, no. 7–8, pp. 3521–3526, Feb. 2007.

[121] S. Sakthivel and H. Kisch, “Daylight Photocatalysis by Carbon-Modified Titanium Dioxide,” *Angew. Chemie Int. Ed.*, vol. 42, no. 40, pp. 4908–4911, Oct. 2003.

[122] T. Ohno, T. Tsubota, K. Nishijima, and Z. Miyamoto, “Degradation of Methylene Blue on Carbonate Species-doped TiO₂ Photocatalysts under Visible Light,” *Chem. Lett.*, vol. 33, no. 6, pp. 750–751, 2004.

[123] T. Tachikawa, S. Tojo, K. Kawai, M. Endo, M. Fujitsuka, T. Ohno, K. Nishijima, Z. Miyamoto, and T. Majima, "Photocatalytic Oxidation Reactivity of Holes in the Sulfur- and Carbon-Doped TiO 2 Powders Studied by Time-Resolved Diffuse Reflectance Spectroscopy," pp. 19299–19306, 2004.

[124] Y. Li, D.-S. Hwang, N. H. Lee, and S.-J. Kim, "Synthesis and characterization of carbon-doped titania as an artificial solar light sensitive photocatalyst," *Chem. Phys. Lett.*, vol. 404, no. 1–3, pp. 25–29, Mar. 2005.

[125] D. Gu, Y. Lu, B. Yang, and Y. Hu, "Facile preparation of micro-mesoporous carbon-doped TiO2 photocatalysts with anatase crystalline walls under template-free condition," *Chem. Commun.*, no. 21, pp. 2453–2455, 2008.

[126] C. Di Valentin, G. Pacchioni, A. Selloni, V. Uni, M. Bicocca, and V. R. Cozzi, "Theory of Carbon Doping of Titanium Dioxide," no. d, pp. 6656–6665, 2005.

[127] W. Zhao, W. Ma, C. Chen, J. Zhao, and Z. Shuai, "Efficient Degradation of Toxic Organic Pollutants with Ni2O3/TiO2-xBx under Visible Irradiation," *J. Am. Chem. Soc.*, vol. 126, no. 15, pp. 4782–4783, Mar. 2004.

[128] E. Finazzi, C. Di Valentin, and G. Pacchioni, "Boron-Doped Anatase TiO2: Pure and Hybrid DFT Calculations," *J. Phys. Chem. C*, vol. 113, no. 1, pp. 220–228, Dec. 2008.

[129] H. Geng, S. Yin, X. Yang, Z. Shuai, and B. Liu, "Geometric and electronic structures of the boron-doped photocatalyst TiO 2," *J. Phys. Condens. Matter*, vol. 18, no. 1, pp. 87–96, Jan. 2006.

[130] J. Xu, Y. Ao, M. Chen, and D. Fu, "Low-temperature preparation of Boron-doped titania by hydrothermal method and its photocatalytic activity," *J. Alloys Compd.*, vol. 484, no. 1–2, pp. 73–79, Sep. 2009.

[131] T. Ohno, M. Akiyoshi, T. Umebayashi, K. Asai, T. Mitsui, and M. Matsumura, "Preparation of S-doped TiO2 photocatalysts and their photocatalytic activities under visible light," *Appl. Catal. A Gen.*, vol. 265, no. 1, pp. 115–121, Jun. 2004.

[132] P. V Kamat and D. Editor, "Semiconductor Nanocrystals : To Dope or Not to Dope," no. 7, pp. 2832–2833, 2011.

[133] J. Yu, H. Yu, B. Cheng, M. Zhou, and X. Zhao, "Enhanced photocatalytic activity of TiO2 powder (P25) by hydrothermal treatment," *J. Mol. Catal. A Chem.*, vol. 253, no. 1–2, pp. 112–118, Jul. 2006.

[134] M. Iwase, K. Yamada, T. Kurisaki, and H. Wakita, "Characterization and photocatalytic activity of nitrogen-doped titanium(IV) oxide prepared by doping titania with TiN powder," *Appl. Catal. A Gen.*, vol. 455, pp. 86–91, Mar. 2013.

[135] J. PERAL and D. OLLIS, “Heterogeneous photocatalytic oxidation of gas-phase organics for air purification: Acetone, 1-butanol, butyraldehyde, formaldehyde, and m-xylene oxidation,” *J. Catal.*, vol. 136, no. 2, pp. 554–565, Aug. 1992.

[136] R. a. Spurr and H. Myers, “Quantitative Analysis of Anatase-Rutile Mixtures with an X-Ray Diffractometer,” *Anal. Chem.*, vol. 29, pp. 760–762, 1957.

[137] P. Kubelka and F. Munk, “A contribution to the optics of pigments,” *Z. Tech. Phys*, vol. 12, pp. 593–599, 1931.

[138] J. Tauc, “Optical properties and electronic structure of amorphous Ge and Si,” *Mater. Res. Bull.*, vol. 3, no. 1, pp. 37–46, Jan. 1968.

[139] J. Sanz, J. Soria, I. Sobrados, S. Yurdakal, and V. Augugliaro, “Influence of amorphous TiO 2-x on titania nanoparticle growth and anatase-to-rutile transformation,” *J. Phys. Chem. C*, vol. 116, pp. 5110–5115, 2012.

[140] S. A. Tio, P. Periyat, S. C. Pillai, D. E. Mccormack, J. Colreavy, and S. J. Hinder, “Improved High-Temperature Stability and Sun-Light-Driven Photocatalytic Activity of,” pp. 7644–7652, 2008.

[141] T. Ohsaka, F. Izumi, and Y. Fujiki, “Raman spectrum of anatase, TiO2,” *J. Raman Spectrosc.*, vol. 7, pp. 321–324, 1978.

[142] H. L. Ma, J. Y. Yang, Y. Dai, Y. B. Zhang, B. Lu, and G. H. Ma, “Raman study of phase transformation of TiO2 rutile single crystal irradiated by infrared femtosecond laser,” *Appl. Surf. Sci.*, vol. 253, pp. 7497–7500, 2007.

[143] K. J. A. Raj and B. Viswanathan, “Effect of surface area , pore volume and particle size of P25 titania on the phase transformation of anatase to rutile,” vol. 48, no. October, pp. 1378–1382, 2009.

[144] S. Valencia, J. M. Marín, and G. Restrepo, “Study of the Bandgap of Synthesized Titanium Dioxide Nanoparticules Using the Sol-Gel Method and a Hydrothermal Treatment,” *Open Mater. Sci. J.*, vol. 4, no. 1, pp. 9–14, Feb. 2010.

[145] C. Kormann, D. W. Bahnemann, and M. R. Hoffmann, “Preparation and characterization of quantum-size titanium dioxide,” *J. Phys. Chem.*, vol. 92, no. 18, pp. 5196–5201, Sep. 1988.

[146] M. M. Rahman, K. M. Krishna, T. Soga, T. Jimbo, and M. Umeno, “Optical properties and X-ray photoelectron spectroscopic study of pure and Pb-doped TiO2 thin films,” *J. Phys. Chem. Solids*, vol. 60, no. 2, pp. 201–210, Feb. 1999.

[147] J. Ananpattarachai, P. Kajitvichyanukul, and S. Seraphin, “Visible light absorption ability and photocatalytic oxidation activity of various interstitial

N-doped TiO2 prepared from different nitrogen dopants.," *J. Hazard. Mater.*, vol. 168, no. 1, pp. 253–61, Aug. 2009.

[148] N. Todorova, T. Vaimakis, T. Giannakopoulou, S. Hishita, A. Griniari, E. Varadas, and C. Trapalis, "N-and N, C-Doped TiO 2 Powders and Their Visible Light Activity," *Nanosci. Nanotechnol. Lett.*, vol. 5, no. 4, pp. 475–479, 2013.

[149] I. Materials, "Photodegradation of Rhodamine B on Sulfur Doped ZnO / TiO 2 Nanocomposite Photocatalyst under Visible-light Irradiation," 2010.

[150] H. Fu, C. Pan, W. Yao, and Y. Zhu, "Visible-light-induced degradation of rhodamine B by nanosized Bi2WO6.," *J. Phys. Chem. B*, vol. 109, no. 47, pp. 22432–9, Dec. 2005.

[151] T. Watanabe, T. Takizawa, and K. Honda, "Photocatalysis through excitation of adsorbates. 1. Highly efficient N-deethylation of rhodamine B adsorbed to cadmium sulfide," *J. Phys. Chem.*, vol. 81, no. 19, pp. 1845–1851, Sep. 1977.

[152] T. Inoue, T. Watanabe, A. Fujishima, K. Honda, and K. Kohayakawa, "Suppression of Surface Dissolution of CdS Photoanode by Reducing Agents," vol. 124, no. 5, pp. 5–8.

Title:	Is the Band Gap of Pristine TiO2 Narrowed by Anion- and Cation-Doping of Titanium Dioxide in Second-Generation Photocatalysts?
Author:	Nick Serpone*
Publication:	The Journal of Physical Chemistry B
Publisher:	American Chemical Society
Date:	Dec 1, 2006

This type of permission/license, instead of the standard Terms & Conditions, is sent to you because no fee is being charged for your order. Please note the following:

- Permission is granted for your request in both print and electronic formats, and translations.
- If figures and/or tables were requested, they may be adapted or used in part.
- Please print this page for your records and send a copy of it to your publisher/graduate school.
- Appropriate credit for the requested material should be given as follows: "Reprinted (adapted) with permission from (COMPLETE REFERENCE CITATION). Copyright (YEAR) American Chemical Society." Insert appropriate information in place of the capitalized words.
- One-time permission is granted only for the use specified in your request. No additional uses are granted (such as derivative works or other editions). For any other uses, please submit a new request.

If credit is given to another source for the material you requested, permission must be obtained from that source.

ELSEVIER LICENSE
TERMS AND CONDITIONS
Jul 21, 2014

This is a License Agreement between Pelin Altay ("You") and Elsevier ("Elsevier") provided by Copyright Clearance Center ("CCC"). The license consists of your order details, the terms and conditions provided by Elsevier, and the payment terms and conditions.

All payments must be made in full to CCC. For payment instructions, please see information listed at the bottom of this form.

Supplier	Elsevier Limited The Boulevard,Langford Lane Kidlington,Oxford,OX5 1GB,UK
Registered Company Number	1982084
Customer name	Pelin Altay
Customer address	Bilkent University SB Building

	Ankara, 06800
License number	3433561361348
License date	Jul 21, 2014
Licensed content publisher	Elsevier
Licensed content publication	Applied Catalysis B: Environmental
Licensed content title	A review on the visible light active titanium dioxide photocatalysts for environmental applications
Licensed content author	Miguel Pelaez,Nicholas T. Nolan,Suresh C. Pillai,Michael K. Seery,Polycarpos Falaras,Athanassios G. Kontos,Patrick S.M. Dunlop,Jeremy W.J. Hamilton,J.Anthony Byrne,Kevin O'Shea,Mohammad H. Entezari,Dionysios D. Dionysiou
Licensed content date	21 August 2012
Licensed content volume number	125
Licensed content issue number	None
Number of pages	19
Start Page	331
End Page	349
Type of Use	reuse in a thesis/dissertation
Portion	figures/tables/illustrations
Number of figures/tables/illustrations	1
Format	both print and electronic
Are you the author of this Elsevier article?	No
Will you be translating?	No
Title of your thesis/dissertation	VISIBLE LIGHT-ACTIVE NON-METAL DOPED TITANIUM DIOXIDE MATERIALS FOR PHOTOCATALYTIC OXIDATION
Expected completion date	Aug 2014
Estimated size (number of pages)	107
Elsevier VAT number	GB 494 6272 12
Permissions price	0.00 USD
VAT/Local Sales Tax	0.00 USD / 0.00 GBP
Total	0.00 USD
Terms and Conditions	

INTRODUCTION

1. The publisher for this copyrighted material is Elsevier. By clicking "accept" in connection with completing this licensing transaction, you agree that the following terms and conditions apply to this transaction (along with the Billing and Payment terms and

conditions established by Copyright Clearance Center, Inc. ("CCC"), at the time that you opened your Rightslink account and that are available at any time at http://myaccount.copyright.com).

GENERAL TERMS

2. Elsevier hereby grants you permission to reproduce the aforementioned material subject to the terms and conditions indicated.

3. Acknowledgement: If any part of the material to be used (for example, figures) has appeared in our publication with credit or acknowledgement to another source, permission must also be sought from that source. If such permission is not obtained then that material may not be included in your publication/copies. Suitable acknowledgement to the source must be made, either as a footnote or in a reference list at the end of your publication, as follows:

"Reprinted from Publication title, Vol /edition number, Author(s), Title of article / title of chapter, Pages No., Copyright (Year), with permission from Elsevier [OR APPLICABLE SOCIETY COPYRIGHT OWNER]." Also Lancet special credit - "Reprinted from The Lancet, Vol. number, Author(s), Title of article, Pages No., Copyright (Year), with permission from Elsevier."

4. Reproduction of this material is confined to the purpose and/or media for which permission is hereby given.

5. Altering/Modifying Material: Not Permitted. However figures and illustrations may be altered/adapted minimally to serve your work. Any other abbreviations, additions, deletions and/or any other alterations shall be made only with prior written authorization of Elsevier Ltd. (Please contact Elsevier at permissions@elsevier.com)

6. If the permission fee for the requested use of our material is waived in this instance, please be advised that your future requests for Elsevier materials may attract a fee.

7. Reservation of Rights: Publisher reserves all rights not specifically granted in the combination of (i) the license details provided by you and accepted in the course of this licensing transaction, (ii) these terms and conditions and (iii) CCC's Billing and Payment terms and conditions.

8. License Contingent Upon Payment: While you may exercise the rights licensed immediately upon issuance of the license at the end of the licensing process for the transaction, provided that you have disclosed complete and accurate details of your proposed use, no license is finally effective unless and until full payment is received from you (either by publisher or by CCC) as provided in CCC's Billing and Payment terms and conditions. If full payment is not received on a timely basis, then any license preliminarily granted shall be deemed automatically revoked and shall be void as if never granted. Further, in the event that you breach any of these terms and conditions or any of CCC's Billing and Payment terms and conditions, the license is automatically revoked and shall be void as if never granted. Use of materials as described in a revoked license, as well as any use of the materials beyond the scope of an unrevoked license, may constitute

copyright infringement and publisher reserves the right to take any and all action to protect its copyright in the materials.

9. Warranties: Publisher makes no representations or warranties with respect to the licensed material.

10. Indemnity: You hereby indemnify and agree to hold harmless publisher and CCC, and their respective officers, directors, employees and agents, from and against any and all claims arising out of your use of the licensed material other than as specifically authorized pursuant to this license.

11. No Transfer of License: This license is personal to you and may not be sublicensed, assigned, or transferred by you to any other person without publisher's written permission.

12. No Amendment Except in Writing: This license may not be amended except in a writing signed by both parties (or, in the case of publisher, by CCC on publisher's behalf).

13. Objection to Contrary Terms: Publisher hereby objects to any terms contained in any purchase order, acknowledgment, check endorsement or other writing prepared by you, which terms are inconsistent with these terms and conditions or CCC's Billing and Payment terms and conditions. These terms and conditions, together with CCC's Billing and Payment terms and conditions (which are incorporated herein), comprise the entire agreement between you and publisher (and CCC) concerning this licensing transaction. In the event of any conflict between your obligations established by these terms and conditions and those established by CCC's Billing and Payment terms and conditions, these terms and conditions shall control.

14. Revocation: Elsevier or Copyright Clearance Center may deny the permissions described in this License at their sole discretion, for any reason or no reason, with a full refund payable to you. Notice of such denial will be made using the contact information provided by you. Failure to receive such notice will not alter or invalidate the denial. In no event will Elsevier or Copyright Clearance Center be responsible or liable for any costs, expenses or damage incurred by you as a result of a denial of your permission request, other than a refund of the amount(s) paid by you to Elsevier and/or Copyright Clearance Center for denied permissions.

LIMITED LICENSE

The following terms and conditions apply only to specific license types:

15. **Translation**: This permission is granted for non-exclusive world **English** rights only unless your license was granted for translation rights. If you licensed translation rights you may only translate this content into the languages you requested. A professional translator must perform all translations and reproduce the content word for word preserving the integrity of the article. If this license is to re-use 1 or 2 figures then permission is granted for non-exclusive world rights in all languages.

16. **Posting licensed content on any Website**: The following terms and conditions apply as follows: Licensing material from an Elsevier journal: All content posted to the web site

must maintain the copyright information line on the bottom of each image; A hyper-text must be included to the Homepage of the journal from which you are licensing at http://www.sciencedirect.com/science/journal/xxxxx or the Elsevier homepage for books at http://www.elsevier.com; Central Storage: This license does not include permission for a scanned version of the material to be stored in a central repository such as that provided by Heron/XanEdu.

Licensing material from an Elsevier book: A hyper-text link must be included to the Elsevier homepage at http://www.elsevier.com . All content posted to the web site must maintain the copyright information line on the bottom of each image.

Posting licensed content on Electronic reserve: In addition to the above the following clauses are applicable: The web site must be password-protected and made available only to bona fide students registered on a relevant course. This permission is granted for 1 year only. You may obtain a new license for future website posting.

For journal authors: the following clauses are applicable in addition to the above: Permission granted is limited to the author accepted manuscript version* of your paper.

***Accepted Author Manuscript (AAM) Definition:** An accepted author manuscript (AAM) is the author's version of the manuscript of an article that has been accepted for publication and which may include any author-incorporated changes suggested through the processes of submission processing, peer review, and editor-author communications. AAMs do not include other publisher value-added contributions such as copy-editing, formatting, technical enhancements and (if relevant) pagination.

You are not allowed to download and post the published journal article (whether PDF or HTML, proof or final version), nor may you scan the printed edition to create an electronic version. A hyper-text must be included to the Homepage of the journal from which you are licensing at http://www.sciencedirect.com/science/journal/xxxxx. As part of our normal production process, you will receive an e-mail notice when your article appears on Elsevier's online service ScienceDirect (www.sciencedirect.com). That e-mail will include the article's Digital Object Identifier (DOI). This number provides the electronic link to the published article and should be included in the posting of your personal version. We ask that you wait until you receive this e-mail and have the DOI to do any posting.

Posting to a repository: Authors may post their AAM immediately to their employer's institutional repository for internal use only and may make their manuscript publically available after the journal-specific embargo period has ended.

Please also refer to Elsevier's Article Posting Policy for further information.

18. **For book authors** the following clauses are applicable in addition to the above: Authors are permitted to place a brief summary of their work online only.. You are not allowed to download and post the published electronic version of your chapter, nor may you scan the printed edition to create an electronic version. **Posting to a repository:** Authors are permitted to post a summary of their chapter only in their institution's

repository.

20. **Thesis/Dissertation**: If your license is for use in a thesis/dissertation your thesis may be submitted to your institution in either print or electronic form. Should your thesis be published commercially, please reapply for permission. These requirements include permission for the Library and Archives of Canada to supply single copies, on demand, of the complete thesis and include permission for UMI to supply single copies, on demand, of the complete thesis. Should your thesis be published commercially, please reapply for permission.

Elsevier Open Access Terms and Conditions

Elsevier publishes Open Access articles in both its Open Access journals and via its Open Access articles option in subscription journals.

Authors publishing in an Open Access journal or who choose to make their article Open Access in an Elsevier subscription journal select one of the following Creative Commons user licenses, which define how a reader may reuse their work: Creative Commons Attribution License (CC BY), Creative Commons Attribution – Non Commercial - ShareAlike (CC BY NC SA) and Creative Commons Attribution – Non Commercial – No Derivatives (CC BY NC ND)

Terms & Conditions applicable to all Elsevier Open Access articles:

Any reuse of the article must not represent the author as endorsing the adaptation of the article nor should the article be modified in such a way as to damage the author's honour or reputation.

The author(s) must be appropriately credited.

If any part of the material to be used (for example, figures) has appeared in our publication with credit or acknowledgement to another source it is the responsibility of the user to ensure their reuse complies with the terms and conditions determined by the rights holder.

Additional Terms & Conditions applicable to each Creative Commons user license:

CC BY: You may distribute and copy the article, create extracts, abstracts, and other revised versions, adaptations or derivative works of or from an article (such as a translation), to include in a collective work (such as an anthology), to text or data mine the article, including for commercial purposes without permission from Elsevier

CC BY NC SA: For non-commercial purposes you may distribute and copy the article, create extracts, abstracts and other revised versions, adaptations or derivative works of or from an article (such as a translation), to include in a collective work (such as an anthology), to text and data mine the article and license new adaptations or creations under identical terms without permission from Elsevier

CC BY NC ND: For non-commercial purposes you may distribute and copy the article and include it in a collective work (such as an anthology), provided you do not alter or modify

the article, without permission from Elsevier

Any commercial reuse of Open Access articles published with a CC BY NC SA or CC BY NC ND license requires permission from Elsevier and will be subject to a fee.

Commercial reuse includes:

- Promotional purposes (advertising or marketing)
- Commercial exploitation (e.g. a product for sale or loan)
- Systematic distribution (for a fee or free of charge)

Please refer to Elsevier's Open Access Policy for further information.

21. **Other Conditions**:

v1.7

If you would like to pay for this license now, please remit this license along with your payment made payable to "COPYRIGHT CLEARANCE CENTER" otherwise you will be invoiced within 48 hours of the license date. Payment should be in the form of a check or money order referencing your account number and this invoice number 501356620.
Once you receive your invoice for this order, you may pay your invoice by credit card. Please follow instructions provided at that time.

Make Payment To:
Copyright Clearance Center
Dept 001
P.O. Box 843006
Boston, MA 02284-3006

For suggestions or comments regarding this order, contact RightsLink Customer

Support: customercare@copyright.com or +1-877-622-5543 (toll free in the US)

or +1-978-646-2777.
Gratis licenses (referencing $0 in the Total field) are free. Please retain this printable license for your reference. No payment is required.
